EFFECT OF MICROBIAL BIOCEMENTATION ON PHYSICO-CHEMICAL AND MECHANICAL PROPERTIES OF MORTAR MADE FROM PORTLAND CEMENTS

DANIEL KARANJA MUTITU
B830/174/2016

A THESIS SUBMITTED IN PARTIAL FULFILLMENT OF THE REQUIREMENTS FOR THE AWARD OF THE DEGREE OF DOCTOR OF PHILOSOPHY IN CHEMISTRY OF THE UNIVERSITY OF EMBU

NOVEMBER, 2020

DECLARATION

This thesis is my original work and has not been presented for a Degree in any other University.

Signature……... Date…….…….
Daniel Karanja Mutitu
Department of Physical Sciences
B830/174/2016

This thesis has been submitted for examination with our approval as the University Supervisors:

Signature ……..……..…… Date…….…..…….
Prof. Jackson Wachira Muthengia
Department of Physical Sciences
University of Embu

Signature ……..……..…… Date…….…..…….
Prof. Romano Mwirichia
Department of Biological Sciences
University of Embu

Signature ……..…….. Date…….…..…….
Prof. Joseph Karanja Thiong'o
Department of Chemistry
Kenyatta University

DEDICATION

This and other achievements I may realize through this work are dedicated to my loving wife, Hannah Nduta, and our wonderful children, Lauryn, Caren, Clarence, and Lily. Their amazing love, patience, encouragement, and financial support have enabled me to see the light of this degree.

ACKNOWLEDGMENT

I express my sincere and deepest gratitude to my esteemed and worthy supervisors, Prof. Wachira Muthengia and Prof. Romano Mwirichia of the University of Embu and Prof. Karanja wa-Thiong'o of Kenyatta University for their valuable discussion, brainstorming, critical reviews, challenges, insights, and guidance throughout this research study. It was through their overwhelming supervision and inspiration that kept me developing new insights and ideas during this research. Their call for 'high-quality work' made me remain focused and aflame.

I owe my thanks to my siblings and exceptionally to my love Hannah, for generously allowing me to utilize any family resource in pursuant of my academic thirst. May the Almighty God always bless them. I am also grateful to the technical staff of Savannah Cement Ltd. and in particular, Mr. Onesmus Munyao for allowing me to use their Cement Laboratory facilities for my laboratory works as well as their technical support and guidance. I would also like to pass my gratitude to the entire staff of the Microbiology laboratory, University of Embu, and in particular Prof. Romano Mwirichia for their guidance in culturing my bacteria and preparation of the microbial solution. My gratitude also goes to the entire staff of Microscopy and Microanalysis Instrumentation Laboratory, University of Pretoria, South Africa for their assistance in conducting my cement sample analysis. It would have been a nightmare without their support.

Special thanks to my student colleagues both at the University of Embu and Kenyatta University for sharing their time and the logistical support during my research.

TABLE OF CONTENTS

LIST OF TABLES

LIST OF FIGURES

APPENDICES

LIST OF ABBREVIATIONS, SYMBOLS, AND ACRONYMS

Cement Chemical Nomenclature and Symbols

$A = Al_2O_3$, $H = H_2O$, $S = SiO_2$, $\bar{S} = SO_3$

$C\bar{S}H_2 = CaSO_4.2H_2O$	Gypsum
$C_4A\bar{S}H_{12} = 3CaO.Al_2O_3.CaSO_4.12H_2O$	Calcium Aluminate Monosulphate hydrate
$C_6A\bar{S}_3H_{32} = 3CaO.Al_2O_3.3CaSO_4.32H_2O$	Ettringite (Ettr)
$C_3A = 3CaO.Al_2O_3$	Tricalcium Aluminate
$C_2S = 2CaO.SiO_2$	Dicalcium Silicate
$C_3S = 3CaO.SiO_2$	Tricalcium Silicate
$CH = Ca(OH)_2$	Calcium hydroxide
CAH	Calcium Aluminate Hydrate
C_4AF	Tetracalcium Aluminoferrite
CSH	Calcium Silicate Hydrate

Abbreviations and Acronyms used

ANOVA	Analysis of Variance
ASTM	American Standard for Testing and Materials
BF	Big Four agenda
BS	British Standards
C_s	Surface Concentration
D_{app}	Apparent Diffusion Coefficient
D_{mig}	Migration Diffusion Coefficient
DC	Direct Current
DIC	Dissolved Inorganic Carbon
DSMZ	Deutsche Sammlung von Mikroorganismen und Zellkulturen
EAS	East Africa Standard
EDAX	Energy Dispersive X-ray Analyzer
EDX	Energy-Dispersive X-ray spectrum

FTIR	Fourier Transform-Infrared
ISO	International Standards of Organizations
KS	Kenya Standard
LOI	Loss on Ignition
MICP	Microbiologically Induced Calcite Precipitation
Mpa	Mega Pascal
MR	Modulus Rapture
OD	Optical Density
OPC	Ordinary Portland Cement
OPC-BM (BM)	OPC mortar prepared and cured using *Bacillus megaterium* microbial solution
OPC-BM (H)	OPC mortar prepared using *Bacillus megaterium* microbial solution and cured in water
OPC-BP (BP)	OPC mortar prepared and cured using *Sporosarcina pasteurii* microbial solution
OPC-BP (H)	OPC mortar prepared using *Sporosarcina pasteurii* microbial solution and cured in water
OPC-H (BM)	OPC mortar prepared using water and cured in *Bacillus megaterium* microbial solution
OPC-H (BP)	OPC mortar prepared using water and cured in *Sporosarcina pasteurii* microbial solution
OPC-H (H)	OPC mortar prepared and cured using water (Control/Non-bacterial treated)
OPC-H (LB)	OPC mortar prepared using water and cured in *Lysinibacillus sphaericus* microbial solution
OPC-LB (H)	OPC mortar prepared using *Lysinibacillus sphaericus* microbial solution and cured in water
OPC-LB (LB)	OPC mortar prepared and cured using *Lysinibacillus sphaericus* microbial solution
PPC	Portland Pozzolana Cement

PPC-BM (BM)	PPC mortar prepared and cured using *Bacillus megaterium* microbial solution
PPC-BM (H)	PPC mortar prepared using *Bacillus megaterium* microbial solution and cured in water
PPC-BP (BP)	PPC mortar prepared and cured using *Sporosarcina pasteurii* microbial solution
PPC-BP (H)	PPC mortar prepared using *Sporosarcina pasteurii* microbial solution and cured in water
PPC-H (BM)	PPC mortar prepared using water and cured in *Bacillus megaterium* microbial solution
PPC-H (BP)	PPC mortar prepared using water and cured in *Sporosarcina pasteurii* microbial solution
PPC-H (H)	PPC mortar prepared and cured using water (Control/Non-bacterial treated)
PPC-H (LB)	PPC mortar prepared using water and cured in *Lysinibacillus sphaericus* microbial solution
PPC-LB (H)	PPC mortar prepared using *Lysinibacillus sphaericus* microbial solution and cured in water
PPC-LB (LB)	PPC mortar prepared and cured using *Lysinibacillus sphaericus* microbial solution
SD	Standard Deviation
SDG	Sustainable Development Goal
SEM	Scanning Electron Microscopy
T_{calc}	Calculated T-test value
UV-Vis	Ultraviolet-Visible
w/c ratio	Water to Cement ratio
XRD	X-ray Diffraction
XRF	X-Ray Fluorescence

ABSTRACT

Microorganisms in soil and water play a significant role in physico-chemical and mechanical properties as well as the durability of building materials. The microorganisms can either contribute to the improvement or deterioration of the materials. Beneficial microorganisms may deposit calcium carbonate in cement mortar or concrete through a process called microbial biocementation. These deposits exhibit binding properties for protecting and consolidating various building materials. Whereas the effect of *Bacillus* bacteria on fully hardened/cured mortar/concrete is well documented, the effect of such microorganisms on fresh mortar and concrete paste has not been fully investigated. Further, this study examined the microorganisms' biominerals, their chemical composition, and their role in the enhancement of nucleation on cement hydration. The *Bacillus* species under this study are commonly found in soil/water, are non-pathogenic and are urease active. Bacterial species, *Lysinibacillus sphaericus, Sporosarcina pasteurii,* and *Bacillus megaterium* were incorporated separately into the mortar-making mixing water at a concentration of 1.0×10^7 cells/mL. Mortar prisms with 0.5 water-cement (w/c) ratio were cast using selected commercial Ordinary Portland Cement (OPC) and Portland Pozzolana Cement (PPC). Some prisms were then cured at room temperature in a microbial solution composed of bacteria, urea, and calcium acetate/calcium chloride, while others were cured in tap water. Lower normal consistency results from microbial mortar pastes than non-microbial pastes in both OPC and PPC were observed. This implied reduced water demand and improved workability. Initial and final setting time were generally lowered, with the OPC paste with *Lysinibacillus sphaericus* showing the highest reduction. The resultant chemical compounds formed in the mortar were analyzed using Scanning Electron Microscopy (SEM), powder X-ray Diffraction (XRD), and Fourier Transform Infrared (FTIR). Bavenite, $Al_2Be_2Ca_4H_2O_{28}Si_9$, and calcite, $CaCO_3$, were found to be the resultant microbial cement hydration products. Compressive and flexural strength gain was observed after the 14th day of curing with the highest compressive and flexural strength gain observed at the 56th day of curing at 19.8 % and 37.0 % respectively for OPC mortars that had *Lysinibacillus sphaericus*. Rapid accelerated chloride and sulphate penetration tests were performed on the mortar prisms by exposing them to a media of 3.5 % by mass of sodium chloride and sodium sulphate separately for thirty-six hours using a 12V DC power source. The migration diffusion coefficient, $D_{mig,}$ and apparent diffusivity coefficient, D_{app}, for both the Cl^{1-} and SO_4^{2-} for mortar prisms were determined. D_{app} was lowered from 3.5340×10^{-10} m^2/s to 2.5449×10^{-10} m^2/s and from 6.4810×10^{-10} m^2/s to 4.5179×10^{-10} m^2/s for Cl^{1-} and SO_4^{2-} respectively in PPC mortars that had *Bacillus megaterium*. After the 28th day of curing, water sorption change was determined across the mortar categories. Water sorption was lowered in the range of 47.8 % to 68.4 %. PPC mortars that had *Bacillus megaterium* exhibited a water sorptivity coefficient reduction from 0.0289 to 0.0093. The results show that the incorporation of the selected *Bacillus* species under this study improves the physico-chemical and mechanical properties of the test cements significantly.

CHAPTER ONE
INTRODUCTION

1.1 Background

Concrete/mortar is one of the most broadly utilized construction materials by mankind and it is the main fabric used for infrastructure development worldwide (Muthengia, 2009; Mutitu, 2013). Cement is a hydraulic binder with adhesive and cohesive properties which makes it capable of bonding mineral fragments together (Mutitu, 2013; Reddy, *et al.*, 2013; KS EAS 18-1:2017; Yu, *et al.*, 2018). The cementing or bonding action of calcareous types of cement is attained through a chemical reaction involving lime or lime compounds (Castanier, *et al.*, 1999). Mortar/concrete exhibits inherent micro-cracks capacity. The presence of non-hydrated excess cement particles in the matrix, which undergoes delayed or secondary hydration upon reacting with ingress water could be attributed to this phenomenon.

Microorganisms in soil and water play a major role in physico-mechanical properties and durability of concrete/mortar through the process generally referred to as microbial biocementation. The process is affected by variation in temperatures, humidity, type of cement, type and concentration of bacteria, soil/water pH among others. Through the process, calcium carbonate is deposited in a cement mortar or concrete matrix. Such sediments have of late emerged as promising binders for securing and consolidating a variety of building materials (Johanneson and Geiker, 2012).

It is generally acknowledged that the durability of concrete/mortar is related to the characteristics of its pore structure (Khan, *et al.,* 2010; Chahal, *et al.*, 2012). Deterioration mechanisms of concrete/mortar commonly depend in the way aggressive substances can enter the concrete/mortar, conceivably causing degradation (Nosouhian, *et al.*, 2016; Munyao, *et al.*, 2020). The porosity of the concrete/mortar depends on its pore network (Chahal, *et al.*, 2012; Mutitu, *et al.*, 2020). The more open the pore structure of the concrete/mortar, the more susceptible the material is to debasement components caused by ingressive substances (Muthengia, 2009, Munyao, *et al.*, 2019).

Cracks have a severe negative influence in an aggressive environment with regard to chloride and sulphate penetration (Maes and De Belie, 2016).

Despite the various concrete/mortar benefits, it has a high crack formation inclination allowing aggressive substances to permeate the structure. Permeability of concrete/mortar initiates deterioration and sets off durability decrease. Treatment of cracks and pores in concrete/mortar is generally divided into passive and active therapies. Passive therapy can only remediate the surface cracks, while active therapy heals both internal and peripheral cracks (Jonkers, *et al.,* 2011).

Recently, biomineralization has attracted attention as a novel way of remediating the durability concerns related to active and passive therapies (Jonkers, *et al.,* 2011). The usefulness and versatility of calcium carbonate as a concrete/mortar void, porosity and crack filler is attributed to its abundance in nature and compatibility with cementitious compositions (Luo and Qjan, 2016). This innovative treatment makes these microbial treated concrete/mortars to act as intelligent systems that are different from the ordinary prepared cement structures (Jonkers, *et al.,* 2011; Tziviloglou, *et al.*, 2016). These smart structures have self-sensing properties towards external factors such as a change in temperature, pH, stress, humidity, and concrete/mortar pore solution chemistry. This characteristic leads to microcracks self-healing.

Bacterial species used in most biocementation processes are not harmful to human beings and are capable of withstanding wide temperature and pH range. These bacteria precipitate inorganic crystals that plug the cracks/voids in the concrete/mortar (De Jong, 2013). Microbially induced calcium carbonate precipitation (MICP) extensive significance has triggered great responsiveness at both basic and applied cement chemistry as well as civil engineering perspectives (Ramakrishnan, *et al.*, 2007; Karanja, *et al.,* 2019; Munyao, *et al.,* 2019).

Ureolysis pathway, which is the decomposition of urea by bacterial urease enzyme has been studied most compared with aerobic oxidation, denitrification, photosynthesis,

ammonification, sulphur reduction, and methane oxidation. Perhaps, this is because ureolytic bacteria are hydro-anaerobic and as such, they grow effectively inside the mortar/concrete matrix in absence/limited oxygen supply. They can also thrive for long as endospores until favorable conditions and the presence of food is available (Vijay and Murmu, 2018). The favourable condition includes future cracks formation where the bacteria get activated and through a suitable pathway deposits calcium carbonate which fills the cracks (Salifu, *et al.*, 2016; Vijay, *et al.*, 2017). Due to the negative-charged bacterial cell membrane and the high surface area to volume ratio of the bacteria, the bacteria attract cations from the surrounding microenvironment, including Ca^{2+} which sediment on their cell membrane (Alghamri, *et al.*, 2016). The Ca^{2+} react with the CO_3^{2-} forming a calcium carbonate encapsulation around them. This way, the bacteria cell wall provides a nucleo-site for cement hydration (Mostavi, *et al.*, 2015). Ureolytic MICP reactions can be summarized as given in Equations 1.1 to 1.7.

$$CO(NH_2)_2 + H_2O \rightarrow NH_2COOH + NH_3 \quad 1.1$$

$$NH_2COOH + H_2O \rightarrow NH_3 + H_2CO_3 \quad 1.2$$

$$2NH_3 + 2H_2O \leftrightarrow 2NH_4^{1+} + 2OH^{1-} \quad 1.3$$

$$H_2CO_3 \leftrightarrow HCO_3^{1-} + H^{1+} \quad 1.4$$

$$HCO_3^{1-} + H^{1+} + 2OH^{1-} \leftrightarrow CO_3^{2-} + 2H_2O \quad 1.5$$

$$Ca^{2+} + \text{Bacterial Cell} \rightarrow \text{Bacterial Cell} - Ca^{2+} \quad 1.6$$

$$\text{Bacterial Cell - } Ca^{2+} + CO_3^{2-} \rightarrow \text{Cell} - CaCO_3 \quad 1.7$$

Polymers attached to the outer cell membrane of Gram-positive and Gram-negative bacteria in the form of peptidoglycan macromolecules (PGM) and lipopolysaccharide (LPS) respectively are highly anionic. This results in an overall electronegatively charged bacterial cell wall, which is highly interactive with metal ions. This cation-philic nature makes them ideal nucleation sites for diverse crystal development (Rodriguez-Navarro, *et al.*, 2007; Botusharova, 2017). The bacteria cell wall thus attracts the Ca^{2+} followed by CO_3^{2-} which deposits as calcium carbonate on their cell surface (Thompson, *et al.*, 1997; Stocks-Fischer, *et al.*, 1999). This process results to complete encapsulation of the bacteria due to significant crystal precipitates around the cell wall (Rodriguez-Navarro,

et al., 2007; De Jong, *et al.,* 2013).

A diagrammatic representation of varied mechanisms for bacterial-catalyzed $CaCO_3$ precipitation is summarized in figure 1.1.

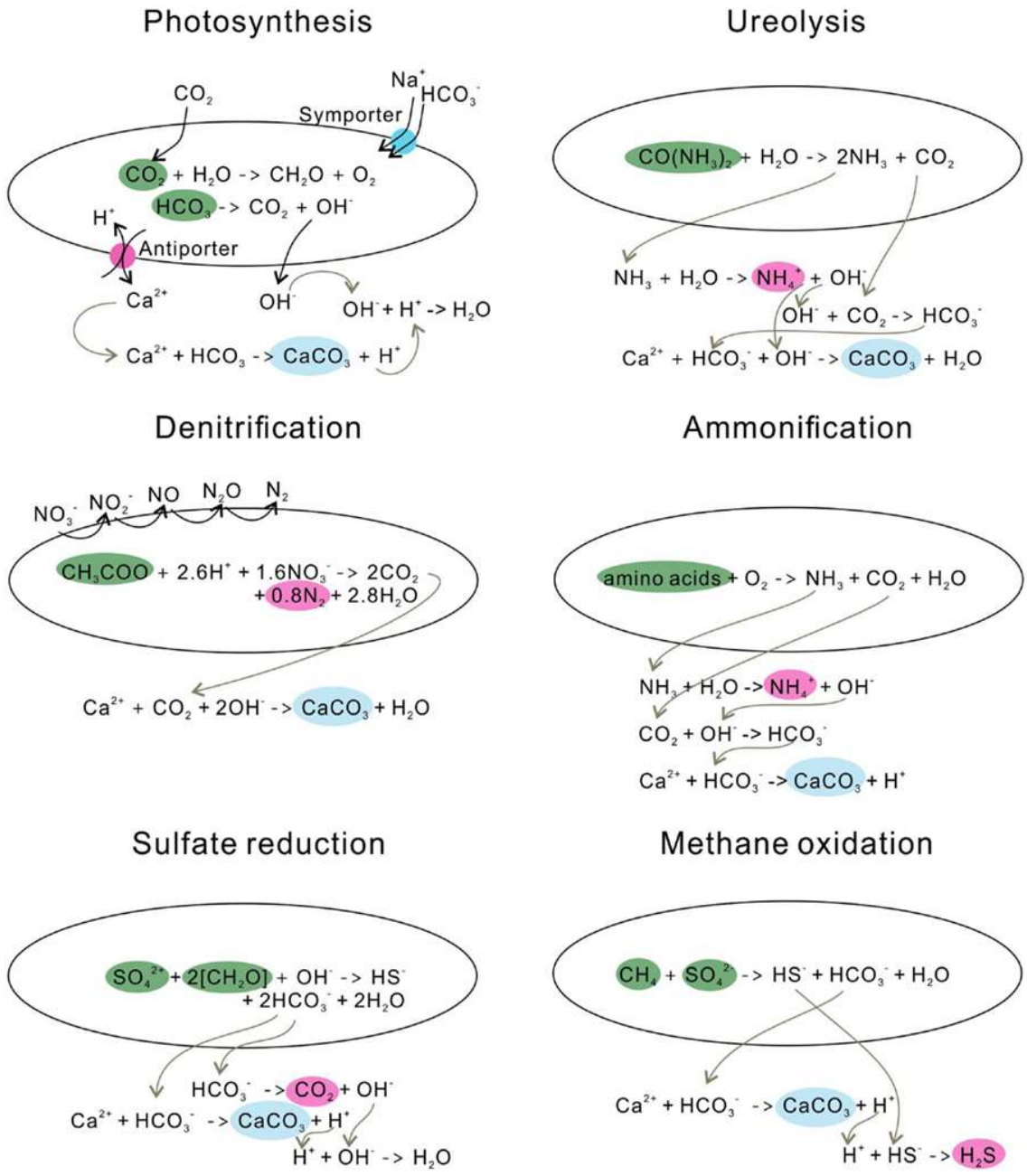

Figure 1.1: Microbially induced calcium carbonate precipitation (figure reproduced from Zhu and Dittrich, 2016)

Comparative studies have exhibited that there are both merits and limitations on bacterial healing agents and strategy (Jonkers, *et al.*, 2011; Mutitu, *et al.*, 2020). The merits include, self-sensing and self-healing capabilitiy, bacteria self regeneration, microenvironment adaptability and tolerance, and calcium carbonate compatibility with cement hydration products. The limitations included bacterial interference with the ground water and commercial use of ureolytic bacterial strains may cause problem as urease enzyme is associated with increased virulence among pathogenic bacterial strains (Lee and Calhoun, 1997). Moreover, most studies have focused more on the durability side such as compressive strength and microcrack repair. Very little knowledge is documented on the physico-chemical properties beneficiation such as setting time, normal consistency, sorptivity and aggressive ion ingress (Maheshwaran, *et al.,* 2014; Munyao, *et al.,* 2019). Thus, there is a need to further investigate to establish a more efficient self-healing strategy as well as examine the physico-chemical and mechanical effects of MICP on mortar/concrete. Most MICP studies have focused on one durability aspect with one bacteria species at a time. Studies, such as the ones summarized in table 2.1, are seen as being too cautious not to negate the pre-defined merits or bring out the limitations of a given bacteria species under certain conditions.

Certain MICP merits under certain conditions could pose limitations under certain different conditions (Jonkers, *et al.,* 2011; Liu, *et al.,* 2015; Karanja, *et al.,* 2019). MICP is an emerging technology in mitigating degradation of concrete/mortar. Varied bacteria cell concentrations and species may expose concrete/mortar to the risk of failure (Munyao, *et al.,* 2019). Certain *Bacillus* species at certain cell concentrations act as concrete/mortar crack fillers, strength development enhancers, and water sorption inhibitors (Maes and De Belie, 2016; Nosouhian, *et al.,* 2016). They exhibit beneficial properties when they ingress or are part of the cementing material.

1.2 Statement of the problem

Cement and cementitious materials are subject to being degraded by aggressive environments. Several measures are used to mitigate the degradation of concrete/mortar. Such measures include the use of special types of cement including water-resistant

cement. Additives to cement, including Pozzolana and other fillers, are also used to increase the resistance of concrete/mortar. These additives may become discordant with concrete/mortar with time, they may emit toxic gases in their expiring process or they may loose aesthetic value with time. It is therefore important to investigate the performance of selected Portland Cement with selected bacteria species under identical controlled conditions. While us the effect of *Bacillus* bacteria on fully hardened concrete/mortar is well documented, the effect on fresh paste has not been fully investigated. There is need to examine microorganisms' biominerals, composition and role in cement hydration process. Further work is, therefore, necessary for a better understanding of the self-healing efficiency and its variability. This will allow proper selection of the best suited MICP bacteria and the optimum conditions for the production of an alternative and high-quality concrete/mortar. When all this is achieved and documented, then engineers, contractors, and construction proprietors could be convinced of the suitability to practice the application of specific *Bacillus* species. Such a practice could be adopted either as an environmentally responsible course of action, for mortar/concrete surface crack healing, to improve the durability properties, to improve the physico-chemical and mechanical properties of mortar/concrete paste or to lower the ingress of ions into the cement matrix on large scale or in the field. From the aforesaid, therefore, there is a need to further investigate the effect of the select bacteria on the physico-chemical and mechanical properties of cement materials. Quality control in Kenya cement standards do not address the requirements for microorganism effect, yet most constructions are done in areas with microorganisms, for example, sewerage, ex-garbage sites, and agricultural farms. The standard does not provide any cement deterioration test nor any advice on possible precautions or remedies.

1.3 Null Hypotheses

H_{01} *Sporosarcina pasteurii, Lysinibacillus sphaericus,* and *Bacillus megaterium* have no microbial biocementation activity onto OPC and PPC mortar.

H_{02} *Sporosarcina pasteurii, Lysinibacillus sphaericus,* and *Bacillus megaterium* have no effect on normal consistency, soundness, and setting time on OPC and PPC fresh paste.

H_{03} *Sporosarcina pasteurii, Lysinibacillus sphaericus,* and *Bacillus megaterium* do not affect hydration, porosity, flexural, and compressive strength development, water sorptivity coefficient or aggressive ion ingress into OPC and PPC mortar.

1.4 Objectives

1.4.1 General Objective

To determine the effects of microbial biocementation on the physico-chemical and mechanical properties of select OPC and PPC mortar.

1.4.2 Specific Objectives

1. To investigate the development of MICP by *Sporosarcina pasteurii, Lysinibacillus sphaericus* and *Bacillus megaterium* in the Kenyan made OPC and PPC mortars using SEM, XRD, and FTIR.
2. To determine the effect of the selected bacteria on normal consistency, soundness, setting time, hydration, and porosity of selected Kenyan made OPC and PPC mortars.
3. To investigate the effect of the selected bacteria on the compressive strength and flexural strength of Kenyan made OPC and PPC mortars.
4. To analyze the water sorptivity coefficients and diffusion coefficients of chloride and sulphate ions in the MICP-containing Kenyan made OPC and PPC mortars.

1.5 Justification of the Study

There is an inherent desire by Kenyans to own decent, affordable, and gorgeous houses. The cost of built environment repair/maintenance though enormous is even not well documented (NCA, 2017). Lack of sewerage and other organic waste disposal systems (NEMA, 2018) creates a conducive environment for bacteria and other microorganism's growth and development. The bacteria-containing water effluents or surface water run-offs come into contact with either, the already constructed building surfaces or as a contaminant with concrete/mortar making, mix-water. This probably either poses a great threat or is of benefit to the cement concrete/mortar in the construction industry. In nature, a given bacteria species does not exist in isolation. The merits of a given bacteria

species to a specific physico-chemical and mechanical parameter may pose some limitations to another bacteria species towards another parameter. There is a need therefore to investigate several bacteria effects on a variety of parameters, independently, but under similar conditions. This will provide information on the best choice of bacterial species and the optimum conditions to remediate specific mortar/concrete property. Kenyan cement standards only rely on physico-mechanical properties without relating the same to microbial effect. The results of this study will make available these vital physico-chemical and mechanical bacteriological requirements. This will allow decision-making on the suitability or otherwise of concrete/mortar in bacteria presence environment, and hopefully lay a foundation for future standards on the use.

Improved infrastructure enhances the opportunities for people to participate in economic activities by supporting macroeconomic development. This is in line with the current Government of Kenya; first of the five-year (2017 to 2022) Kenya development goals (Big – Four Agendas); manufacturing competitiveness and value of Kenyan-made products, and the second goal of creating access to an affordable and decent shelter by cutting the costs of construction by using innovative technologies.

The attainment of the 9th SDG includes the need to build resilient infrastructure, promote inclusive and sustainable industrialization, and foster innovation. The 11th SDG requires that we make cities and human settlements inclusive, safe, resilient, and sustainable, the 15th SDG; protect, restore and promote sustainable use of terrestrial ecosystems, sustainably manage forests, combat desertification and halt and reverse land degradation and halt biodiversity loss. This study will promote the construction of resilient infrastructure that is self-healing and can withstand harsh environments and therefore help in the realization of the above SDGs related to construction in one way or the other.

Manufacture of synthetic resins/epoxy used to remediate the cracks emit toxic/greenhouse gases during their manufacture as well as after use once they expire or become incompatible (Karol, *et al.*, 2003; Bojes and Pope, 2007; Lassen, *et al.*, 2015). These synthetic resins/epoxy disposal is an environmental pollutant. MICP is a smart

technology with no toxic/greenhouse gas effect. This will contribute significantly to the mitigation of climate change effects especially in developing and middle-income countries like Kenya.

1.6. Scope and Limitations

This study used select bacteria; *Sporosarcina pasteurii, Lysinibacillus sphaericus,* and *Bacillus megaterium* that are known to synthesize active urease. Laboratory-investigations were carried out as opposed to field investigations.

CHAPTER TWO
LITERATURE REVIEW

2.1 Durability Properties of Hydrated Cement

Constructions of structures such as bridge decks, parking structures, marine structures, sewage pipes, structures for solid and liquid wastes containing toxic substances requires high durability cement. This durability requirement for cement concrete/mortar exposed to aggressive environments and underground constructions may not be achieved using ordinary Portland cement (OPC) alone (Karanja, *et al.,* 2019; Munyao, *et al.,* 2019). Cement with properties that cannot be affected or that can withstand aggressive ion effect is a necessity. The durability of concrete/mortar is related to the characteristics of its pore structure (Khan, *et al.,* 2010; Mutitu, 2013).

Concrete/mortar has various advantages while used in construction. These include adhesive properties for binding and dressing the surfaces of adjacent blocks, pliable with blocks whether regular/irregular or smooth/rough. Concrete/mortar also exhibit resistance to water, wind and fire attack. Concrete/mortar application requires minimal maintenance, heat retention ability, ability to mix, and be compatible with waste materials, among other multimodal application characteristics. Concrete/mortar structures, however, have a high tendency to form cracks allowing aggressive substances to penetrate the structure. Permeability or cracks are one of the main causes of concrete/mortar deterioration and thus decrease in expected durability service-life (Tziviloglou, *et al.*, 2016). These cracks have a severe negative influence in an aggressive environment with regard to chloride and sulphates penetration (Maes and De Belie, 2016; Mutitu, *et al.*, 2019).

Degradation mechanisms of concrete/mortar often depend on the way potentially aggressive media can penetrate it. The permeability to such a structure depends on the porosity and the inter-connectivity of the pores. The more open the pore structure of the concrete/mortar, the more vulnerable it is to degradation mechanisms caused by penetrating substances. The deterioration of structures usually involves movement of

aggressive gases, ions, or fluids from the surrounding environment into such a structure accompanied by physical and/or chemical reactions within its internal structure, possibly leading to irreversible damage (Nosouhian, *et al.*, 2016; Supritha, *et al.*, 2016). This implies that transport/migration properties and mechanical properties are important factors for concrete/mortar durability. The durability and life of cement-based specimens are estimated by the capillary water movements into it. Higher absorption of water by the specimen would imply higher damage.

To decrease the susceptibility of crack development, organic solvents and synthetic polymers, hollow fibers, microencapsulation, epoxy, resins, epoxy mortars among other synthetic fillers are applied (Qian, *et al.*, 2018). To control structural decay, water repellants and stone consolidating synthetic/mineral admixtures are currently being applied. These admixtures may with time be discordant or result in harmful surface films (Verma, *et al.*, 2015; Qian, *et al.*, 2018). All these methods are expensive and have proven to be unsatisfactory (Munyao, *et al.,* 2019). Ghosh, *et al.*, (2009) postulated a sustainable, cheaper, alternative green and clean methodology, the use of a biological self-healing repair technique. This process is necessary for saving enormous structures from damage (Supritha, *et al.*, 2016).

Bacterial treated concrete/mortar specimens are found to have better resistance towards chloride and or sulphate penetration as compared to non-bacterial treated concrete/mortar specimens (Damidot and Glasser, 1997; Karanja, *et al.*, 2019). A decreased water permeability of bioremediated cement-based cubes treated by *Sporosarcina pasteurii* was reported by Achal *et al.,* (2013) with a six times reduction in water absorption. Several studies have documented compressive strength improvements on bacterial treated cementitious material of between 9 % and 25 % by 28^{th} day of curing (Chahal, *et al.*, 2012; Ersan, *et al.*, 2015; Achal, *et al.*, 2016; Thiyagarajan, *et al.*, 2016). Different researchers have documented both positive and negative effects on compressive strength depending on the bacterial strain, bacteria feed, cell concentration, or concrete age (Ghosh, *et al.*, 2009; Park, *et al.*, 2010). Wang, (2013) found out that calcium nitrate as a bacterial nutrient accelerated cement hydration while yeast extract significantly delayed

the hydration and resulted in a lowered cement hydration. Wang, (2013), on embedding encapsulated *Bacillus sphaericus* in a cracked mortar, obtained a decrease in compressive strength of between 15 % and 34 % between the 7^{th} and 28^{th} day of curing. Achal *et al.,* (2013) reported a reduction in compressive strength on using *Sporosarcina pasteurii* at a cell concentration of 5×10^8 cells/mm^3. Ersan *et al.*, (2015) used encapsulated *Sporosarcina pasteurii* and reported a decrease in compressive strength on concrete in the 7^{th} and 28^{th} day of curing by 63 % and 60 %, respectively. However, generally, there is a significant increase in compressive strength in bacterial treated concrete/mortar as compared to the conventional concrete/mortar. The type of biocementatious bacteria used determines the extent of compressive strength enhancement. This could be attributed to the activity of different bacterial species such as ureolytic, photosynthetic, methane-oxidizing bacteria, cyano-bacteria, aerobic oxidation, or denitrifying bacteria.

Chloride and sulphate ingress in cement-based materials is mainly through capillary absorption, permeation, and diffusion. Chloride and sulphate ingress, however, may also occur through a multiple of the aforementioned mechanisms. Diffusion is the most prevalent process through which chlorides and sulphates ingress in cement-based materials (Machard, *et al.*, 1998; Wang, *et al.*, 2014). The ingress of chlorides/sulphates into concrete/mortar due to the various transport mechanisms obeys different laws (Crank, 1975). Fick‘s second law of diffusion is commonly applied to quantify the aggressive ion ingress due to the multiple transport phenomena.

Chlorides react with C_3A and the C_4AF present in Portland cement to produce Friedel‘s salt, $Ca_6Al_2O_6.CaCl_2.10H_2O$ or calcium chloroferrite, $Ca_6Fe_2O_6.CaCl_2.10H_2O$ respectively (; Muthengia, 2009; Mutitu, 2013). No deleterious effect is associated with these products. The reaction between the C_3A phase and free chlorides in hydrated cement leads to a reduction of Cl^- from pore solution (Cheng and Cord-Ruwisch, 2013). This lowers the risk of rebar corrosion (Rasheeduzzafar, *et al.*, 2004). However, these chloride salts are both expansive and soft which increases mortar/concrete porosity. Permeation of water and oxygen necessary for rebar corrosion as well as aggressive ions, which act as corrosion accelerators become a necessary factor to consider. When using cement in

structures requiring reinforcement bars, the depth of cover and the type of cement becomes a necessary factor to consider (Mutitu, 2013).

Biocementation in Portland cement concrete/mortars lowers ion ingress and permeability into its matrix (Dousti, *et al.*, 2011). This is due to the refinement of the pore structure (Mutitu, 2013; Muthengia, 2009). Microbiologically induced calcite precipitation (MICP) can be achieved extracellularly either through heterotrophic processes, or autotrophic processes. Both of these processes follow the urea decomposition, oxidation of organic acids, or nitrate reduction pathways (De Muynck, *et al.*, 2010; Salifu, *et al.*, 2016).

The $CaCO_3$ deposit has emerged as a promising sealant for the protection and the consolidation of various construction materials (Adolphe, *et al.*, 1990). Adolphe, *et al.,* (1990) as pioneers of MICP, incorporated calcite precipitation in the restoration of ornamental stone surfaces. However, the results from the durability tests conducted by Cheng, *et al.*, (2013), on sand columns show that MICP-cemented samples are highly durable to the freeze-thaw abrasion but less durable to the acid rain corrosion. In their work, the $CaCO_3$ crystals were scoured by the hydrogen ions from the acid rain leading to the destruction of cementitious products - $CaCO_3$ bond. This resulted in severe damage affecting the sample's mechanical properties. The results of the scoured samples reflected that no obvious damage occurred at the bottom part of the sand column. However, the strength of the top part of the sand column was decreased by about 40%. This could imply that the potential of MICP as a viable alternative process, could offer long term benefits if it occurs within the mortar/concrete matrix than as a surface application technique.

The deposits enhance nucleation of cement hydration on early cement compressive and flexural strength and as well improve the reactivity of Pozzolana and other non-cementitious material. Furthermore, the microbial biocementation increases the resistivity of the resultant mortar/concrete to aggressive media (Luo and Qjan, 2016). The abundant and cementitious-compositions-compatibility nature of calcium carbonate

makes it the most necessary and versatile grout to plug the voids, seal porosities, and fill the cracks in concrete/mortar (Luo and Qjan, 2016). This innovative treatment makes these microbial treated concrete/mortars to act as intelligent systems that are different from the ordinary prepared cement structures (Jonkers, *et al.*, 2011; Tziviloglou, *et al.*, 2016). These smart structures have self-sensing and self-healing properties toward external factors such as a change in temperature, pH, stress, humidity, and concrete/mortar pore solution chemistry (Salifu, *et al.*, 2016). *Bacillus* species are extensively distributed in most soils and can continually deposit calcite sediments under favourable conditions, they are harmless to human beings, and should be able to withstand a wide range of temperature and pH. The nucleo-crystal precipitation causes the healing of the cracks and voids as well as lowers the pores in the concrete/mortar (Salifu, *et al.*, 2016).

In concrete/mortar structures, cracking is a common phenomenon due to relatively low tensile strength (Yu, *et al.*, 2018). Concrete/mortar cracking may be caused by concrete/mortar internal/chemical processes as a result of plastic shrinkage/settlement. Plastic shrinkage/settlement cracks occur mostly in freshly prepared structures when the rate of water loss through evaporation exceeds the rate at which water is reaching the cement matrix (Vijay and Murmu, 2018). High tensile stresses can result either from external loads or imposed deformations due to temperature gradients which cause differential volume variations and against structure rigidity, tensions arise causing cracking. Microcracks may also develop due to cement hydration heat which results in internal stresses. At times, micro-cracks develop due to the continuous vibration of a machine in later works in the same or adjacent cement structure. Other causes of cracks include long-term shrinkage and creep as a result of constant loads over time on concrete/mortar structures (Reddy, *et al.*, 2013; Achal, *et al.*, 2016). Cracks are one of the main causes of concrete/mortar deterioration and a decrease in durability. The presence of cracks results in increased porosity and permeability. The permeability of the mortar/concrete is dependent on the porosity and the connectivity of the pores. The more open the pore structure of the mortar/concrete, the more vulnerable the material is to degradation mechanisms (Muthengia, 2009). Cracks provide pathways for the penetration

of potentially aggressive substances in the mortar/concrete, possibly causing damage (Nosouhian, *et al.*, 2016).

Treatment of cracks and pores in concrete is generally divided into passive and active treatments. Passive treatments can only heal the surface cracks. In this treatment, sealants are sprayed or injected into the cracks (Pacheco-Torgal and Labrincha, 2013; Wang, 2013). The sealants comprise of chemical materials such as epoxy resins, chlorinated rubbers, polyurethane, acrylics, and siloxanes. Passive treatments have proven to have many limitations that hinder their usage (Van Tittelboom and De Belie, 2013). Active treatments can heal both interior and exterior cracks. Active treatment techniques also referred to as self-healing techniques can operate independently in different conditions regardless of the crack position. Once the crack is formed, they activate immediately and seal the crack. The suitable treatment of concrete/mortar cracks should have quality, long shelf-life, pervasiveness, and the ability to repeatedly heal the cracks on an unlimited number of times (Li and Herbert, 2012). Self-healing mechanisms can be established either through autogenous healing, encapsulation of polymeric materials, or through microbial production of calcium carbonates (Johanneson and Geiker, 2012).

Recently, biomineralization approaches have attracted researcher's attention as a novel way to address the durability issues related to active and passive treatments. The abundance in nature and compatibility with cementitious compositions of calcium carbonate makes it the most useful and versatile fillers to plug the voids, porosities, and cracks in mortar/concrete (Seifan, *et al.*, 2016; Supritha, *et al.*, 2016). This innovative treatment makes the microbially treated cement mortars/concrete to act as intelligent systems that are different from the ordinary prepared cement structures (Jonkers, *et al.*, 2011; Tziviloglou, *et al.*, 2016). These smart structures have self-sensing and self-healing properties toward external factors such as change in temperature, pH, stress, humidity, and concrete/mortar pore solution chemistry. MICP is a relatively green and sustainable improvement structural technique (Carmona, *et al.*, 2016; Williams, *et al.*, 2016; Vijay, *et al.*, 2017). However, as highlighted under section 2.1, calcite surface remediation is prone to acid rain degradation.

Corrosion of rebar in concrete causes micro-cracks. To initiate reinforcement corrosion, it is necessary for the chloride to penetrate a cementitious substance from outside and to exceed the chloride critical corrosion-inducing limit (Florea and Brouwers, 2012). Chloride ions penetrate the concrete/mortar pore system and form chloride salts which may crystallize within the pores inducing internal cracks (Dousti, *et al.*, 2011). The cracks affect the mechanical and durability properties of concrete/mortar (Dousti, *et al.*, 2011). For iron bar reinforced concrete, the condition will be much worse as the presence of chloride ions affect rebar through pitting (Luping and Gulikers, 2007). The concrete/mortar around the reinforcement, thus making it possible to initiate reinforcement corrosion. Corrosion is a major problem and millions of dollars are spent every year to repair the deterioration it causes (Bamforth, 2003; Bertolini, *et al.*, 2004). Inclusion of bacteria in concrete/mortar preparation or curing regime leads to sealing of the chloride ingress pathways eliminating/lowering the reinforcement corrosion. The MICP in heterotrophic bacteria during aerobic oxidation occurs according to equations 2.4 to 2.9. This microbial metabolism consumes the oxygen necessary for reinforcement corrosion and the hydroxide ions important for expansive oxychlorides formation.

The high alkalinity of the mortar/concrete introduced during the bacteria MICP prevents the breakup of the passive film (De Belie and Wang, 2016). The carbonation of concrete/mortar accompanied by the presence of chloride ions lowers the alkalinity of pore water. Rasheeduzafar *et al.,* (2004), Dousti *et al.,* (2011), and Rao and Meena, (2017), observed the amount of free chloride decrease with increasing C_3A and the amount of bound chloride decreased with increasing OH^- concentration from the hydrated cement structures. Given this, the high corrosion of rebars exposed to chloride media can be assumed to be due to low alkalinity of pore solution (Venkateswara, *et al.*, 2011; Theodore and Karen, 2012; De Weerdt, *et al.*, 2016). Solutions with high Cl^{1-} concentration, may cause chemical attacks within the cement matrix which may lead to a drop in pore water pH and a disruption of the matrix (Wachira, 2012). This is due to the consumption of the sparingly soluble calcium hydroxide. $MgCl_2$ reacts with portlandite as shown in Equation 2.1.

$$MgCl_{2(aq)} + Ca(OH)_{2(s)} + 2H_2O_{(l)} \rightarrow CaCl_2.2H_2O_{(aq)} + Mg(OH)_{2(S)} \qquad 2.1$$

The chemical attack may lead to a drop in pore solution pH and a disruption of the cement matrix (Rasanen and Pentalla, 2004; Mutitu, *et al.*, 2014). The resultant pore solution may cause rebar pitting (Larbi, 1993; Muthengia, 2009; Dong, *et al.*, 2011). The consumption of $Ca(OH)_2$ by $MgCl_2$ may also cause interruption to the hydration process inhibiting the formation of the additional beneficial C-S-H crystals.

The damaging effect of cement by chloride ions is due to the formation of expansive oxychlorides from portlandite (Al-Mouldi, *et al.*, 2011). The C_4AF and C_3A are the cement phases attacked by the chlorides forming the expansive oxychlorides and Friedel's salt as shown in Equation 2.2 and 2.3:

$$2NaCl + Ca_4Al_2O_3.Fe_2O_3.6H_2O + Ca(OH)_2 + 4H_2O \rightarrow Ca_4Al_2O_3.Fe_2O_3.CaCl_2.10H_2O + 2NaOH \quad 2.2$$

$$2NaCl + Ca_3Al_2O_6.6H_2O + Ca(OH)_2 + 4H_2O \rightarrow 3CaO.Al_2O_3.CaCl_2.10H_2O + 2NaOH \quad 2.3$$

Incorporation of microorganisms in concrete/mortar leads to the formation of increased content of C-S-H and CAH gels and ettringite during the cement hydration process (Vijay, *et al.*, 2017). These gels seal the microbial mortar pore connectivity inhibiting the Cl^{1-} ingress. MICP precipitates in mortar hydrates, form cement compatible $CaCO_3$ further decreasing permeability. The imperviousness of the resultant concrete/mortar by the Cl^{1-} lowers the probability of the formation of the expansive oxychlorides hence no/limited internal cracks would be formed. This characteristic correlates with what was observed by Chahal *et al.*, (2012), Nosouhian *et al.*, (2016) and Karanja *et al.*, (2019) though involving varied types of *Bacillus species* bacteria.

2.2 Calcite Precipitating Bacteria

Microbiologically induced calcium carbonate precipitation (MICP) in a cement concrete/mortar is a complex mechanism (Chahal *et al.*, 2012). In nature, the $CaCO_3$ precipitation is accompanied by biological processes. The process can occur inside or outside the microbial cell or even some distance away within the concrete/mortar (Siddique and Chahal, 2011). Bacterial activities often trigger a change in solution chemistry that leads to over-saturation and mineral precipitation. Based on continuous

research, several innovations have been made from time to time to improve the strength and durability performance of biomineralized concrete/mortar (Douglas and Beveridge, 1998; Ramakrishnan, *et al.,* 2007; Mehta, 2011).

Microbiologically, calcium carbonate precipitation is assumed to be controlled by four key factors namely calcium ion concentration, the concentration of dissolved inorganic carbon (DIC), the pH and the availability of nucleation sites (Powers, 1958; Otsuki, *et al*., 2003; Patrick, *et al.*, 2012). $CaCO_3$ precipitation requires sufficient calcium and carbonate ions so that the ion activity product exceeds the solubility constant. The concentration of carbonate ions is related to the concentration of DIC and the pH of a given aquatic system (Patrick, *et al.*, 2012). The concentration of DIC depends on several environmental parameters such as temperature and the partial pressure of carbon (IV) oxide for systems exposed to the atmosphere (Damidot and Glasser, 1997; Castanier, *et al.,* 1999; Cook, 2006). Microorganisms can thus influence MICP either through one or a combination of the above-mentioned factors.

The presence of MICP in the cement concrete/mortar has been analyzed and reported that the crystallization of $CaCO_3$ is as vaterite (least stable), aragonite (metastable), calcite (most thermodynamically stable) (Stutzman and Clifton, 2015). The morphology and physico-chemical properties of the precipitate formed during induced bio-mineralization depend upon factors such as the initial supersaturation of ions in solution, type of organic matrix present, pH, and temperature (; Bang, *et al.*, 2010; Zhu and Dittrich, 2016; Botusharova, 2017). It has been reported that amorphous calcium carbonate can be seen in the early stages of precipitation by microorganisms. As growth and agglomeration of bacterial precipitates occur, they transform into more crystalline and stable forms, such as calcite (Castanier, *et al.,* 1999).

Although the cement concrete/mortar is relatively strong mechanically, it may exhibit low tensile strength, permeability to liquid and consequent corrosion of reinforcement, susceptibility to chemical attack, and low durability. Concrete/mortar is not usually expected to resist the direct tension due to its low tensile strength and brittleness, thus the

determination of its tensile strength is necessary to determine the load at which the cement concrete/mortar might crack (De Muynck, *et al.*, 2010; Jonkers, *et al.*, 2011). The presence of MICP in cement concrete/mortar has been observed to increase both the compressive strength and split tensile strength at varied bacterial cell concentration (Ghosh, *et al.*, 2009; De Muynck, *et al.*, 2010; Achal, *et al.*, 2013). The biodeposition treatment has also been attributed to increased resistance of cement concrete/mortar towards carbonation, chloride infiltration, and freezing–defrosting (De Muynck, *et al.*, 2010; Jonkers, *et al.*, 2011).

Pei *et al.*, (2013) and Sookie *et al.*, (2014) suggested that bacteria cell wall serves as nucleation sites for calcite precipitation in biochemical reactions. *Bacillus* species for example precipitate calcite which is highly insoluble around their cell wall which acts as a nucleation site, increasing the impermeability of the mortar/concrete in the bacterial environment. The bacteria cell walls act as a nucleation site by providing a growth-inducing environment where the calcium silicate hydrate (C–S–H) nucleation and growth appears to be due to the interactions between a filler surface and calcium ions in the pore solution.

2.3 Mechanism of microbe induced calcite precipitation

The healing agent can be introduced in the concrete/mortar matrix through a vascular network technique/immobilized or can be introduced directly during concrete/mortar preparation. The vascular technique has been said to be almost impractical on a large scale by most researchers for some three main shortcomings. Firstly, due to the inability of the healing agent to maintain constant viscosity throughout its lifespan in the concrete/mortar lifespan (Van Tittelboom and De Belie, 2013). Secondly, it would be difficult to distribute the vessels homogenously throughout the concrete/mortar matrix (Mostavi, *et al.*, 2015; Khaliq and Ehsan, 2016), and thirdly, the incorporated vessels in the mortar/concrete matrix may lead to structural delamination. It has thus by convention, been generally agreed that the introduction of the beneficial bacteria during mortar/concrete preparation is more effective in remediating and improving the physico-chemical and mechanical properties of the resultant mortar/concrete.

Some bacteria achieve MICP by the production of a urease enzyme. This enzyme uses urea as the main source of nitrogen, catalyzing the hydrolysis of urea into ammonium ion. This creates a micro-gradient concentration of carbonate and increases the pH at the site of cell attachment. This is achieved through multiple reactions leading to calcium carbonate precipitation.

MICP can also occur due to an increase in pH and production of carbonate by heterotrophic bacteria during aerobic oxidation of specific feed sources under alkaline conditions as shown in Equations 2.4 to 2.9.:

(I) Use of lactate.

$$CaC_6H_{10}O_6 + 6O_2 \rightarrow CaCO_3 + 5CO_2 + 5H_2O \quad 2.4$$

$$5CO_2 + 5Ca(OH)_2 \rightarrow 5CaCO_3 + 5H_2O \quad 2.5$$

(II) Use of acetate / Aerobic oxidation.

$$CH_3COO^{1-} + 2O_2 \rightarrow 2CO_2 + OH^{1-} + H_2O \quad 2.6$$

$$CO_2 + OH^{1-} \rightarrow HCO_3^{1-} \quad 2.7$$

$$HCO_3^{1-} + OH^{1-} \rightarrow CO_3^{2-} + H_2O \quad 2.8$$

$$Bacterial - Cell - Ca^{2+} + CO_3^{2-} \rightarrow Cell - CaCO_3 \quad 2.9$$

The biogenic CO_2 produced in equation 2.6 may also react with $Ca(OH)_2$ produced during the cement hydration process to form additional $CaCO_3$ (Thompson, *et al.*, 1997). This reaction is shown in Equation 2.10:

$$CO_2 + Ca(OH)_2 \rightarrow CaCO_3 + H_2O \quad 2.10$$

Bacterial denitrification process causes a localized pH rise due to the production of hydroxyl ions which initiates MICP without pH buffering (Arunachalan, *et al.*, 2010). The carbon (IV) oxide gas produced in the presence of rising pH produces the carbonate ion which when in contact with calcium ion results in MICP as shown by Equations 2.11 to 2.13.

(I) Dissimilatory nitrate reduction

$$\text{Organic compound} + aNO_3^{1-} + bH^{1+} \rightarrow cCO_2 + dH_2O + eN_2 \quad 2.11$$

$$CO_2 + 2OH^{1-} \rightarrow CO_3^{2-} + H_2O \quad 2.12$$

$$Ca^{2+} + CO_3^{2-} \rightarrow CaCO_3 \quad 2.13$$

(II) Dissimilatory sulphate reduction.

$$CaSO_4 + 2(CH_2O) \rightarrow CaS + 2CO_2 + 2H_2O \quad 2.14$$

$$CaS + 2H_2O \rightarrow Ca(OH)_2 + H_2S \quad 2.15$$

$$2CO_2 + 2H_2O \rightarrow 2H_2CO_3 \quad 2.16$$

$$Ca(OH)_2 + H_2CO_3 \rightarrow CaCO_3 + 2H_2O \quad 2.17$$

The dissimilatory sulphate reduction may not be a suitable concrete/mortar remediation process as it uses up gypsum as shown in equation 2.14 – 2.17. It may also produce acidic products hence deleterious to concrete/mortar. The sulphides formed reacts with available metal ions forming insoluble sulphides which clogs the pores in the cement matrix binding the particles together. This is beneficial in the short term as the compaction created by the formation of the sulphides is unstable as they can chemically or biologically be oxidized to sulphuric acid or sulphates under aerobic conditions. The formed acid or sulphates may internally attack the mortar/concrete (Alexander and Karen, 2012; Munyao, *et al.*, 2020).

Table 2.1 gives the details of the mechanism of precipitation of various bacteria, source of calcium nutrients, and mode of healing agent embedment into the mortar/concrete matrix. Ureolysis is the most studied pathway for MICP. This could be attributed to the fact that urea hydrolyzing microorganisms are abundant in nature. This makes the urea hydrolysis process common to soil worldwide (Mobley and Hausinger, 1989). Urease active producing microorganisms are known to induce MICP in the presence of urea and calcium ion (Cheng and Cord-Ruwish, 2013).

Table 2.1: Mechanism of MICP reactions

Mechanism of Precipitation	Microorganism	Nutrients	Embedment in Concrete / Mortar	Reference
Bacterial metabolic conversion of organic acid	*Bacillus pseudofirmus*	Calcium lactate, calcium glutamate, yeast extract, and peptone	Direct	Jonkers, *et al*., (2011)
	Bacillus pseudofirmus	Calcium lactate, calcium acetate, yeast extract, and peptone	Direct	
Ureolysis	*Bacillus sphaericus*	Urea, Calcium nitrate and yeast extract	Encapsulated	Wang, (2013)
	Bacillus sphaericus	Urea and Calcium chloride	Direct	Achal, *et al.*, (2013)
	Bacillus sphaericus	Urea, Calcium chloride, Calcium nitrate, and yeast extract	Encapsulated	Van Tittelboom & De Belie, (2013)
	Sporosarcina pasteurii,	Urea and Calcium Chloride	Direct	Park, *et al.,* (2010)
	Bacillus cereus,	Urea, Calcium chloride and nutrient broth	Direct	Maheswaran, *et al.*, (2014)
Denitrification	*Bacillus sphaericus*	Urea, Calcium formate, calcium nitrate, and yeast extract	Encapsulated	Ersan, *et al.,* (2015)

Ureolytic bacteria are also able to produce urease in the presence of urea causing the production of the carbonate ion necessary for the MICP process. These bacteria are also able to withstand relatively high pH levels compared to the pH of the mortar/concrete matrix without suppressing their microbial growth/processes. Most of the other abundant bacteria that are non-ureolytic suppress urease in the presence of ammonia and other nitrogen-containing compounds (Mobley and Hausinger, 1989).

2.3.1 Encapsulation of MICP microbes into cement mortar matrix

The introduction of a good protective capsule/carrier is necessary for achieving the desired MICP results. Numerous porous-expanded microbe protective carriers have been applied in sheltering self-healing bacteria. Xu *et al*., (2018) used ceramsite, Amiri *et al.,* (2018) applied expanded clay particles, Zhang *et al.,* (2017) incorporated expanded perlite particles while Wang *et al.,* 2014, employed diatomaceous earth. All these carriers were observed to prolong the survival life of the microbes inside the mortar/concrete matrix and consequently improved their self-healing capacity. However, in all the resultant self-healing mortar/concrete, there was a compromise on their mechanical properties as well as these carriers' incompatibility with mortar/concrete.

Liu *et al.,* (2020) used the low alkaline, more porous and high water absorption recycled aggregate derived from the condensation of natural aggregates and cement-based hydrates as the bacteria carrier. This carrier exhibited better mechanical properties than those used previously by other researchers (Xu, *et al.*, 2018; Liu, *et al.*, 2020). This improvement is attributed to the pozzolanicity reaction that this carrier undergoes forming additional cementitious products.

2.4 Portland Pozzolana Cement

Pozzolana material addition introduces fine particles into cement which physically decreases the void space in the cement matrix (Blanks and Kennedy, 1955; Sarsale, 1980; Muthengia, 2009; Jeffrey, *et al.*, 2012). The fine particles of pozzolana pack between the aggregates and cement grains thereby improving on the densification of the resultant

cement (Dousti, *et al.*, 2011; Mortureux, *et al.*, 2011; Cheng, *et al.*, 2013). The presence of pozzolana also provides pozzolanicity to concrete/mortar during the hydration process.

Pozzolana is blended with cement to amplify compressive strength and to enhance the durability of resultant concrete/mortar (Resheidat and Ghama, 1997; Otsuki, *et al.*, 2003; Cook, 2006). Ready-mixed concrete/mortar with compressive strength of nearly 135 Mpa (20,000 psi) has been produced in U. S. using silica fume as the pozzolana combined with other admixtures (Theodore and Karen, 2012; Cheng, *et al.*, 2013). In Kenya, concrete/mortar with compressive strength of 52.5 Mpa (7,778 psi) has been manufactured (KS EAS 18-1:2017) using natural volcanic tuff as the pozzolana. Silica fume and natural tuff, as pozzolana, enhances durability primarily by decreasing the permeability of concrete/mortar. With its reduced permeability (Dhir, *et al.*, 1996; Kawai, *et al.*, 2008), pozzolana concrete/mortar has been extensively used in reducing the permeability of chlorides into structures such as bridge decks, parking structures and marine structures (Holden, *et al.*, 1983; Dousti, *et al.*, 2011).

2.5 Bacterial Concrete/mortar

Bacterial concrete/mortar biologically produce calcium carbonate (limestone) to seal pores that appear within the concrete/mortar matrix or heal cracks that appear on the surface of concrete/mortar structures (De Muynck, *et al.,* 2010). Specific types of the bacteria genera such as *Bacillus* and *Lysinibacillus* along with a calcium-based nutrient known as calcium lactate/acetate, nitrogen, and phosphorus, are added to the ingredients of the concrete when it is being mixed (Bang, *et al.,* 2010). These self- healing agents can lie dormant within the concrete/mortar for up to 200 years (Stocks-Fischer, *et al.,* 1999; Ramakrishnan, *et al.,* 2007; Bang, *et al.,* 2010). However, when a concrete/mortar structure is damaged and water starts to seep through the cracks that appear in the concrete/mortar, the spores of the bacteria germinate on contact with the water and the nutrients. Once activated, the bacteria start to feed on the calcium-containing nutrient and consuming oxygen. The soluble calcium-containing nutrient is converted to insoluble calcium carbonate (Stocks-Fischer, *et al.,* 1999). The calcium carbonate solidifies on the cracked surface, thereby sealing it up.

2.5.1 Optimum conditions for biocementation

The concrete/mortar matrix has a pH range of between 11.5 and 13.5. pH levels may affect bacterial growth/survival. The pH is conducive for the degradation of organic compounds into carbon (IV) oxide and water through the action of MICP bacteria. Sahoo *et al.,* (2016) observed that due to the high pH of the mortar/concrete matrix, bacterial cells grow slowly at the initial curing period as they accustom themselves to the new high pH environment. If the pH media is beyond what a given bacteria can withstand, the bacteria either die or turn into an endospore. Sookie *et al.*, (2014), tested the effect of pH on the bacterial growth. In their studies, they used both *Sporosarcina pasteurii* and *Bacillus sphaericus* and exposed them to nutrients with a pH range of 4 – 12. They found out that *Sporosarcina pasteurii* had optimum growth in the pH range of 7.0 – 9.0 while *Bacillus sphaericus* optimum growth was at the pH range of 8.0 – 9.0. Cheng, *et al.*, (2013) cultured both *Bacillus cereus* and *Bacillus sphaericus* in Luria Bertani broth at the pH range of 8.0 – 12.5 both at 37 °C and 50 °C for 24 hours. They found out that *Bacillus cereus* did not survive above pH 9.0 while *Bacillus sphaericus* survived in the media in the pH range of 8.0 – 12.5 both at 37 °C and 50 °C and thus suitable for fresh mortar/concrete with pH of about 11.5 – 12.5 and the temperature of 37.0 – 50.0 °C. Sahoo *et al.,* (2016) on culturing *Bacillus megaterium*, found out that the maximum pH was 8.9 at both 37 °C and 50 °C after 24 hours of curing till 120 hours. Schwantes-Cezaro *et al.*, (2019) in their work observed that the optimum pH for *Bacillus subtilis* in the phosphate-buffered nutrient media is 9.0. Arunachalan *et al.*, (2010) in their work observed that the optimum pH for urease enzyme is in the range of 7.5 – 8.0. They further found that the urease activity increased gradually from pH 6.0 to 8.0. However, the pH of the reactant medium was found to increase gradually during the urea hydrolysis due to the production of ammonia. Carbon (IV) oxide, produced during microbial respiration, acts as a buffer to the pH change. The influence of pH on MICP is complex because it affects various processes such as microbial activity, urease activity, and calcite solubility. The initial pH medium increases during the precipitation for all MICP bacterial species, thus changing the environment for optimum precipitation. Various species of MICP-forming bacteria adapt to a given pH range to optimize calcite precipitation with an alkaline media being favourable to the process.

The microbial activity and growth are less sensitive to the temperature within the range of 20 – 30 °C. The rate of urea hydrolysis is insignificantly higher at 30 °C as compared to 20 °C. An increase in temperature beyond 30 °C does not promote the decomposition rate of urea (Dhami, *et al.*, 2012). Temperatures mainly vary with latitude, altitude, incident solar radiation, moisture content, conduction, the thickness of the structure among other factors. In terms of urease enzyme, Dhami *et al.,* (2012), while studying the effect of temperature on urease activity of *Bacillus megaterium* found out that the activity increased with increasing temperature from 10 °C and reached an optimum at 60 °C. Urease activity was inhibited above 100 °C. Dhami *et al.*, (2012) findings were consistent with the findings of both Arunachalan *et al.*, (2010) and Cheng *et al.*, (2011). The optimum temperature for bacterial activity is different from the optimum temperature for calcite precipitation. Urease was found to be active at temperatures between 10 °C and 60 °C, with the urease activity being at its peak at 60 °C, while calcite precipitation increased between 20 °C and 30 °C with calcite precipitation being at its peak at 30 °C. In the temperature range of 30 – 50 °C, there is a significant decrease in calcite precipitation, with the least precipitation observed at 50 °C. Perhaps there is no direct correlation between temperature and MICP deposits since calcite solubility decreases with an increase in temperature, thus affecting calcite precipitation.

The source of calcium ion during biocementation dictates the type of crystal formed, the size, morphology, and the degree of crystallization. Numerous studies have reported the use of 3 g/l of nutrient broth, with different chemicals for different bacteria species into the treatment solution to sustain the growth and viability of urease producing bacteria (Van Tittelboom and De Belie, 2013; Maheshwaran, *et al.*, 2014). The supply of nutrients is to ensure the bacteria can subsist long enough to support MICP to achieve the desired structural performance. Several studies have illustrated that these bacteria form thick membrane spores, which can survive without nutrients for up to 200 years (Van Tittelboom and De Belie, 2013). The endospores are also postulated to be able to remain dormant and be able to withstand environmental changes, chemicals, ultraviolet radiation as well as mechanical stresses for hundreds of years (Jonkers, *et al.*, 2011; Van Tittelboom and De Belie, 2013). The supply of enough, appropriate, and sufficient

nutrients to bacteria ensures that they get the energy sources that can initiate their growth from the endospores and sustain them long enough. The concentration of nutrients and their salinity influences the MICP process. High salinity has an inhibitory effect on microbial activity and MICP. The urease enzyme, supplied directly into the mortar/concrete or produced by the incorporated bacteria, decompose urea through a chemical reaction known as hydrolysis of urea as shown in Equation 2.18:

$$CO(NH_2)_2 + 2H_2O \xrightarrow{\text{urease}} 2NH_4^+ + CO_3^{2-} \qquad 2.18$$

The ammonium ions released from urea hydrolysis results in local pH rise and commences the MICP process. The high pH at a localized area increases the tendency for the bacteria cell wall to act as a nucleation site for calcite precipitation. Calcite precipitation is through the combination of carbonate ion (CO_3^{2-}) from the hydrolysis of urea and the calcium ion (Ca^{2+}) from calcium supplied from a soluble calcium salt or the bacteria cell wall. The calcite precipitated is responsible for the biocementation of mortar/concrete.

The bacteria cell wall acts as the nucleation site and also influences the type of biomineral to be precipitated. Hammad, *et al.*, (2013) and Karanja, *et al.*, (2019) reported that urease activity affects the chemical process associated with the formation of biominerals through four different factors; pH, dissolved inorganic carbon (DIC) concentrations, calcium concentrations and the availability of nucleation sites. The first three parameters influence the CO_3^{2-} concentration while the last factor promotes stable and continuous $CaCO_3$ formation (Stocks-Fischer, *et al.*, 1999; Vijay and Murmu, 2018).

2.6 Ingress ion Profile Analysis

Chloride and sulphate profiling is widely used for the analysis of chloride/sulphate ions concentration, whether they are free (water-soluble), bound (acid-soluble) or both versus depth of ingress into cement mortar or concrete (Suryavanshi, *et al.,* 1996; Muthengia, 2009; Mutitu, 2013). The ingress ion profile is used to monitor the extent of ion ingress as well as ion diffusivity into concrete/ mortar (Yang and Cho, 2003). The methods of analysis of the ingress ion from the extracts vary from laboratory to laboratory depending

on the availability of facilities and the ion under analysis. Some of the common analytical techniques for chloride ion analysis include chloride analyzer (Atkins *et al.,* 1996; Suryavanshi, *et al.,* 1996), potentiometric titration, chloride ion-selective electrode, inductively coupled plasma spectroscopy and colour based titrations (Golterman, 1978; Bertolini, *et al.,* 2004).

The majority of the researchers have used a Rapid chloride permeability test to investigate chloride ion ingress. Chahal *et al.*, (2012) on using *Sporosarcina pasteurii* bacterial concrete observed 380 coulombs chloride penetration as compared with their control concrete which allowed 762 coulombs penetration. Nosouhian *et al.*, (2016) in their work observed the reduced chloride ion penetration in their concrete containing *Sporosarcina pasteurii* and *Bacillus subtilis* bacteria and fly ash separately compared with concrete without bacteria. Siddique *et al.*, (2016) on using *Bacillus aerius* bacterial cells in their work, noted reduced total charge passed through their bacterial concrete by 55.8 %, 49.9 %, and 48.4 % compared to the control concrete at the curing age of 7, 14, and 56 days respectively. Maes and De Belie (2016) focused on using encapsulated polyurethane with concrete containing-induced cracks of 100 and 300 mm. They observed 83 % and 67 % decrease in chloride ingress on the exposure of the cracks to encapsulated polyurethane followed by the chloride ingress. The same researchers also observed that autonomous healing can seal crack widths of 100 and 300 mm for chloride penetration in 67 % and 33 % of the cases respectively.

Therefore, there is a significant reduction in chloride ion permeability in bacterial concrete/mortar for all *Bacillus* species considered. This could imply that the service life of concrete/mortar structures exposed to aggressive ions is well defined by the ability of the concrete/mortar to resist the penetration of either chloride ions or sulphate ions.

2.7 Water permeability

Permeability of concrete/mortar depends on the pore network of cementitious material. Permeability is thus an important property for the ingress of substances that may cause

degradation of concrete/mortar. Permeability is considered to be a fundamental property for portraying the durability of cement concrete/mortar.

Chahal and Siddique, (2012) and Chindara, *et al.*, (2014) in their work, observed a decrease in water permeability in their concrete containing *Sporosarcina pasteurii* bacteria and fly ash compared with concrete without the bacterial content. Achal *et al.,* (2013) cast cubes with the addition of *Bacillus megaterium* and its nutrients. They observed water absorption reduction of more than three times in the bacterial concrete than in the control one. Siddique *et al.,* (2016) added *Bacillus aeris* in concrete and observed a reduction in water absorption. All these studies attributed the decrease in water permeability and porosity in the bacterial concrete to calcium carbonate precipitation within the cured concrete pores. Several researchers have investigated the effect of MICP on water permeability and porosity. A comparative summary involving different bacteria after 28 days of curing and their results are summarized in Table 2.2.

Table 2.2: Water absorption by varied bacterial concrete samples after 28 days of curing

Bacteria	Water absorption after 28 days of curing	Author
Bacillus sphaericus	45 – 50 % less than the controlled concrete sample	De Muynck *et al.*, (2010); Achal V. *et al.,* (2013); Majunathan *et al.*, (2014)
Bacillus subtilis	Nearly 50 % less than the controlled concrete sample	Reddy *et al.*, (2013); Muhammad *et al.*, (2014); Pei *et al.*, (2013)
Bacillus megaterium	46 % less than the controlled concrete sample	Dhami *et al.*, (2012)
Sporosarcina pasteurii	50 – 70 % less than the controlled concrete sample	Achal *et al.*, (2013); Pei *et al.*, (2013); Chindara *et al.*, (2014)
Bacillus cohnii	Nearly 35 % less than the controlled concrete sample	Sierra-Betran *et al.*, (2014)
Bacillus flexus	Nearly 40 % less than the controlled concrete sample	Kumar-Jagdeesha *et al.*, (2013)
Bacillus pseudofirmus	50 % less than the controlled concrete sample	De Muynck *et al.*, (2010); Maheshwaran, (2014)

From the studies it is evident that bacterial concrete/mortar has a higher water permeability resistance than control concrete/mortar regardless of the species of *Bacillus* used. Amongst all the *Bacillus* species used, the water porosity reduced by between 35 % and 50 %, except for *Sporosarcina pasteurii* where the reduction was up to 70 %. All these studies attributed a decrease in water permeability and porosity in the bacterial concrete to calcium carbonate precipitation within the cured concrete pores.

2.8 Powder X-Ray Diffraction (XRD) Analysis

X-ray spectroscopic analysis is utilized in studying the crystallinity of the precipitated compound as well as in determining the mineralogical composition of the precipitate. In MICP, calcium carbonate precipitated exists in calcite, aragonite, and vaterite polymorphic forms depending on the type of nutrient and species of bacteria used. The most stable and least soluble form is calcite (Liu, *et al.*, 2015). XRD is used to characterize the material by analyzing the crystal structure, and comparing it against a database of known structures (Artioli, *et al.*, 2015; Bossa, *et al.*, 2015). In previous studies, XRD analysis has mainly been used to either establish the polymorphic form of $CaCO_3$ precipitated or to determine the formation of additional C-S-H crystal. This technique can provide phase, grain size, and texture, and percent crystallinity information about a material (Jupe, *et al.*, 2012). Currently, most XRD is coupled with Energy Dispersive X-Ray Analyser (EDX). EDX usually determines the chemical identification of elements and their concentration.

2.9 Fourier Transform-Infrared (FT-IR) Analysis

The spectroscopic FT-IR method has several advantages in analyzing cementitious materials. Some of the major advantages associated with this technique include the use of a little amount of the sample (Horgnies, *et al.,* 2013). It is a rapid analytical technique analyzing samples within minutes and with a simplified sampling protocol (Del Bosque, *et al.*, 2014). One of the novelties of this technique in studying cementitious materials is its ability to utilize ATR to detect both organic functional groups, hydrated cement phase functional groups, and calcite which effloresces at the surface of hardened

concrete/mortar. It also displays unique spectral peaks/deeps at an interface between the hydrated cement compounds and any admixture in the matrix (Horgnies, *et al.,* 2013; Chollet and Horgnies, 2011). However, its two major drawbacks are its inability to provide quantification interpretation and specificity to certain compounds. To use an IR spectrum table, first find the frequency or compound in the first column, depending on which type of chart you are using. Then find the corresponding values for absorption band wavelength. Table 2.3 summarizes the band wavelengths of the most common hydrated cement functional groups.

Table 2.3: FT-IR detectable bands of the hydrated cement functional groups/phases.

		Wave-number (cm^{-1})						
	Phase	O-H	O-H (from H_2O)	Si-O (Ass. Stretching)	Si-O	Al-O	Si-O (in-plane)	C-O, CO_3^{2-}
Main Hydrated phases	C-S-H (Ca/Si = 1.5)		3356, 1640	1000, 950	950		667, 496	
	Portlandite, $Ca(OH)_2$	3642						
Clinker phases	Ca_3SiO_5, C_3S			935 - 883			522	
	Ca_2SiO_4, C_2S			995 - 900			518	
	$Ca_3Al_2O_6$, C_3A					898, 786, 740, 704, 521	456	
Aluminate (Aft/AFm) phases	Ettringite, $Ca_6Al_2(SO_4)_3(OH)_{12}.26H_2O$	3637	3431, 1680-1640			857, 537		
	Monosulphoaluminate $Ca_4Al_2(SO_4)(OH)_{12}.6H_2O$	3672, 3549	3423, 1650			579, 525		1380
Polyamide								2510, 1420, 872, 710

Source: Hydrated cement functional groups modified from Horgnies *et al.*, 2013, Materials Characterization VI, Lafarge, France.

CHAPTER THREE

MATERIALS AND METHODS

3.1 Sampling and Preparation of test materials

3.1.1 Sampling and Preparation of test Cement and Standard sand

Materials were sampled from their respective areas; Savannah Cement Ltd. Company OPC and PPC were sampled from appointed distributors in Thika Town (1.0388°S, 37.0834°E), Kitengela Township (1.4758°S, 36.9570°E) and Nairobi City (1.2921°S, 36.8219°E) in Kenya. For each cement category, chemical analysis was done in accordance with KS EAS 18-1: 2017. Fifty kilograms (50 kg) cement was bought from the appointed distributors in the three towns respectively. Some ten kilograms (10kg) of each cement category were then mixed thoroughly to make a thirty kilogram (30 kg) sample in each cement category. The cement used to prepare the mortar/paste per cement category was obtained from the thirty kilograms (30 kg) sample. ISO standard sand conforming to EN 196 – 1: 2016 was obtained from Savannah Cement Ltd company, Kitengela, (1.4758°S, 36.9570°E), Kenya.

3.1.2 Analytical Reagents

In this chapter, whenever water is mentioned, it refers to distilled water unless specified. De-ionized water was used as the solvent for the laboratory preparation of aggressive ion solutions including their requisite dilution where necessary. Distilled water was used for rinsing the apparatus. Analytical grade chemicals were used in the preparation of the solution. Glassware and plastic containers were washed with a suitable detergent using tap running water, rinsed with distilled water, and dried appropriately.

3.1.3 Preparation of microbial culture solution

Microbial cultures were obtained from Leibniz DSMZ – Deutsche Sammlung von Mikroorganismen und Zellkulturen GmbH culture collection, Germany. Bacterial cultures were grown in accordance with BS EN 12322 (1999). One thousand milliliters or One Litre (1000 ml/1L) broth medium were prepared for each bacterial strain in

accordance with each bacterial species nutrient and media preparation procedure to obtain a microbial solution with optical density (OD) at 600 nm of 1.0 OD in the UV/VIS Spectrometer. The different bacterial solutions were kept separately for 120 hours (5 days) to ensure a stable pH state was achieved.

A freeze-dried culture of *Sporosarcina pasteurii* was obtained from DSMZ culture collection Germany (DSM 33) and revived using protocols supplied with the microbial culture. The medium used for culturing contained 30 g Tryptone Soya Agar (Bacto) and 20 g urea (filter sterilized) per litre of deionized water. Flasks containing bacterial solutions were placed in a Stuart BJPX-200B orbital shaking incubator at 150 rpm for 24 hours. Test cultures were obtained after the OD had reached 1.0. For the induction of calcium carbonate precipitation, the bacteria were re-suspended in a medium (referred to as "cementation medium" in this work) which contained 30 g Oxoid Cm131 nutrient broth, 15 g peptone from casein, 5 g peptone from soymeal, 5 g NaCl, 7.35 g $CaCl_2.2H_2O$, 20 g urea (filter sterilized) and 10 mg $MnSO_4.2H_2O$ per litre of deionized. The medium pH was adjusted to 7.3. This medium preparation procedure was adopted from De Jong *et al.,* (2006), DSMZ GmbH (2007). Before utilizing the strain in experiments the cultures were pelleted by centrifuging at a relative centrifugal force (RCF) of 3200 for between 20 to 25 min in a Heraeus Varifuge 3.0 Centrifuge (Heraeus GmbH; Wehrheim, Germany). The supernatant was discarded and exchanged with the same volume of phosphate-buffered saline (PBS) which contained 8 g NaCl, 1.42 g Na_2HPO_4, and 0.24 g KH_2PO_4 per litre of deionized water: with a pH of 7.2.

Bacillus megaterium was grown in Luria-Bertani medium which contained 10 g tryptone, 5 g yeast extract, 5 g NaCl, 4.2 g $NaHCO_3$, and 5.3 g Na_2CO_3 per litre of deionized water. The last two components were added by filter sterilization after autoclaving. The pH of the medium was adjusted to 9.7. The modified medium used for calcium carbonate precipitation contained 4 g yeast extract and 10 g dextrose, 2.5 g calcium acetate per litre of deionized water, with pH adjusted to 9 (Boquet, *et al.,* 1973). Induction of sporulation in *Bacillus megaterium* was achieved through a highly alkaline mineral medium which contained 0.1g yeast extract, 0.2 g NH_4Cl, 0.02 g KH_2PO_4, 0.225 g $CaCl_2$, 0.2 g KCl, 0.2

g $MgCl_2.6H_2O$, 0.01 g $MnSO_4.2H_2O$, 1 ml trace element Solution SL12B, 5.16 g citric acid trisodium Salt, 4.2 g $NaHCO_3$ and 5.3 g Na_2CO_3 per litre of deionized water with a pH was close to 10 (Jonkers, *et al.,* 2011).

Lysinibacillus sphaericus liquid medium chosen for culturing the bacteria consisted of 5.00 g of peptone added to 3.00 g of meat extract, 10 mg $MnSO_4.2H_2O$, and 3.95 g of calcium acetate per liter of distilled water. This mixture was sterilized for 20 minutes at a temperature of 121 °C by autoclaving. After cooling, a sterile 1M Na-sesquicarbonate solution (1.0 ml in 10.0 ml) prepared by mixing 4.2 g $NaHCO_3$ with 5.3 g anhydrous Na_2CO_3 and made up-to 1 liter using distilled water was added to the stock culture to achieve a pH of 9.7.

3.1.4 Assesment of bacterial growth

A spectrophotometric method for the determination of cell concentrations in bacterial cultures was used. Optical density was determined by placing 1 ml of the solution under test in optical polystyrene (PS), 1.6 ml cuvette before recording the optical density (light absorbance) of the specimen at a wavelength of 600 nm in a Hitachi UV-1900 UV-visible wavelength spectrophotometer. OD – 600 nm measurements were used to assess bacterial growth, to determine cell numbers at the onset of experiments, and to construct growth curves of bacteria. This microbial culture concentration was maintained throughout the mortar samples preparation as well as in prism curing solution.

3.2 Cement Chemical Analysis

In this study, the Ordinary Portland Cement (OPC 42N) and the Portland Pozzolana Cement (PPC 32.5N), used were tested according to Kenyan Cement Standards specifications, KS EAS 18 - 1: 2017. The standard sand manufactured according to ISO EN 196 – 1 (2016) was used. Test cement sample weighing 100 g was ground to pass through a 76 μm mesh sieve. The ground sample was used for chemical analysis of cement oxides using X-ray fluorescence in the usual manner (KS EAS 18 – 1 (2017).

Loss on Ignition was done in accordance with ASTM D7348: 2013. Raw experimental data is represented in Appendix A, Table A1.

3.3 Fresh Paste Tests preparation

Two categories of fresh cement paste tests; normal consistency, soundness, and setting time were separately prepared. The first category of the cement paste both for OPC and PPC was prepared using distilled water as the mix media and was labeled OPC (H) and PPC (H) respectively. The second category for each cement of fresh cement paste was prepared using the microbial solution as the mix media across the three bacteria under study; *Lysinibacillus sphaericus, Sporosarcina pasteurii* and *Bacillus megaterium* separately and were labeled as OPC (LB), OPC (BP) and OPC (BM) for OPC cement and PPC (LB), PPC (BP) and PPC (BM) for PPC cement respectively.

Normal Consistency test required a cement paste for OPC (H) weighing 300.0 g prepared in accordance with IS 4031 – 4:1988. Standard consistency was calculated using Equation 3.1.

$$\text{Standard Consistency}\,(\%) = \frac{\text{Weight of water added}}{\text{Weight of cement}} \times 100 \qquad 3.1$$

The weight of water added for OPC (H) fresh cement paste refers to the weight of distilled water used. A cement paste for PPC (H) weighing 300.0g was prepared similarly as OPC (H) and the same procedure for determining the standard consistency repeated. For OPC fresh cement paste prepared using the microbial solution of *Lysinibacillus sphaericus*, it was labeled as OPC (LB). In this microbial fresh cement paste category, the weight of water added refers to the weight of microbial solution used to make the microbial fresh cement paste. Across all other bacterial cement pastes for both OPC and PPC, the weight of water added refers to their separate respective microbial solutions. The cement paste samples were labeled as OPC (BP) and OPC (BM) for OPC cement pastes prepared using the microbial solution of *Sporosarcina pasteurii* and *Bacillus megaterium* respectively. The cement samples prepared with PPC using the microbial solution from *Lysinibacillus sphaericus*, *Sporosarcina pasteurii,* and *Bacillus megaterium* were labeled as PPC (LB), PPC (BP) and PPC (BM) respectively.

Normal consistency tests in this study were performed on three samples per category for obtaining average results.

The soundness test was done in accordance with KS EAS 148 – 3: 2017. A lightly oiled mould was placed on a lightly oiled glass sheet and filled with mortar paste formed by gauging cement with 0.78 times the distilled water to prepare OPC (H) fresh cement paste. The same procedure was repeated using PPC fresh cement paste in place of OPC to prepare PPC (H). The same procedure was repeated but now with 0.78 times of the microbial solution instead of distilled water for both OPC and PPC and labeled OPC (LB), OPC (BP) and OPC (BM) for OPC fresh cement paste and PPC (LB), PPC (BP) and PPC (BM) for PPC fresh cement paste to give a paste of standard consistency for each cement paste category (IS 4031 – 4 (1988), KS EAS 148 – 3 (2017). A similar test was repeated on three fresh cement pastes samples per category to obtain averages.

The Initial Setting time fresh sample of cement paste for each category was prepared in accordance with KS EAS 148 - 3: 2017. This test was done across all fresh cement pastes under study; OPC (H), PPC (H), OPC (LB), OPC (BP), OPC (BM), PPC (LB), PPC (BP) and PPC (BM). Initial setting time tests in this study were performed on three samples per cement paste category for obtaining average results (Elvira, 2012).

Final Setting time for a fresh sample of cement paste for each category was prepared in accordance with KS EAS 148-3: 2017. This test was done across all test fresh cement pastes under study; OPC (H), PPC (H), OPC (LB), OPC (BP), OPC (BM), PPC (LB), PPC (BP) and PPC (BM). Final setting time tests in this study were performed on three samples per cement paste category for obtaining average results (Elvira, 2012). Raw experimental data is represented in Appendix A, Table A3.

3.4 Mortar Preparation and Curing

Mortar mix prisms were fabricated according to KS EAS 18 - 1: 2017. Four hundred and fifty grams (450 g) of the cement was placed in the mixing basin of an automatic programmable mixer model number JJ-5. Two hundred and twenty five mililitres (225.0

ml) of distilled water or 225.0 ml of bacterial solution were added to make a 0.5 w/c ratio mortar of blank and bacterial respectively. The mix basin and its contents were clamped onto the automatic programmable mixer and allowed to run for three minutes. 1350 ± 5 g of the standard sand was placed in an automatic pour-trough little by little until all 1350 ± 5 g sample was added while the mixer was still running at a speed of 30 revolutions per minute (rpm). The machine was let to run for ten minutes. The mortar prepared had a w/c ratio of 0.5. The mortar was used to prepare three mortar prisms as follows; Once the mortar was mixed, it was poured into steel moulds of 40 mm x 40 mm x 160 mm. Using a trowel, the mortar paste was scooped from the automatic programmable mixing basin and placed in a compaction mould of a jolting compaction machine which was set to run at 60 rpm vibrations for 2 minutes. Leveling of the paste was done with a mould trowel in each of the three chambers of the mould after every jolting cycle until a good finish was achieved at the surface. The mould with the mortar paste was then placed in a humid chamber maintained at 95 % humidity at 27.0 °C for 24 hours. The mortar was then demoulded from the moulds after 24 hours. The distilled-water prepared mortars were categorized into two depending on their subsequent curing regime: The first category of the OPC mortar prepared and was to be cured in distilled water was labeled as OPC-H (H). The second category, prepared using distilled water but was to be cured in *Lysinibacillus sphaericus* microbial solution was labeled as OPC-H (LB). The above procedure was repeated but this time using 225 ml of *Lysinibacillus sphaericus* microbial solution as mix media instead of distilled water which resulted to the third and fourth categories.

The third category was the OPC mortar prepared using the microbial solution and cured in distilled water, labeled as OPC-LB (H), while the fourth category was the OPC mortar prepared using the microbial solution and cured in microbial solution, labeled as OPC-LB (LB). The mortars were labeled for identification and placed in requisite water or microbial solution for curing in a chamber maintained at 27 ± 1 °C for curing. The same procedure for preparing OPC mortar categories two, three, and four were repeated with the other two bacteria. *Sporosarcina pasteurii* (BP) mortars for categories two, three, and four were labeled as OPC-H (BP), OPC-BP (H), and OPC-BP (BP) respectively.

Similarly, for *Bacillus megaterium* (BM) mortars for categories two, three, and four were labeled as OPC-H (BM), OPC-BM (H), and OPC-BM (BM) respectively.

The same procedure used to prepare OPC mortars was repeated to prepare PPC mortars across the three bacteria under investigation. The mortars obtained were labeled accordingly to obtain; PPC-H (H) category one mortars. On using *Lysinibacillus sphaericus* (LB) bacteria, mortars in category two, three, and four were labeled as PPC-H (LB), PPC-LB (H), and PPC-LB (LB) respectively. On using *Sporosarcina pasteurii* (BP) bacteria, mortars in category two, three, and four were labeled as PPC-H (BP), PPC-BP (H), and PPC-BP (BP) respectively. On using *Bacillus megaterium* (BM) bacteria, mortars in category two, three, and four were labeled as PPC-H (BM), PPC-BM (H), and PPC-BM (BM) respectively.

3.5 Scanning Electron Microscopy

Dried and powdered calcium carbonate, produced by bacteria, was visualized by a dual-beam Scanning Electron Microscope (SEM) model XB1540 (Carl Zeiss, Germany). Samples were coated with Au/Pd (80/20) using a sputter coater (Agar Scientific, Stansted, UK). The scanning electron micrographs of bacterial and control mortars were taken with an energy dispersive X-ray analyzer (EDAX) at the accelerating voltage of 200 V to 30 kV. The samples were subjected to the SEM usual manner for surface analysis.

3.6 Powder X-Ray Diffraction

The mineralogy of the newly formed cement hydration/bacterial material was determined using an X-Ray Diffraction (XRD) Instrument PW1710 Phillips. Prior to running the XRD analysis samples were oven-dried at 100 ºC and powdered with a mortar and pestle, they were then placed in a zero-background silicon sample holders. The goniometer was calibrated using a silicon standard. Samples were analyzed using PANalytical software, with goniometer start and end angles at 5.00 and 80.00 2 ºTheta, step size of 0.020 2 ºTheta, and scan step time of 0.5 second at an adjusted current and voltage of 40 mA and 35 kV respectively. The samples' functional groups were identified by comparing the X-

ray profile of the samples with standards established by the International Center for Diffraction Data. Raw experimental data are represented in Appendix A, Table A7, and Table A8.

3.7 Fourier Transform-Infrared Spectroscopy (FT-IR)

FT-IR spectroscopy is one of the powerful techniques normally used for molecular characterization. Recently, FT-IR has been found to be very useful in delineating the complex chemistry involved in the hydration of cement. In particular, the FT-IR results have been used to resolve the hydroxyl bands, in understanding the degree of silicate polymerization occurring, and in monitoring the dynamics of changes during hydration reactions.

3.8 Determination of Compressive Strength

Compressive strength was done in accordance with KS EAS 148 – 1: 2017. Compressive strength for non-bacterial mortars and bacterial-mortars for both OPC and PPC were determined using a Compressive Strength Machine at the 2^{nd}, 7^{th}, 14^{th}, 28^{th}, and 56^{th} day of curing. The compressive strength machine model YAW-300 was used.
The machine was started and run at 5000 psi/min.

The percent compressive strength gain for each OPC microbial mortar at a given curing age was determined using Equation 3.2:

$$n^{th}\,\text{day};\ \%\,\text{C.S.gain} = \frac{(\text{C.S.}_{\text{BOM}}) - (\text{C.S.}_{\text{NOM}})}{\text{C.S.}_{\text{NOM}}} \times 100 \qquad 3.2$$

where n^{th} day is the duration the mortar had cured; in this study, n was at 14^{th}, 28^{th} or 56^{th} day), % C.S. gain is the calculated percent gain in compressive strength; C.S._{BOM} refers to the compressive strength of the bacterial treated OPC mortar while C.S._{NOM} is the compressive strength of the OPC mortar without bacterial treatment.

The percent compressive strength gain for PPC mortar categories used the same equation

as equation 3.2 where the OPC mortar was replaced by PPC mortar categories. Raw experimental data is represented in Appendix A, Table A5.

3.9 Determination of Flexural Strength

Flexural strength is a measure of an unreinforced concrete/mortar beam or slab to resist failure in bending. Flexural strength is expressed as Modulus of Rupture (MR) in MPa. Flexural strength for control mortars and the three bacteria under study bacterial-mortars for both OPC and PPC was determined using ASTM C293:1990 (Walker and Bloem, 1994), Centre-Point Loading method at the 2^{nd}, 7^{th}, 14^{th}, 28^{th} and 56^{th} day of curing. The flexural strength machine model UTC - 5502 was used.

The percent flexural strength gain for each OPC microbial mortar at a given curing age was determined using Equation 3.3:

$$n^{th}\ \text{day};\ \%\ \text{F.S.gain} = \frac{(\text{F.S.}_{\text{BOM}}) - (\text{F.S.}_{\text{NOM}})}{\text{F.S.}_{\text{NOM}}} \times 100 \qquad 3.3$$

where the n^{th} day is the duration the mortar had cured; in this study, n was at 14^{th}, 28^{th} or 56^{th} day; % F.S. gain is the calculated percent gain in flexural strength; F.S._{BOM} refers to the flexural strength of the bacterial treated OPC mortar while F.S._{NOM} is the flexural strength of the OPC mortar without bacterial treatment.

The percent flexural strength gain for PPC mortar categories used the same equation as equation 3.4 where the OPC mortar was replaced by PPC mortar categories. Raw experimental data is represented in Appendix A, Table A6.

3.10 Sorptivity test

Sorptivity test was carried out following the method prescribed by Achal *et al.,* (2013) on all the mortar categories across the three bacteria under study. To calculate the sorptivity coefficient, the 28^{th} day cured mortar prism was dried at 100 °C in a ventilated oven. The mortar prism was coated with two layers of waterproof resin of ISO 0081 at all outer

surfaces except top and bottom-base to ensure unidirectional absorption through the non treated side only. Water was placed into a beaker up to a height of 50 mm. The mortar prism was then submerged with the non-coated side facing downward at 2 mm above the bottom base of the mortar prism as shown in Figure 3.1. Raw experimental data is represented in Appendix D, Table D6.

(a) (b)

Figure 3.1: Water Sorptivity test Set-up (a) OPC-BP (BP) Mortar, (b) Varied OPC Mortars

After each time intervals (0.25 hr., 0.5 hr., 1 hr, 1.5 hrs., 3 hrs., 5 hrs., 8 hrs., 24 hrs., 72 hrs., 96 hrs., 120 hrs., 144 hrs., and 168 hrs.), the mortar prisms were removed from the water and weighed after drying the surface with a clean wet towel. Immediately after the measurement, the mortar prism was re-submerged again into water and the new weight taken after a given time interval. This was continued, to obtain a saturated weight of water of infiltration. The sorptivity coefficient (k) was obtained by using Equation 3.4:

$$\frac{Q}{A} = kt^{1/2} \qquad 3.4$$

where Q is the amount of water absorbed, A is the cross-section of the specimen that is in contact with water and t is time. On plotting a graph of Q/A against the square root of

time, values of k were determined graphically. Varied graphical Sorptivity coefficients are represented in Appendix B, Figure B7 to Figure B16.

The percent water sorption gain at each interval across all test mortars was determined using Equation 3.5:

$$\%\ H_S gain\ = \frac{(W_{iS}) - (W_{BS})}{W_{BS}} \times 100 \qquad 3.5$$

where % H_S gain is the calculated percent water sorption gain of the mortar; W_{nS} is the weight of the mortar prism after the i^{th} interval of immersion into water, where i in this study ranged from 15 minutes to 168 hours; W_{BS} is the weight of the prism before immersion into water.

The percent water sorption drop for the mortars was determined by using Equation 3.6:

$$\%\ H_S drop\ = \frac{(W_{nS}) - (W_{BS})}{W_{BS}} \times 100 \qquad 3.6$$

where % H_S drop is the calculated percent water sorption drop of the mortar; W_{nS} is the weight of the mortar prism after the n^{th} duration of immersion into water, where n in this study was 120 hours while W_{BS} is the weight of the prism before immersion into water.

3.11 Ion Diffusing Test

Diffusing test was done in accordance with ASTM C1556 (2004) and EN 196-21 (2001) on all the mortar categories from both OPC and PPC, across the three bacteria species under study. The cement mortar prism cured for 28 days was reduced to 100 mm length using a cutting machine. The mortar specimen was then placed between two cells and covered with a fabric material. The anodic compartment was filled with 500 ml of water. An equal volume of 3.5 % NaCl or Na_2SO_4 was placed in the cathodic compartment.

Stainless steel electrodes were placed on two sides of the specimen as the electrodes. The electrodes were then connected to a 12 ± 0.1 V direct current (DC) power source. The current between the electrodes through the mortar was recorded using a milli-ampere (mA) ammeter after every thirty (30) minutes. The top of the container was then covered

with a polyethylene paper and the entire set up maintained at 22 ± 1 °C for thirty-six hours. During the experimental period, the solutions were stirred periodically using a glass rod. The mortar sample was then removed from the electrochemical cell set up and allowed to drain for 30 minutes.

Three mortar cubes for each ingress ion were electrically drilled through the core center into a 10 mm interval along the length using a 15 mm radius drill bit up to 80 mm per mortar category along the length using a water-lubricated rotary hammer drill Becker-Decker drilling machine. The obtained powder per 10mm depth was dried at 105 °C to a constant mass. The mortar powder obtained was pulverized to pass through a 76 µm mesh sieve using a pulverizer. The ground mortar was placed in a 20-ml glass sample holder and shaken to mix. Before another sample was ground, the pulverizer-basins were thoroughly cleaned with water and dried to avoid sample cross-contamination. The ground samples were then subjected to SO_4^{2-} and Cl^{1-} analysis. Triplicate analyses were done for every mortar category. Raw experimental data are represented in Appendix C, Table C1 to Table C40.

3.11.1 Chloride and Sulphate ion Profiling

The chlorides and sulphates ions at each depth of penetration were analyzed in accordance with KS EAS 18 - 1: 2017 procedure in all the mortar categories. The estimation of apparent ion diffusion coefficients was achieved under non-steady state conditions assuming boundary conditions $C_{(x,t)} = 0$ at $t = 0$, $0 < x < \infty$, $C_{(x,t)} = C_s$ at $x = 0$, $0 < t < \infty$, constant effects of coexisting ions, linear chloride/sulphate binding, and one-dimensional diffusion into semi-infinite solid (Muthengia, 2009; Crank, 1975). Crank's solution to Fick's second law of diffusion is given by Equation 3.7.

$$C_{(x,t)} = C_{(s)}\left\{1 - \text{erf}\left(\frac{x}{(4D_{mig}t)^{1/2}}\right)\right\} \qquad 3.7$$

where $C_{(x,t)}$ is the concentration of Cl^-/SO_4^{2-} at any depth x in the mortar bulk at time t, C_s is the surface concentration, and D_{mig} is the accelerated migration diffusion coefficient. The error correction function, erf, is the Gaussian error function. The chloride and

sulphate ions profiles were obtained by fitting equation 3.7 for each ion separately to experimentally determined chloride and sulphate profile concentrations, thus determining the values of D_{mig} and C_s mathematically for Cl^-/SO_4^{2-}.

By using the accelerated migration diffusion coefficient D_{mig} determined graphically, D_{app} can be determined by using Equation 3.8.

$$D_{app} = \frac{RT}{ziF} D_{mig} \frac{Int^2}{\Delta Ø} \qquad 3.8$$

where D_{app} is the apparent diffusion coefficient, R is the Gas constant, F is the Faraday constant, T is the temperature of the electrolyte in Kelvin, zi is the valency of the ion i, $\Delta Ø$ is the Effective Applied Voltage in V, t is the duration of the test/exposure in seconds.

3.12 Data Analysis

Triplicate results were obtained for each category of results. Averages were done to obtain statistical means. The change between each category of the sample was analyzed for a significant difference between the same and different samples using the T-test. ANOVA statistical analysis was performed to determine the statistical significance of the results as well as assess the relationship between MICP and the mortar's physico-mechanical properties. Microsoft Excel statistical functions were used to calculate standard deviations and Spearman's rank correlation to compare the various bacteria species and their MICP deposits. Graphical methods have been used to present the results for chloride profile, sulphate profile, compressive and flexural strength, porosity, and permeability analysis. T-Test Summary for test cement of varied microbial preparation and curing regime is represented in Appendix D, Table D1 to Table D6.

CHAPTER FOUR

RESULTS AND DISCUSSION

4.1 Introduction

Chemical analysis results for the OPC and PPC categories showed that they met the minimum requirements as per Kenya Cement Standard KS EAS 18-1:2017 as presented in table 4.1. The fresh cement mortar paste tests prepared using the selected bacteria for both OPC and PPC as presented in Table 4.2 complied with the Kenya Cement Standard for fresh pastes KS EAS 148-3: 2017. The SEM morphological test results as well as the XRD diffractograms for mortar without bacterial treatment showed no Bavenite hydrate or Calcium carbonate precipitate formation. The FT-IR spectral analysis exhibited the presence of hydrated mortar functional groups within the expected cement hydration products wavelengths for the non-bacterial mortars. Further, the FT-IR spectral results for mortar with bacterial treatment showed the presence of additional vibrational wavelengths which were attributed to the functional groups present in Bavenite and Calcium carbonate crystals. Strengths gain was observed across all bacterial treated mortars across both OPC and PPC mortars with the highest gain observed in OPC bacterial categories. The strength gains were attributed to more calcium silicate hydrate bonds and increased densification as a result of Bavenite. Additionally, the water sorption percent drop was exhibited across all bacterial test mortars due to calcium carbonate and Bavenite crystals densification. The results for the apparent diffusion coefficient, D_{app}, of chloride and sulphate ions in microbial mortars were lower than for the non-microbial mortar categories due to the refinement of the pore structure resulting from calcium carbonate and Bavenite precipitation/crystallization.

4.2 Cement oxides

The results for the chemical analysis of cement oxides and LOI in percent by mass for the OPC and PPC test cement are given in Table 4.1.

Table 4.1: OPC and PPC Chemical Analysis Results

Sample	Cement metal oxides composition % w/w ± S.D									
	Al_2O_3	SiO_2	SO_3	Na_2O	K_2O	CaO	MgO	Fe_2O_3	MnO	LOI
OPC	3.643	22.182	2.695	0.410	0.975	64.627	2.084	3.403	0.173	1.519
	±0.010	±0.010	±0.021	±0.001	±0.006	±0.042	±0.025	±0.012	±0.006	±0.001
PPC	5.284	33.422	1.449	0.975	1.846	47.426	1.880	4.618	0.234	2.668
	±0.010	±0.036	±0.010	±0.006	±0.006	±0.306	±0.015	±0.034	±0.006	±0.003

The chemical analysis results show that the test OPC and PPC met the minimum chemical composition requirements (KS EAS 18 - 1: 2017, ASTM D7348: 2013). Using Bogues formula (Bogue, 1977), the average phase composition for the test OPC is 65.115 ± 0.854 %, 14.485 ± 0.913 %, 3.899 ± 0.013 % and 10.355 ± 0.018 % for C_3S, C_2S, C_3A and C_4AF respectively. The average phase composition for PPC is 28.259 ± 0.146 % C_3S, 58.571 ± 0.893 % C_2S, 6.190 ± 0.170 % C_3A and 4.053 ± 0.147 % C_4AF. These study results confirm that the test cement has the major cement phases that meet the Kenya Standards for cement, acceptable cement phases range (KS EAS 148 - 3: 2017).

4.3 Normal consistency, Setting time and Soundness for Control and Microbial OPC

Table 4.2 gives the results for normal consistency, Setting time, and Soundness for control and microbial OPC and PPC.

Table 4.2 Normal consistency, Setting time and Soundness for control and microbial OPC and PPC paste

Test Cement Mortar paste	Setting Time (min)		Normal consistency (%)	Soundness (mm)
	Initial	Final		
OPC (H)	98.0 ± 5.0	178.0 ± 5.0	28.0 ± 0.05	1.0 ± 0.05
PPC (H)	150.0 ± 5.0	220.0 ± 5.0	31.2 ± 0.05	0.8 ± 0.05
OPC (LB)	78.0 ± 5.0	167.0 ± 5.0	26.4 ± 0.05	1.0 ± 0.05
PPC (LB)	130.0 ± 5.0	190.0 ± 5.0	29.1 ± 0.05	1.0 ± 0.05
OPC (BM)	80.0 ± 5.0	170.0 ± 5.0	27.5 ± 0.05	1.0 ± 0.05
PPC (BM)	135.0 ± 5.0	200.0 ± 5.0	30.2 ± 0.05	1.0 ± 0.05
OPC (BP)	89.0 ± 5.0	175.0 ± 5.0	22.3 ± 0.05	1.0 ± 0.05
PPC (BP)	140.0 ± 5.0	209.0 ± 5.0	29.4 ± 0.05	1.0 ± 0.05

All microbial mortar pastes showed a significant difference in the fresh paste tests. PPC (H) showed a higher Normal consistency and setting time values than OPC (H). There was a significant difference in Normal consistency for OPC (H) and PPC (H) ($t_{calc.}$ 0.000163, p = 0.05) implying that PPC (H) required more amount of water to form a workable paste than OPC (H). Patrick, *et al.*, (2012) and Okoya, (2013) made similar observations. They attributed this to the pore fineness present in PPC (H) due to its pozzolanic nature. A similar trend where PPC bacterial pastes exhibited higher normal consistency than OPC pastes of the same bacterial solution was made in this study. The water demand effect of the pozzolana had overridden the beneficial effect of the bacteria or the bacteria feed/biomass addition.

The incorporation of *Lysinibacillus sphaericus*, *Bacillus megaterium,* or *Sporosarcina pasteurii* to OPC and PPC paste lowered the initial setting time just like the final setting time, as well as the normal consistency (Table 4.2). The addition of either of the test *Bacillus* bacteria did not influence the cement paste soundness. These observations could be attributed to the availability of the calcium acetate or sodium chloride in the microbial

biomass or the added microbial feed present in the mix solution. Collepardi, *et al.*, (1972) and Hamdy, *et al.*, (1999) observed in their work that the addition of calcium acetate, calcium nitrate, calcium formate, or sodium chloride act as setting time accelerator. The two authors attributed the shortened setting time and lowered normal consistency to accelerated hydration of dicalcium silicate, (C_2S) cement phase by the acetate ion. In this study, both the acetate or chloride anion, contributed to the setting time acceleration and lowering of the normal consistency. The appreciable lowered initial and final setting time just as normal consistency across all microbial cement pastes for both OPC and PPC is beneficial. It implies that the resultant mortar pastes have reduced water demand and improved workability.

The incorporation of bacteria in OPC fresh pastes, significantly accelerated the setting time or water required for normal consistency. OPC-BP statistically exhibited the lowest normal consistency than all other microbial OPC fresh pastes. This was in agreement with the findings of Sahoo *et al.*, (2016) in a study on the effect of *Bacillus megaterium* on fresh cement paste properties. It was found that, the soundness of OPC-LB, OPC-BM, OPC-BP, and OPC-H cement fresh pastes exhibited no significant difference ($t_{calc} = 0.5$, $p = 0.05$). This could imply that either the microbial biomass or the calcite precipitated by these microbes has cementitious properties. It does not expose the resultant mortars to undergo any appreciable change in volume upon setting.

PPC in both non-bacterial and bacterial treated cement pastes exhibited raised setting time and normal consistency compared to OPC prepared using the same bacterial solution as the paste making mix regime as shown in Table 4.2. The use of the microbial solution as mix media for both OPC and PPC lowered both initial and final setting time as well as the normal consistency of the fresh cement paste. The use of the microbial solution as mortar paste mix media had no effect on soundness for both OPC and PPC fresh mortar pastes. Maheshwaran, *et al.*, (2014), on incorporating *Bacillus pasteurii* in a calcium acetate feed and Jonkers, *et al.*, (2011), on incorporating *Bacillus pseudofirmus* in calcium chloride nutrients, observed accelerated setting time and lowered water of consistency. They attributed the accelerated setting time and lowered water of

consistency to the presence of acetate and chloride ions respectively. In the alternative, Ersan, *et al.*, (2015) observed retarded setting time and lowered water consistency. In their study, they grew *Bacillus pasteurii* in calcium formate nutrients. They attributed the retardation to the presence of formate ions.

The bacterial effect on setting time and water for normal consistency in OPC paste was not as pronounced as was the case with PPC fresh paste. Perhaps, the addition of $CaCl_2$, NaCl, or $Ca(CH_3COO)_2$ in the microbial biomass or feed, as well as the presence of bacterial cell wall as a nucleation site, establish fineness. The fine particles with increased surface area create adsorption sites. PPC having a higher content of C_2S than OPC exhibits an improved surface area of hydration which accelerates both initial and final setting time and lower water demand for normal consistency.

The cement paste prepared using a microbial solution containing *Lysinibacillus sphaericus* and *Bacillus megaterium* exhibited lower setting time and normal consistency than the paste prepared using *Sporosarcina pasteurii* solution across both OPC and PPC paste. This was in agreement with the observations made by both Maheshwaran, *et al.*, (2014) while using *Bacillus pasteurii* and Jonkers, *et al.*, (2011) while using *Bacillus pseudofirmus*. They attributed their observations to the presence of either acetate or chloride ion in the bacterial nutrients. The bacteria feed for both *Lysinibacillus sphaericus* and *Bacillus megaterium* contained $Ca(CH_3COO)_2$ while the one for *Sporosarcina pasteurii* contained $CaCl_2$. The two biomass ingredients could be attributed to the variation in the setting time and normal consistency. Perhaps, the presence of CH_3COO^{1-} and Cl^{1-} in the bacterial solution could imply that CH_3COO^{1-} is a better setting time accelerator than the Cl^{1-}.

4.4 Scanning Electron Microscope (SEM) analysis

The SEM morphologies for non-bacterial treated OPC and the bacterial treated OPC test mortars are represented in Figure 4.1 (a) to (d), Figure 4.2 (a) to (c), and Figure 4.3 (a) to (c) after the 28^{th} day of curing.

Figure 4.1 (a) represents the non-bacterial treated mortar SEM morphology. Figure 4.1 (b) to (d) represents SEM morphologies for bacterial treated, mortar prepared using tap water and cured in a solution containing *Lysinibacillus sphaericus*, mortar prepared using a solution containing *Lysinibacillus sphaericus* and cured in tap water, and a mortar prepared and cured using a solution containing *Lysinibacillus sphaericus* respectively.

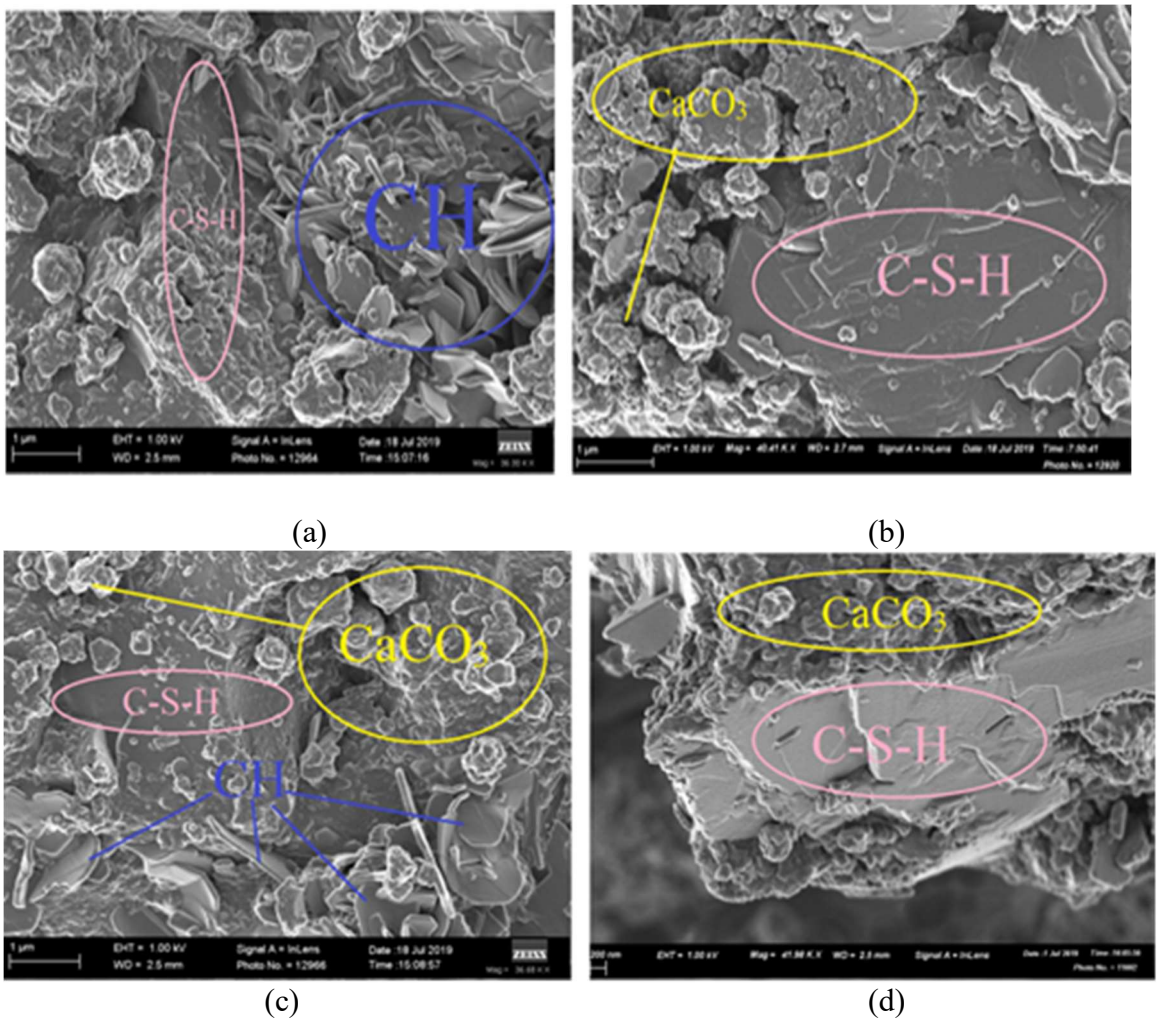

Figure 4.1: SEM analysis for (a) OPC-H (H), (b) OPC-H (LB), (c) OPC-LB (H) and (d) OPC-LB (LB).

The SEM images exhibit the development of calcium-silicate-hydrate , C-S-H, as a crystalline gel, across all the test mortars. There is the formation of hexagonal crystals which is portlandite, CH, within mortars that were either prepared using water and cured in water or the mortars prepared using the microbial solution but cured in water as shown

by Figures 4.1 (a) and 4.1 (c). Across all mortars either prepared or cured using the microbial solution or prepared and cured in microbial solution there is the trigonal/rhombohedral crystals of calcium carbonate, $CaCO_3$. deposition. As exhibited by Figures 4.1, there was more $CaCO_3$ deposition in Figures 4.1 (b) and 4.1 (c) as compared with Figure 4.1 (d). Figure 4.1 (d) exhibited more/denser C-S-H gel compared with the others. These SEM results could imply that the presence of bacteria either in mortar preparation or curing regimes causes the consumption of CH during cement hydration and subsequent formation of $CaCO_3$ and more C-S-H crystals.

Figure 4.2 (a) to (c) represents SEM morphologies, for *Bacillus megaterium* treated, mortar prepared using tap water and cured in a solution containing *Bacillus megaterium*, mortar prepared using a solution containing *Bacillus megaterium* and cured in tap water, and a mortar prepared and cured using a solution containing *Bacillus megaterium* respectively.

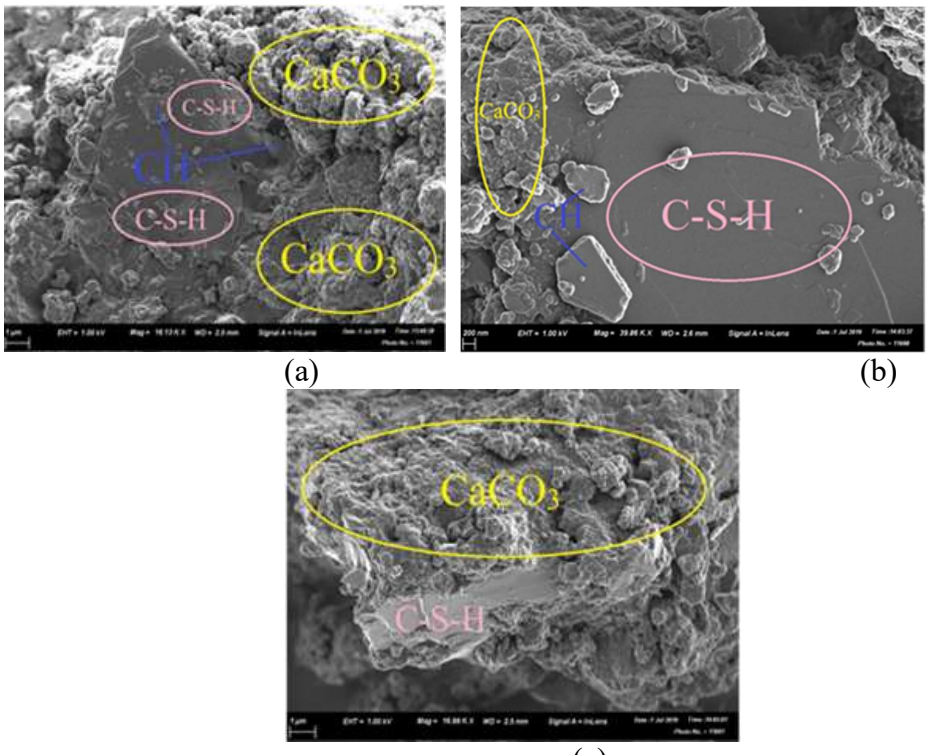

(a) (b)

(c)

Figure 4.2: SEM analysis for (a) OPC-H (BM), (b) OPC-BM (H) and (c) OPC-BM (BM)

Figure 4.3 represents SEM morphologies for *Sporosarcina pasteurii* treated mortars. Figure 4.3 (a) represents a mortar prepared using tap water and cured in a solution containing *Sporosarcina pasteurii*, Figure 4.3 (b) represents a mortar prepared using a solution containing *Bacillus megaterium* and cured in tap water, and Figure 4.3 (c) represents a mortar prepared and cured using a solution containing *Sporosarcina pasteurii*.

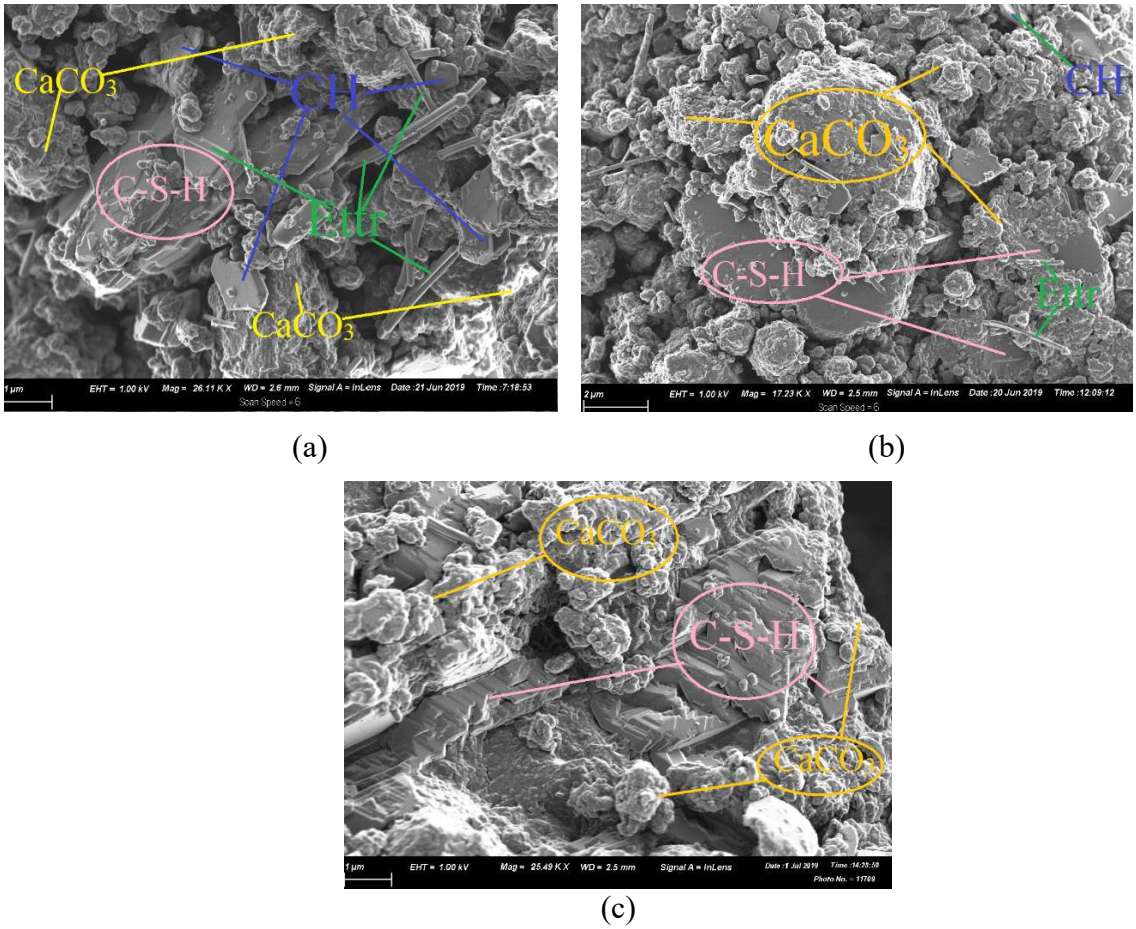

Figure 4.3: SEM analysis for (a) OPC-H (BP), (b) OPC-BP (H), and (c) OPC-BP (BP).

SEM image for OPC-H (H) mortar as shown in Figure 4.1 (a) had no evidence of calcium carbonate sedimentation. Conversely, significant calcium carbonate sedimentation occurred as shown by the SEM images in Figure 4.1 (b) to (d), Figure 4.2 (a) to (c) as well as in Figure 4.3 (a) to (c), the microbial mortars OPC-H (LB), OPC-H (BM), OPC-H (BP), OPC-LB (H), OPC-BM (H), OPC-BP (H), OPC-LB (LB), OPC-BM (BM) and

OPC-BP (BP) respectively. This is attributed to the MICP deposits by *Lysinibacillus sphaericus, Bacillus megaterium* and *Sporosarcina pasteurii* either present in mix media or present in the cultured curing solution. A similar SEM morphological observation was made by Hammad, *et al.*, (2013) and Vijay and Murmu, (2018) while using *Bacillus pasteurii* and *Bacillus subtilis* respectively. They attributed their observations to the deposition of calcite and crystallization of calcium silicate hydrate. In this study, the morphology of C-S-H densifies from Figure 4.1 (b) through (c) to (d), Figure 4.2 (a) to (c) as well as in Figure 4.3 from (a) through (b) to (c). This implies that there is additional calcium silicate hydrate crystallization based on the mortar preparation or curing regime. The densification could also be attributed to calcite precipitation as seen across the SEM micrographs for the three bacteria under study. Image (d) from Figure 4.1 and image (c) from Figures 4.2 and 4.3, visibly demonstrate biodeposition over Ettringite spurs resulting in the formation of biofilms on their surface and plugging of the pores on the mortar structure.

Calcite biodeposition was more crystalline and dense in microbial mortars prepared and cured using a bacterial solution than the mortars either prepared or cured using tap water. This can be deduced from figures 4.1 (d), 4.2 (c), and 4.3 (c). This improved calcite crystallinity and more densification were more in microbial mortars prepared or cured using *Lysinibacillus sphaericus* than in the mortars prepared using *Bacillus megaterium* or *Sporosarcina pasteurii* bacteria. This calcite crystallinity and densification difference based on the mortar preparation and curing regime could be attributed to the availability of nucleation sites. The mortars prepared and cured using the bacterial solution are in an environment with a relatively higher bacteria population. This avails a higher concentration of Ca^{2+} and increased nucleation sites than in the other mortar categories. Mutitu, *et al.*, (2020) on using both *Bacillus megaterium* and *Lysibacillus sphaericus* in their study for the biocementation effect on chloride ingress and Stocks-Fischer, *et al.*, (1999) using *Bacillus pasteurii* in their study to investigate the physical and biochemical properties of $CaCO_3$ precipitate induced by their alkaliphilic soil microorganism, made similar observations. They attributed this observation to the stable and continuous $CaCO_3$ formation promoted by the availability of sufficient nucleation sites.

The SEM morphologies for non-bacterial treated PPC and the bacterial treated PPC test mortars are represented in Figure 4.4 (a) to (d), Figure 4.5 (a) to (c), and Figure 4.6 (a) to (c) after the 28th day of curing. Figure 4.4 (a) represents the non-bacterial treated mortar SEM morphology. Figure 4.4 (b) to (d) represents SEM morphologies for bacterial treated, mortar prepared using tap water and cured in a solution containing *Lysinibacillus sphaericus*, mortar prepared using a solution containing *Lysinibacillus sphaericus* and cured in tap water, and a mortar prepared and cured using a solution containing *Lysinibacillus sphaericus* respectively.

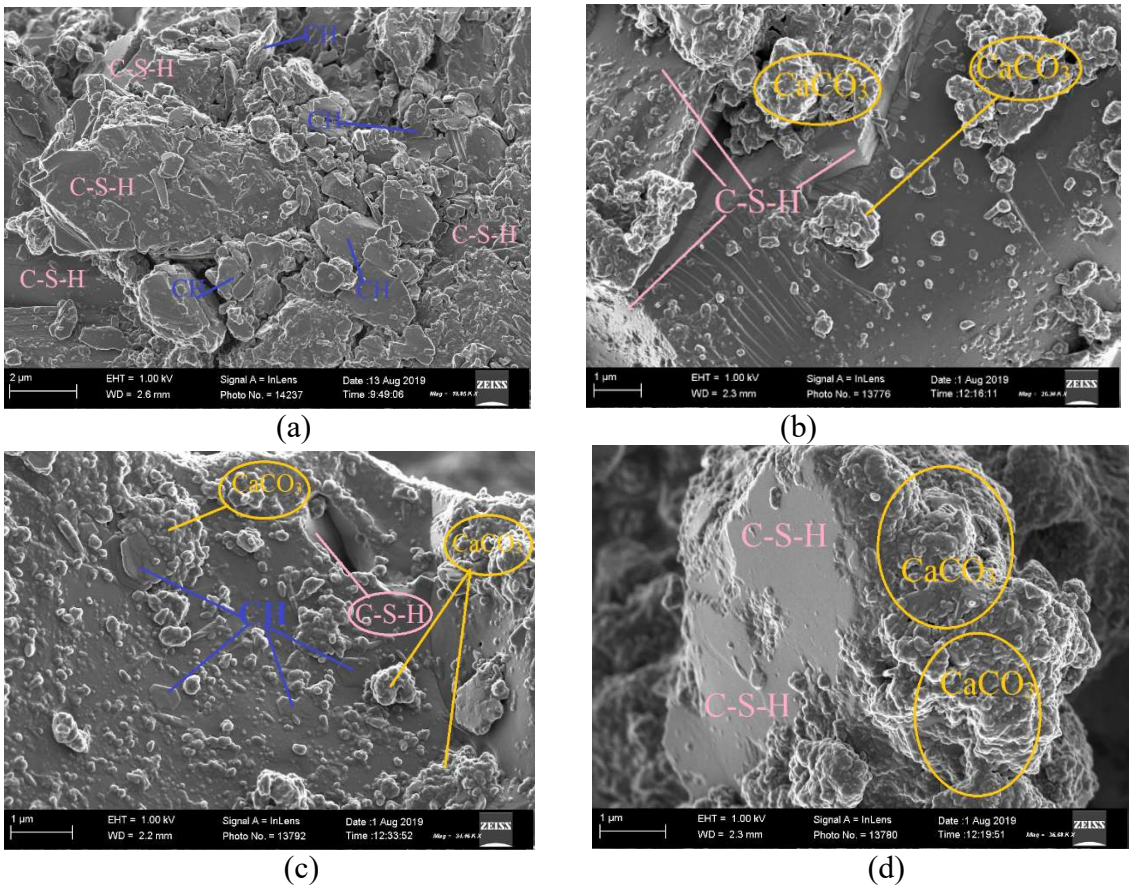

Figure 4.4: SEM analysis for (a) PPC-H (H), (b) PPC-H (LB), (c) PPC-LB (H) and (d) PPC-LB (LB).

The non-microbial mortar cured in water exhibited no calcite deposition as shown by Figure 4.4 (a). This mortar was non-bacterial treated. There was no MICP process within this mortar matrix and hence it had no $CaCO_3$ precipitation. Both microbial prepared and the non-microbial prepared mortars which were cured in microbial solution exhibited

$CaCO_3$ precipitation as shown by Figures 4.4 (b), (c), and (d). Across both microbial and non-microbial prepared mortars, there is the formation of C-S-H. The C-S-H crystallization was more/denser in the microbial mortars cured in a *Lysinibacillus sphaericus* bacterial solution. Verma, *et al.*, (2015) and Achal, *et al.*, (2016) made similar observations. They reported that urease produced by the ureolytic bacteria they incorporated into their mortars, influences the chemical process associated with the formation of biominerals. In this study, the formation of $CaCO_3$ or C-S-H is attributed to biomineralization either as a result of ureolysis or aerobic oxidation of the bacteria feed urea or acetate ion respectively in the presence of Ca^{2+}. The densification of the precipitation could also be attributed to the presence of other hydration products that have cementitious characteristics.

Figure 4.5 represents SEM morphologies for PPC *Bacillus megaterium* treated mortars. Figure 4.5 (a) represents a SEM morphology of a mortar prepared using tap water and cured in a solution containing *Bacillus megaterium*. Figure 4.5 (b) represents a mortar prepared using a solution containing *Bacillus megaterium* and cured in tap water, while Figure 4.5 (c) represents a mortar prepared and cured using a solution containing *Bacillus megaterium.*

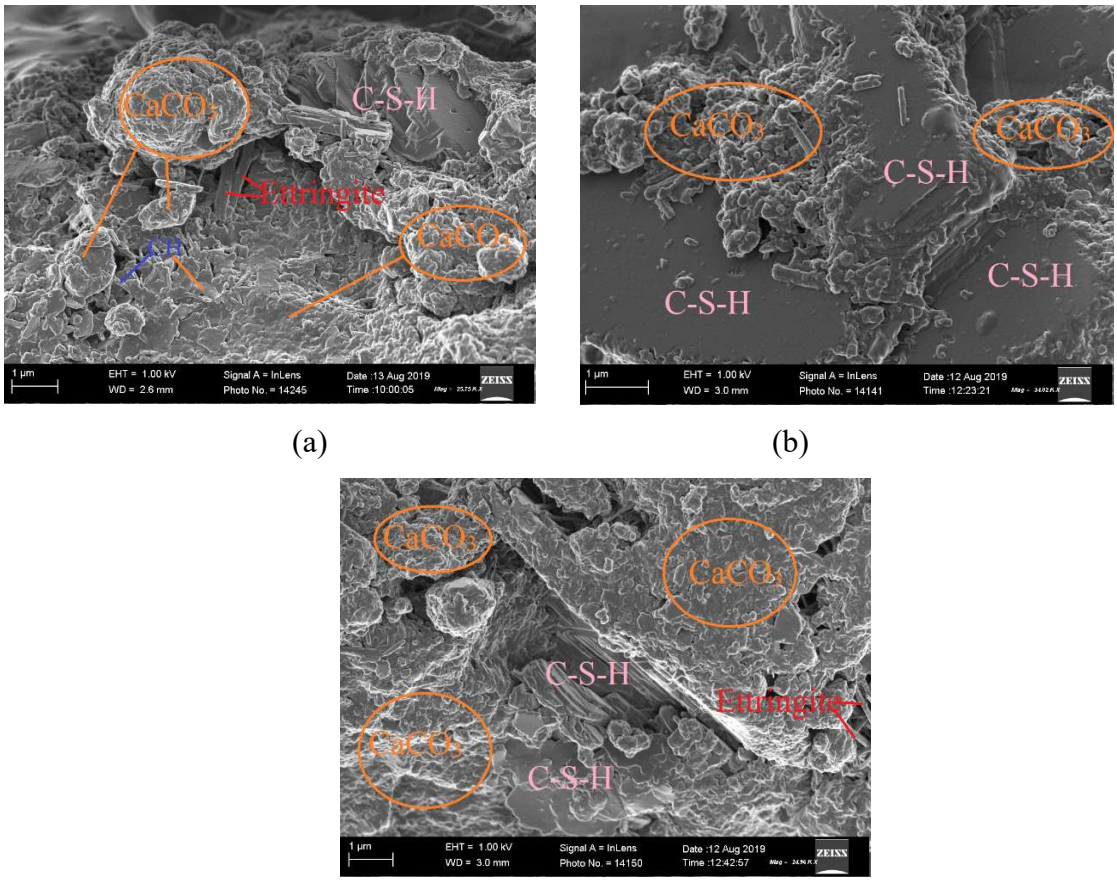

Figure 4.5: SEM analysis for (a) PPC-H (BM), (c) PPC-BM (H) and (d) PPC-BM (BM).

As portrayed by SEM morphologies in Figure 4.5, in addition to C-S-H crystallization, there is the formation of both $CaCO_3$ and ettringite. Ettringite formation could be attributed to internal sulphate attack, where gypsum reacts with calcium aluminate phases, C_3A, or C_4AF to form ettringite (Mutitu, 2013; Nosouhian, *et al.*, 2016; Munyao, *et al.*, 2020). The fewer ettringite crystallization or their covering by C-S-H or $CaCO_3$ could imply that there is limited internal sulphate attack. Further, it could also imply that the calcium aluminate phases are being utilized in the formation of other hydration compounds with cementitious properties.

Figure 4.6 represents SEM morphologies for *Sporosarcina pasteurii* PPC treated mortars. Figure 4.6 (a) represents a mortar prepared using tap water and cured in a solution

containing *Sporosarcina pasteurii*, Figure 4.6 (b) represents a mortar prepared using a solution containing *Bacillus megaterium* and cured in tap water, and Figure 4.6 (c) represents a mortar prepared and cured using a solution containing *Sporosarcina pasteurii.*

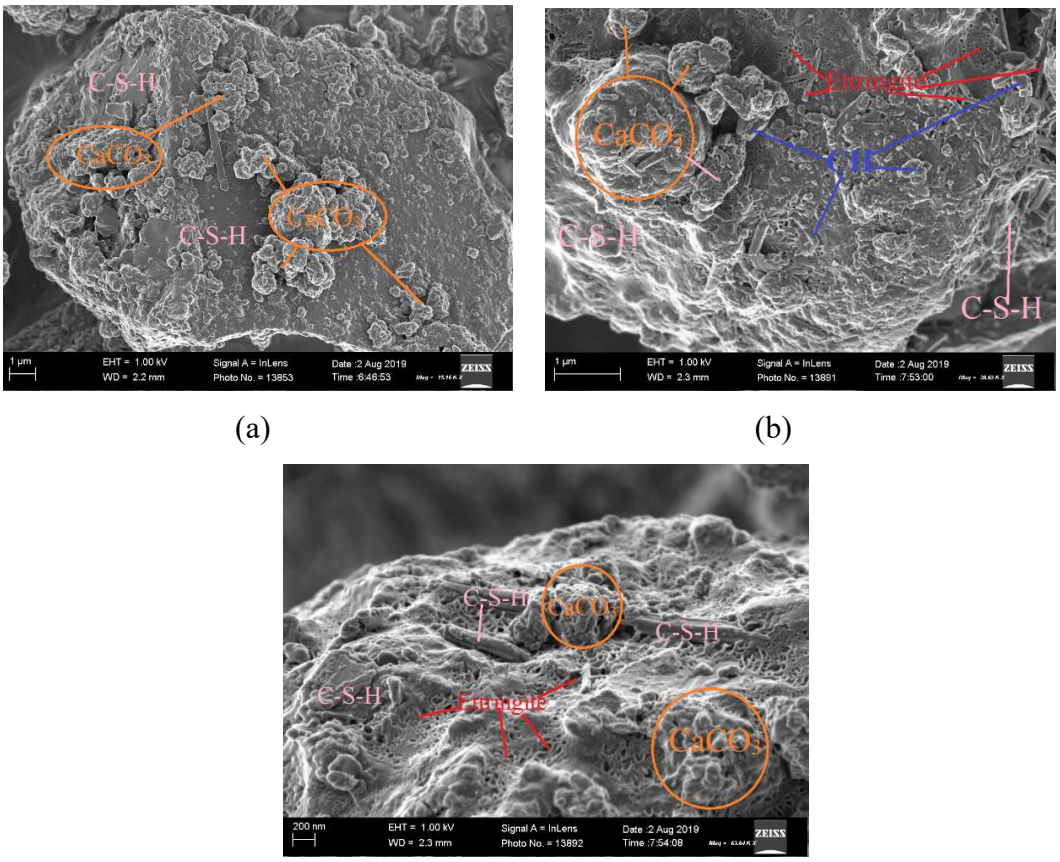

Figure 4.6: SEM analysis for (a) PPC-H (BP), (c) PPC-BP (H) and (d) PPC-BP (BP).

Calcium carbonate and C-S-H formation was observed across the three mortar categories treated with *Sporosarcina pasteurii*. The biomineralization process would be attributed to the formation of these two compounds just like in Figure 4.4 and 4.5 above. The SEM morphologies from *Sporosarcina pasteurii* treated mortars exhibited significant Ettringite crystals as shown by Figure 4.6 (b) and Figure 4.6 (c). Jonkers, *et al.*, (2011) and Nosouhian, *et al.*, (2016) though using *Bacillus pseudofirmus* and *Bacillus subtilis*

bacteria respectively made similar observations. Ettringite formation is not a direct product of biomineralization. Thaumasite, a sulphate attack product, which occurs in nature as ettringite is formed in the presence of $CaCO_3$, SO_4^{2-} and low temperatures (Mingyu, *et al.*, 2006; Mutitu, 2013).

As SEM images in Figure 4.4 (a) illustrate, the non-microbial PPC-H (H) mortar had no visible calcium carbonate deposits. However, all the PPC microbial mortars prepared and or cured using the microbial solution showed significant calcium carbonate precipitates. This could be attributed to the MICP deposits from the *Bacillus* bacteria either present in mix media or present in the cultured curing solution. There are observable differences between the SEMs including morphology of C-S-H and $CaCO_3$ as well as their quantity. These two compounds densification across all the three bacteria under study is more in mortars whose preparation and curing regime had the bacteria. The densification of C-S-H was higher in mortars containing *Lysinibacillus sphaericus* while the densification though with lower crystallinity of $CaCO_3$ was higher in mortars containing *Bacillus megaterium*. These results could imply that the incorporation of *Bacillus* species in mortar causes a mop-up of CH, a product of cement hydration leading to $CaCO_3$ formation. The more C-S-H crystals in these microbial mortars could be attributed to catalytic and accelerating properties of these bacteria leading to a complete cement hydration process. The more densification could also imply that there was the formation of more C-S-H crystals and additional hydration products with cementitious attributes.

4.5 OPC X-Ray Diffraction (XRD) Analysis

Figure 4.7 shows the XRD diffractogram obtained for an OPC mortar prepared using a microbial solution containing *Lysinibacillus sphaericus* as the mix solution and cured in a microbial solution containing the same bacteria.

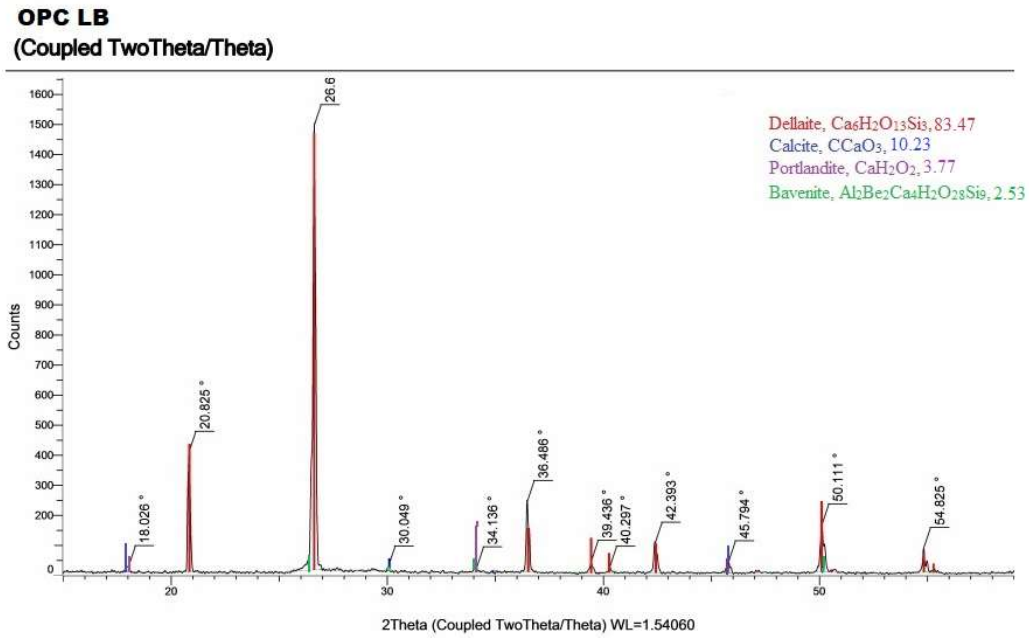

Figure 4.7: XRD Diffractograms for OPC-LB (LB)

Table 4.3 summarizes the % w/w ± S. D. values of hydrated OPC control and microbial mortars after curing them for 28 days.

Table 4.3: XRD (% w/w ± S. D. values) summary for hydrated OPC microbial mortars prepared and cured in respective microbial solution against control OPC mortar after the 28th day of curing

Hydration Compound	Mortar Category (% w/w ± S. D.)			
	OPC-H (H)	OPC-LB (LB)	OPC-BM (BM)	OPC-BP (BP)
Bavenite, ($Al_2Be_2Ca_4H_2O_{28}Si_9$)	-	2.53 ± 0.02	1.33 ± 0.03	2.08 ± 0.07
Dellaite, ($Ca_6H_2O_{13}Si_3$)	83.93 ± 0.03	83.47± 0.02	84.18 ± 0.02	83.69 ± 0.03
Calcite, ($CaCO_3$)	0.64 ± 0.02	10.23 ±0.02	10.27 ± 0.02	10.21 ± 0.02
Portlandite, ($Ca(OH)_2$)	15.47 ± 0.03	3.77 ± 0.02	4.19 ± 0.02	3.81 ± 0.02

The XRD analysis of the OPC mortars, confirms that microbial biocementation introduces new cementitious material. Bavenite, $Al_2Be_2Ca_4H_2O_{28}Si_9$, which is completely absent in the non-microbial treated mortar, OPC-H (H), is present in the microbial mortars, OPC-LB (LB), OPC-BP (BP) and OPC-BM (BM) at 2.53 % 2.08 % and 1.33 % by mass of the cement mortar respectively. The majority of the researchers have not gone to the extent of investigating other biominerals beyond calcium carbonate polymorphs and the additional C-S-H crystallization. Dhami, *et al.*, (2012) in their study, investigating the potential of *Bacillus megaterium* to produce calcite and improve properties of ash bricks, used both SEM and XRD analysis to determine the polymorphic form of precipitated $CaCO_3$. Vijay and Murmu, (2018) in their studies in investigating the effect of calcium lactate on compressive strength and self-healing of cracks in microbial concrete, used both SEM and XRD analysis to confirm the effect of calcite precipitation on microcrack healing and the influence of the additional C-S-H on

compressive strength improvement. The results of this study imply that the test bacteria species influence the biomineralization process differently. The difference is attributed to either the urease activity of a given bacterial species or the bacterial mechanism of solution saturation. SEM and XRD analysis confirm the biomineralization of $CaCO_3$, additional formation of C-S-H as well as bavenite crystallization as an additional cementitious compound.

In this study, the formation of bavenite from bacterial treated OPC is hypothesized to follow a bacterial catalyzed mechanism. The reaction mechanism utilizes the tricalcium aluminate hydrate, ($Ca_3Al_2O_6.6H_2O$) and tricalcium silicate hydrate, ($Ca_3H_2(SiO_4)_2.2H_2O$) as some of the reactants. These two cement hydration compounds are formed within the mortar matrix according to Equation 4.1 and 4.2 respectively:

$$3CaO.Al_2O_3 + 6H_2O \rightarrow Ca_3Al_2O_6.6H_2O \quad 4.1$$

$$2(CaO)_2.SiO_2 + 4H_2O \rightarrow Ca_3H_2(SiO_4)_2.2H_2O + Ca(OH)_2 \quad 4.2$$

The test *Bacillus* species being urease active, selectively activates Beryllium oxide, BeO among the available cement oxides. BeO being amphoteric reacts with hydroxyl ion within the mortar's alkaline pore solution. The reaction produces beryllate complex ion according to Equation 4.3:

$$BeO + 2OH^{1-} + H_2O \rightarrow [Be(OH)_4]^{2-} \quad 4.3$$

The products of equation 4.1, 4.2, and 4.3 react in the presence of urease active bacteria forming bavenite according to Equation 4.4:

$$4[Be(OH)_4]^{2-} + 2Ca_3Al_2O_6.2H_2O + 9Ca_3H_2(SiO_4)_2.2H_2O \xrightarrow{\text{Urease}} 2Ca_4Be_2Al_2Si_9O_{26}(OH)_2 + 25Ca(OH)_2 + 8OH^{1-} + 8H_2O \quad 4.4$$

Biomineralization of Bavenite, a siliceous and aluminous material could be attributed to the additional cementitious property exhibited by the microbial treated OPC mortars.

Calcite, $CaCO_3$ is statistically significantly more in OPC-BM (BM), OPC-LB (LB), and OPC-BP (BP) at 10.27 %, 10.23 %, and 10.21 % by mass of the cement mortar respectively as compared to 0.64 % by mass of the cement mortar in OPC-H (H). This

relates very well with improved calcite, $CaCO_3$, deposits, and depleted Portlandite, $Ca(OH)_2$, (CH), in microbial mortars as seen in SEM morphological images shown in Figures 4.1 (d), 4.2 (c) and 4.3 (c).

The massive amount of calcium carbonate precipitated in the microbial mortars is attributed to a two-mechanism biochemical process. The first mechanism is the direct bacteria nutrient metabolic ureolysis as summarized in equations 1.1 to 1.7, or the metabolic conversion of the acetate ion through aerobic oxidation as shown in equations 2.6 to 2.9. The second mechanism is the indirect chemical reaction between the relatively more soluble portlandite from the cement hydration process with the biogenic carbon (IV) oxide as shown in equation 2.10.

The more densification of C-S-H in microbial treated mortars as compared with the non-microbial treated mortars as seen in SEM micrographs is statistically supported by the high percentage of both Bavenite, $Al_2Be_2Ca_4H_2O_{28}Si_9$, and Dellaite, $Ca_6H_2O_{13}Si_3$ individually or combined in OPC-BP (BP), OPC-BM (BM) and OPC-LB (LB) than in OPC-H (H) as shown in Table 4.3. The XRD quantifications confirm the presence of calcite as well as more C-S-H in microbial mortars. These depositions in the pores maximized the packing density of cement mortar consequently improving the mortar's physico-chemical and mechanical properties.

4.6 OPC Fourier Transform-Infrared Spectroscopy (FT-IR) Analysis

Table 4.4 represents a summary of the functional groups from the FT-IR analysis of hydrated OPC mortars both for the non-microbial as well as the microbial mortars. The analysis was done after the 28^{th} day of curing.

Table 4.4 shows FT-IR detectable bands of the Microbial and Non-microbial treated hydrated cement after 28 days of curing.

	Phase	Wave-number (cm^{-1})					
		O-H	**O-H (from H_2O)**	**Si-O (Assym. Stretching)**	**Al-O**	**Si-O (in-plane)**	**C-O, CO_3^{2-}**
Main Hydrated phases	C-S-H (Ca/Si = 1.5)		3311, 1739	1057, 1097	523	694, 523	
	Portlandite, $Ca(OH)_2$	3642					
MICP phase	Calcite						2971, 2153, 1424, 776
Clinker phases	Ca_3SiO_5, C_3S			1057		523	
	Ca_2SiO_4, C_2S					519	
	$Ca_3Al_2O_6$, C_3A				523		

The stretching vibration frequencies of the polymerized Si-O bond in a microbial environment is 1057 cm^{-1} which is similar to the values reported by Rong and Qian, (2015). The vibrational absorptions at 2971 cm^{-1} and 1424 cm^{-1} correspond to the stretching vibration frequencies of $CaCO_3$ present in OPC as part of cement additive and microbial precipitate respectively. The stretching vibration frequencies for O-H at 3642 cm^{-1} was as a result of $Ca(OH)_2$. The band at 3311 cm^{-1} is due to the presence of crystal water in the mortars (Zhang, *et al.*, 2014). However, all the above vibrational frequencies occurred at different % transmittance levels for different microbial mortars. The above results show the stretching vibration frequencies are different in four different specimens which could be attributed to different binding effects of the resultant bonds. FT-IR peaks of all microbial mortar products formed through chemical precipitation and microbiological sedimentation in mortars are 523cm^{-1}, 694cm^{-1}, 1057 cm^{-1}, 2971 cm^{-1}, 3311 $cm^{-1,}$ and 3642 cm^{-1} which correspond to the stretching vibrations of asymmetric Si-O or Al-O stretch, out-of-plane Si-O, symmetric Si-O, $CaCO_3$ precipitate, $CaCO_3$ additive, O-H of water of hydration and O-H of $Ca(OH)_2$, respectively. These stretch wavelengths are consistent with the reported results in the literature (Zhang, *et al.,* 2014; Rong and Qian, 2015).

The band wavelengths at 2153 cm^{-1} and 1739 cm^{-1} have no literature assigned functional group for hydrated cement. 2153 cm^{-1} fall in the range 3000 and 2000 cm^{-1} which are overtone modes (Horgnies, *et al.*, 2013; Stutzman, *et al.*, 2016). The stretch at 1739 cm^{-1} could be brought up by overlapping of different functional groups. It could be associated with the overlap of CO_3^{2-} from the MICP calcite which was observed at 1424 cm^{-1} and the O-H from the calcium silicate hydrate observed at 3311cm^{-1}. This overlap could be attributed to the presence of $CaCO_3$ which precipitates on the surface of C-S-H. This is corroborated by the SEM images. The non-bacterial treated mortars did not show any absorption spectral at these wavelengths.

At 1424 cm^{-1}, $CaCO_3$ precipitate occasioned by the microbial deposition is visualized. More intense characteristic peaks were observed in the FTIR spectra for the calcite particles from microbial treated hydrated cement mortars than in the spectra for the non-

microbial mortars. The clarity of these absorption bands could be attributed to the formation of the calcite polymorph of $CaCO_3$ particles. At 776 cm^{-1}, an Al-O vibration is detected. This is principally from tricalcium aluminate, C_3A, and to a lesser extent from tetracalcium alumino-ferrite, C_4AF (Horgnies, *et al.*, 2013; Zhang, *et al.*, 2014).

The positions of all of the infrared active modes of calcite, C-S-H, and CH found in both microbial treated mortars and the non-microbial treated mortars, closely match those of the reference bands. These results also confirm the SEM micrographs and XRD analysis results, presented earlier in section 4.4 and 4.5 respectively. These findings confirm that additional cementitious products are formed in microbial treated mortars. Further, these results also confirm that the MICP products are both cementitious and are compatible with the usual cement hydration products.

4.7 PPC X-Ray Diffraction (XRD) Analysis

Figure 4.8 shows hydrated compounds XRD diffractogram for microbial PPC mortar prepared using *Lysinibacillus sphaericus* mix solution and cured in a similar bacteria microbial solution after 28th day of curing.

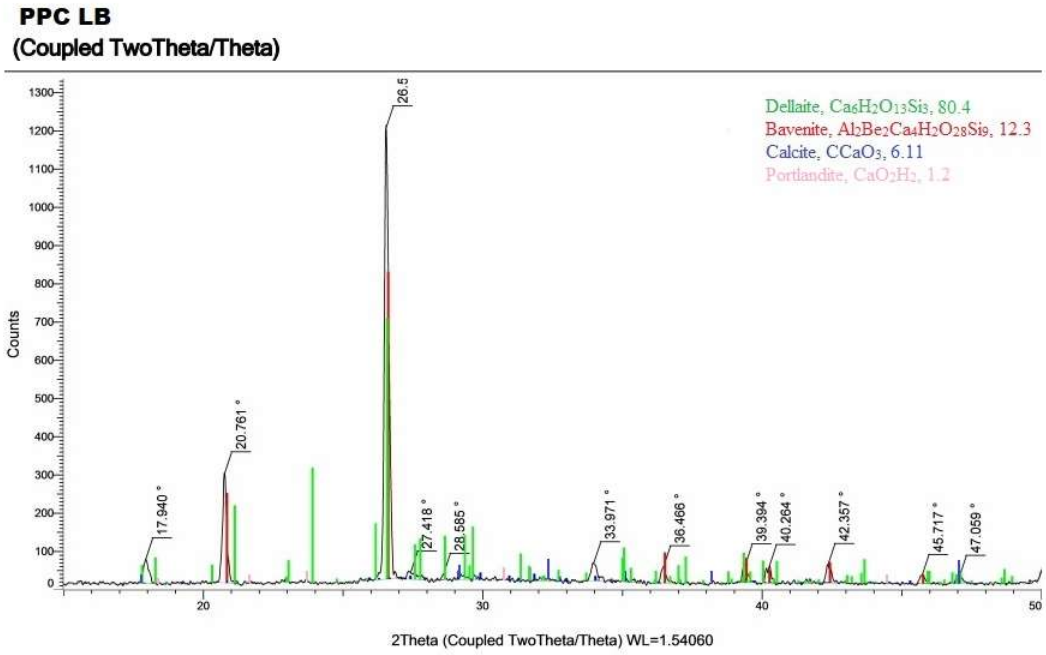

Figure 4.8: XRD diffractograms for PPC-LB (LB).

Similar XRD diffractogram analysis were done for other test mortars and results summarized in Table 4.5.

Table 4.5: XRD (% w/w ± S. D. values) summary for hydrated PPC microbial mortars prepared and cured in respective microbial solutions against control PPC mortar after 28th day of curing.

Hydration Compound	Mortar Category (% w/w ± S. D.)			
	PPC-H (H)	PPC-LB (LB)	PPC-BM (BM)	PPC-BP (BP)
Bavenite, ($Al_2Be_2Ca_4H_2O_{28}Si_9$)	-	12.30 ± 0.02	14.90 ± 0.01	13.87 ± 0.01
Dellaite, ($Ca_6H_2O_{13}Si_3$)	93.80 ± 0.02	80.40± 0.02	75.30 ± 0.02	77.23 ± 0.02
Calcite, ($CaCO_3$)	0.90 ± 0.02	6.11 ±0.02	7.50 ± 0.02	7.20 ± 0.01
Portlandite, ($Ca(OH)_2$)	5.30 ± 0.02	1.20 ± 0.02	2.30 ± 0.02	1.70 ± 0.01

The XRD analysis of the PPC mortars just like the one for OPC, confirms that microbial biocementation introduces new cementitious material, Bavenite, $Al_2Be_2Ca_4H_2O_{28}Si_9$. This hydrated cement compound is not available in the non-microbial treated mortar, PPC-H (H)**.** Bavenite was depicted in the microbial treated mortars, PPC-BM (BM), PPC-BP (BP), and PPC-LB (LB), at 14.90 % 13.87 % and 12.30 % respectively. The bavenite percent in microbial treated PPC is significantly higher than in OPC microbial treated mortars. C_3S and C_2S are the main cement phases that undergo hydration forming siliceous compounds with cementitious properties (Theising, *et al.*, 1986; Mutitu, 2013). C_3S phase hydrates and sets much faster than C_2S. C_2S dictates the later age strength (Muthengia, 2009; Kropp and Hilsdorf, 2010). The test PPC had 58.571 % C_2S while the test OPC had 14.485 % C_2S. C_2S undergoes hydration together with bacterial biominerals

forming additional cementitious products, such as bavenite. This % C_2S variation is attributed to the higher bavenite content in PPC than in OPC across all microbial treated mortars.

In this study, the formation of bavenite from bacterial treated PPC is hypothesized to follow a bacterial catalyzed mechanism. The reaction mechanism utilizes the tricalcium aluminate hydrate, ($Ca_3Al_2O_6.6H_2O$) from the cement's tricalcium aluminate phase. This cement's phase hydration occurs according to equation 4.1. The other reactant for PPC bavenite formation is postulated to come from the additional calcium silicate hydrate, ($CaH_2SiO_4.2H_2O$). This Calcium silicate hydrate results from the pozzolanic, acid-base reaction between the highly soluble portlandite and silicic acid according to Equation 4.5:

$$Ca(OH)_2 + H_4SiO_4 \rightarrow CaH_2SiO_4.2H_2O \qquad 4.5$$

Beryllate ion, $[Be(OH)_4]^{2-}$ hydrolyzed according to equation 4.3 reacts with $Ca_3Al_2O_6.6H_2O$ and $CaH_2SiO_4.2H_2O$ in presence of bacterial urease according to Equation 4.6:

$$2[Be(OH)_4]^{2-} + Ca_3Al_2O_6.6H_2O + 9CaH_2SiO_4.2H_2O \rightarrow Ca_4Be_2Al_2Si_9O_{26}(OH)_2 + \\ + 8Ca(OH)_2 + 4OH^{1-} + 26H_2O \qquad 4.6$$

Bavenite as a biomineral with aluminous and siliceous properties could be attributed to the beneficial cementitious property exhibited by the microbial treated PPC mortars. In addition to bavenite, this biomineralization process avails significant quantities of portlandite which could make the mortar undergo beneficial late hydration. This process would form more C-S-H crystals leading to higher strengths.

Calcite was significantly more in PPC-BM (BM), PPC-BP (BP), and PPC-LB (LB) at 7.50 %, 7.20 %, and 6.11 % respectively as compared with 0.90 % in PPC-H (H). This relates very well with improved calcite, ($CaCO_3$) deposits and lessened Portlandite, $Ca(OH)_2$, (CH), in microbial treated mortars as seen in SEM micrographs. The increased presence of dissolved inorganic carbon from the bacteria feed, the enhanced surface area of Ca^{2+} over the bacteria cell wall and the alkaline nature of the pore solution are the parameters attributed to the high availability of CO_3^{2-} for calcite precipitation. The

stability and continuous production of $CaCO_3$ are attributed to the availability of the bacteria cell wall as the nucleation sites (Stocks-Fischer, *et al.*, 1999; Karanja, *et al.*, 2019).

The more densification of C-S-H in microbial mortars as compared with non-microbial treated mortar as seen in SEM micrographs could be attributed to the presence of both Bavenite in microbial PPC mortars as well as more calcite precipitate as summarized in Table 4.4. The microbial induced calcite and bavenite are highly coherent with the usual hydrated cement compounds. The resultant compound is attributed to the enhanced chemical and physico-mechanical properties of the resultant product.

The XRD quantifications confirm the presence of calcite as well as additional C-S-H in the microbial treated mortars. Vijay and Murmu, (2018), on using both *Bacillus pasteurii* and *Bacillus subtilis* encapsulation for micro-crack healing, observed the formation of similar products using XRD analysis. Schwantes-Cezario, *et al.*, (2019), in their study on mortars with the addition of *Bacillus subtilis* spores, used XRD analysis to reveal $CaCO_3$ precipitation only. The depositions in microbial treated mortars, result from both chemical and microbiological processes. This could result in stronger bonding, improving the mortar's physico-chemical and mechanical properties.

4.8 PPC Fourier Transform-Infrared Spectroscopy (FT-IR) Analysis

Table 4.6 represents a summary of the functional groups from the FT-IR analysis of hydrated PPC mortars both for the non-microbial as well as the microbial mortars. The analysis was done after the 28^{th} day of curing.

Table 4.6 shows FT-IR detectable bands of the Microbial and Non-microbial treated PPC hydrated cement after 28 days of curing.

	Phase	Wave-number (cm^{-1})					
		O-H	O-H (from H_2O)	Si-O (Assym. Stretching)	Al-O	Si-O (in-plane)	C-O, CO_3^{2-}
Main Hydration phases	C-S-H (Ca/Si = 1.5)		3446, 1644	1058, 1097		694, 644	
	Portlandite, $Ca(OH)_2$	3642					
Clinker phases	Ca_2SiO_4, C_2S					518	
	$Ca_3Al_2O_6$, C_3A				779		
Aluminate (Aft/AFm) phases	Ettringite, $Ca_6Al_2(SO_4)_3(OH)_{12}.26H_2O$ or Thaumasite $Ca_6[Si(OH)_6]_2(CO_3)_2(SO_4)_2.24H_2O$		3446,				1741
	Monosulphoaluminate $Ca_4A_{l2}(SO_4)(OH)_{12}.6H_2O$						1427
$CaCO_3$ Polymorphs							2973, 2155, 875.

All the vibrational frequencies occurred at different % transmittance levels for different microbial mortars. FT-IR peaks of all microbial mortar products formed through chemical precipitation and microbiological sedimentation in mortars are 523 – 500 cm^{-1}, 644 cm^{-1}, 694cm^{-1}, 779 cm^{-1}, 1058 cm^{-1}, 1427 cm^{-1}, 1644 cm^{-1}, 1741 cm^{-1}, 2155 cm^{-1}, 2973 cm^{-1}, 3446 $cm^{-1,}$ and 3642 cm^{-1} which correspond to the stretching vibrations of asymmetric Si-O/Al-O stretch, symmetric Si-O, Al-O from C_3A/C_4AF, Si-O stretch from C_3S and Quartz, $CaCO_3$ precipitate, O-H from the hygroscopic $CaCO_3$, $CaCO_3$ precipitate, $CaCO_3$ from the admixture, O-H of water of hydration and O-H of $Ca(OH)_2$, respectively. These stretch wavelengths for cement hydration compounds functional groups are consistent with reported results in the hydrated cement functional groups literature (Horgnies, *et al.*, 2013; Zhang, *et al.,* 2014; Rong and Qian, 2015).

The stretch wavelength at 2973 cm^{-1} to 1741 cm^{-1} has no assigned functional group in the hydrated cement literature values. As earlier indicated 2153 cm^{-1} fall in the range 3000 and 2000 cm^{-1} which are overtone modes (Horgnies, *et al.*, 2013; Stutzman, *et al.*, 2016). Similarly, the stretch at 1741 cm^{-1} could be brought up by overlapping of different functional groups. It could be associated with the overlap of CO_3^{2-} observed at 1424 cm^{-1} and O-H observed at 3311 cm^{-1}. This overlap could be attributed to the presence of $CaCO_3$ which precipitates on the surface of C-S-H.

These wavelengths fall within the range in which $CaCO_3$ is precipitated. Perhaps this could infer the formation of a new polymorphic form of $CaCO_3$. At 875 cm^{-1}, $CaCO_3$ deposition from a ureolytic microbial reaction since it is a polyamide C-O stretch vibration (Horgnies, *et al.*, 2013). The hydrated cement functional groups imply that the microbial treated mortars formed additional hydration products with cementitious properties.

The positions of all of the infrared active modes of calcite, C-S-H, and CH found in each microbial treated mortars as well as in non-microbial treated mortars, closely match those of the reference bands. These results additionally justify the SEM micrographs and XRD analysis results, given earlier in section 4.4 and 4.5 respectively. These findings confirm

that additional cementitious products are formed in microbial treated mortars. Additionally, these results also confirm that the MICP products are both cementitious and are compatible with the typical cement hydration products.

4.9 Compressive Strength

Compressive strength is the capacity of a material or structure to withstand loads tending to reduce its size. It can be measured by plotting applied force against deformation in a compressive strength machine (Young *et al.,* 1998; Thiyagarajan *et al.*, 2016; Munyao, *et al.*, 2020). Some material fracture at their compressive strength limit; others deform irreversibly, so a given amount of deformation may be considered as the limit for the compressive load (KS EAS 148 – 1: 2017).

The compressive strength for all test mortar categories increased with curing age. Across all curing ages, for both microbial treated and non-microbial treated mortars, the OPC categories attained higher compressive strength at an early age compared to their corresponding PPC categories. A similar trend was made by Alexander and Karen, (2012) and Mutitu, (2013). All these authors attributed their observation to the slow strength development on the incorporated pozzolana in PPC. From Bogue's formula analysis, OPC had a higher C_3S content than PPC. C_3S promotes early strength development (Muthengia, 2009; Del Bosque, *et al.*, 2014).

Figure 4.9 is a summary of percentage gain in compressive strength for OPC and PPC bacterial and non-bacterial treated mortars. The percentage gain in compressive strength was determined using equation 3.3 at the 14^{th}, $28^{th,}$ and 56^{th} day of curing.

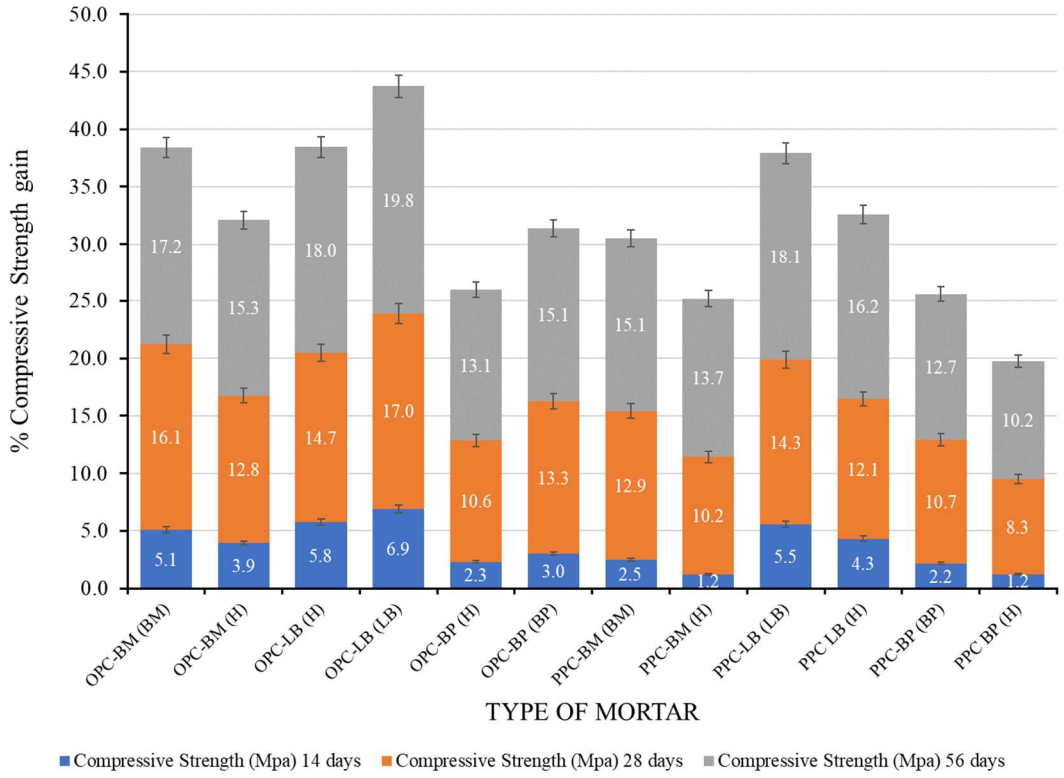

Figure 4.9: Percent gains Compressive strength for varied microbial mortars at 14th, 28th, and 56th day of curing.

Several studies have documented compressive strength improvements on bacterial containing cementitious material of between 9% and 25% by 28th day of curing (Ghosh, *et al.*, 2009; Park, *et al.*, 2010; Vijay and Murmu, 2018). Different researchers have documented both positive and negative effects on compressive strength depending on the bacterial strain, cell concentration, or concrete age (Schwantes-Cezaro, *et al.*, 2019). Bacteria feed nutrients affect compressive strength and cement hydration. Wang, (2013) in his studies using encapsulated *Bacillus sphaericus,* found out that calcium nitrate as a bacterial nutrient accelerated cement hydration while yeast extract significantly delayed the hydration and resulted in lower hydration. The lowered hydration was attributed to a lowered compressive strength on the 90th day of curing. In this study the highest compressive strength and percent compressive strength gain was observed at the 56th day of curing at 19.8 % as shown in Figure 4.9. Statistically significant difference in compressive strength and percentage of compressive strength gain was observed. This

trend was observed both from one curing age to another as well from one microbial mortar category to another across all microbial mortar categories. Microbial treated mortars exhibited higher compressive strength than the non-microbial treated mortars across all the curing ages. The rise in compressive strength could be attributed to the biominerals precipitated by the *Bacillus species* under study. Perhaps, the biomineralization products were involved in the hydration process forming more calcium silicate hydrate bonds. It could also imply that the biominerals precipitated, increased the densification of the hydrated mortar resulting in increased compressive strength.

The added Ca^{2+} together with calcium acetate, in presence of the negative microbial cell-wall, avails a nucleation site that is enriched with Ca^{2+}. (Ersan, *et al.*, 2015; Achal, *et al*., 2016; Thiyagarajan, *et al.*, 2016; Karanja, *et al.*, 2019). The bacterial catalyzed mechanisms, avails the required beryllate ion and other hydrated cement phases, C_3S and C_3A and upon pore saturation, bavenite, $Al_2Be_2Ca_4H_2O_{28}Si_9$ is formed. Bavenite being both siliceous and aluminous, therefore, possess cementitious properties. This characteristic is also similar to other strength contributing compounds in hydrated cement. It can, therefore, be concluded that Bavenite is one of the compressive strength contributing biominerals in the microbial mortars under study.

In this study, it has been found that the microbial biomineralization process enhances the compressive strength hence improving the durability properties of cement-based structures. The enhanced MICP process in this study could also be attributed to the metabolic conversion of the organic acetate added as a microbial feed in form of calcium acetate which was aerobically oxidized under improved alkaline conditions by this ureolytic alkaliphilic *Bacillus spp.* according to equations 2.6 to 2.9.

Amongst the PPC mortar categories, PPC-LB (LB) exhibited the highest compressive strength as well as the highest percentage gain in compressive. Similarly, across all PPC mortar categories, the mortar prisms prepared with or cured in *Lysinibacillus sphaericus* exhibited the highest compressive strength or percent gain in compressive gain amongst

all *Bacillus species* under study. This implies that *Lysinibacillus sphaericus* bacteria precipitate the highest amount of MICP compressive strength development compound.

From the XRD results summarized under Table 4.3 and Table A8 for OPC and PPC mortar categories respectively, it was observed that the percent content of dellaite, $Ca_6H_2O_{13}Si_3$, was highest in the control non-microbial mortar prisms at 83.93 % and 93.80 % for OPC-H (H) and PPC-H (H) respectively, then in any microbial treated mortar. These non-microbial treated mortars did not record any amount of bavenite compound from the XRD analysis.

The sum of both dellaite, $Ca_6H_2O_{13}Si_3$, and bavenite, $Al_2Be_2Ca_4H_2O_{28}Si_9$, in microbial mortar prisms was higher in mortar prisms prepared using *Lysinibacillus sphaericus* than the other microbial mortar prisms. For OPC mortar categories, the average sum of $Ca_6H_2O_{13}Si_3$ and $Al_2Be_2Ca_4H_2O_{28}Si_9$, was 86.00 %, 85.77 %, and 85.51 % for OPC-LB (LB), OPC-BP (BP) and OPC-BM (BM) respectively. A similar trend was observed in PPC mortar categories where the average sum of the two hydration compounds was 92.70 %, 91.10 %, and 90.20 % for PPC-LB (LB), PPC-BP (BP) and PPC-BM (BM) respectively. These two hydration compounds are attributed to the enhanced compressive strength in the microbial mortar prisms than in the control non-microbial mortar prisms. The usual compound responsible for the formation of compressive strength in hydrated mortar/concrete is calcium silicate hydrate, $CaH_2SiO_4.2H_2O$. Empirically, both bavenite and dellaite have a huge/more calcium silicate group than in calcium silicate hydrate compound. This group is present in the two hydrated compounds and could also be attributed to the enhanced compressive strength characteristics, as compared to the control mortar prisms.

The percentage content of dellaite, $Ca_6H_2O_{13}Si_3$ in control OPC-H (H), and PPC-H (H) mortar prisms is higher than in the microbial mortar prisms at 93.80 % and 83.93 % respectively. Even though, these control mortar prisms did not exhibit higher compressive strengths. This implies that the hydrated compound formed in the microbial mortar prisms is a result of the MICP process and contributes to the enriched compressive strength.

4.10 Flexural Strength

The percent gain flexural strength results obtained at 14th, 28th, and 56th day of curing for bacterial treated OPC and PPC test mortar categories are given in Figure 4.10 and Figure 4.11 respectively.

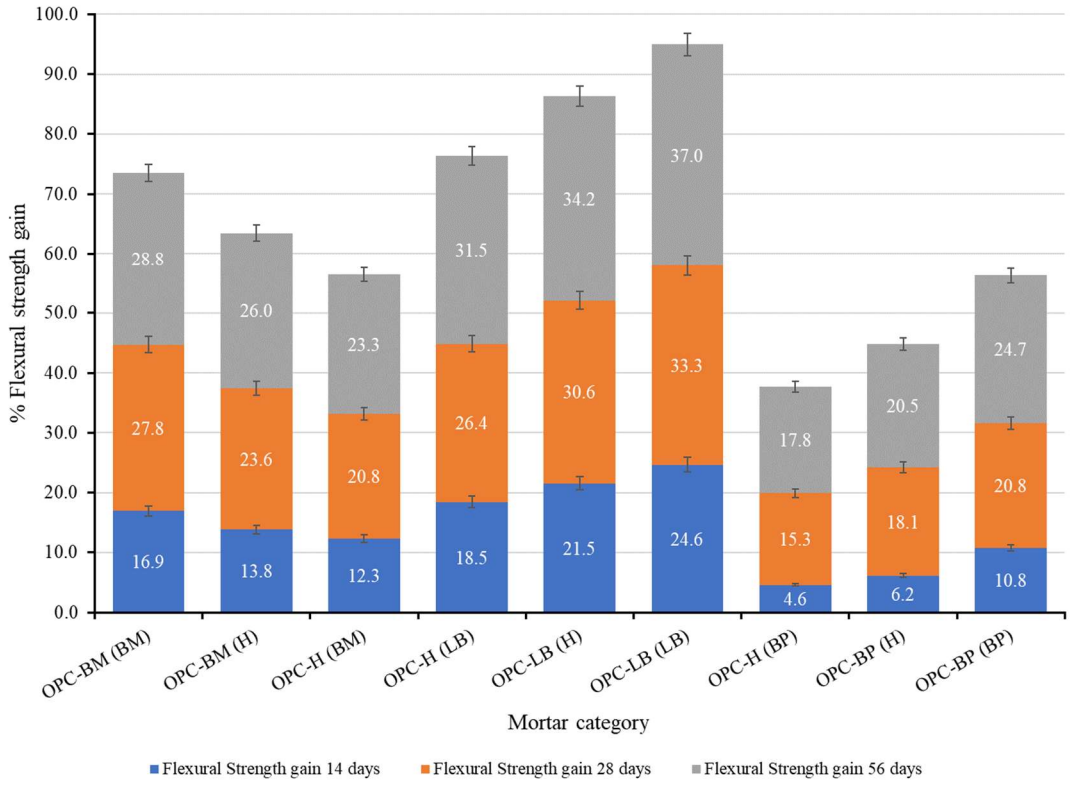

Figure 4.10: Percent gain Flexural strength of OPC-microbial test mortars at 14th, 28th and 56th day of curing

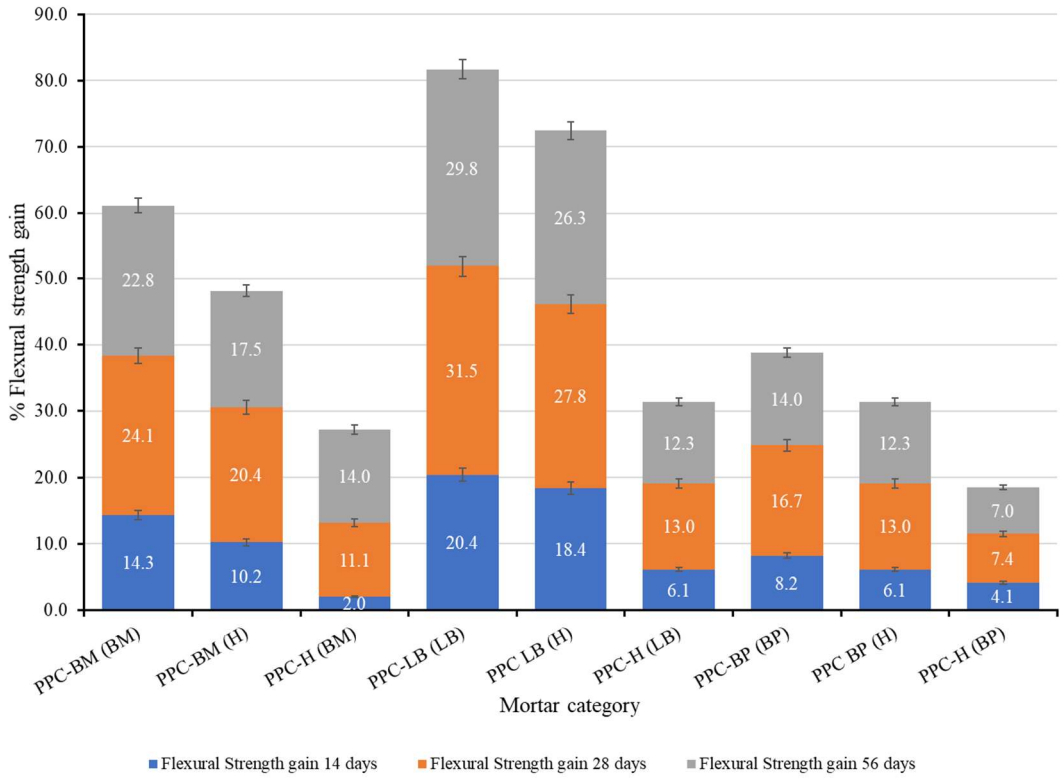

Figure 4.11: Percent gain Flexural strength of PPC-microbial test mortars at 14th, 28th and 56th day of curing

Across all mortar categories under study, there was no significant difference (T_{calc} = 0.5, p = 0.05) in their flexural strengths on the 2nd and 7th day of curing. Perhaps the bacteria had not precipitated significant quantities of calcium carbonate to establish significant nucleation sites or the cement material had not reacted with the precipitation to form a strength beneficial material. The flexural strength across all mortar categories for the three bacteria under study increased with an increase in curing age as depicted in Figure 4.10 and Figure 4.11. Across all the test mortars, the flexural strength increase was higher and more statistically significant between the 14th and 28th day than between the 28th and 56th day of curing. However, among the microbial mortar categories, flexural strength appears to be influenced more both by the type of the bacteria as well as the preparation or curing regime than the curing age.

There was a statistically significant difference in flexural strength across all microbial mortar categories amongst them, as well as between one bacterial treated mortar and another. This could imply that the introduction of the microbial solution, either as preparation or curing regime enhances the formation of C-S-H bond containing material resulting in improved flexural strength. De Muynck, *et al.*, (2010) made similar observations. They attributed this to increased C-S-H bond and $CaCO_3$ precipitate densification.

The flexural strength improvement for mortars of the three bacteria under study was more in the mortar categories where the microbial solution was used as the mortar making mix solution than as the curing regime. Generally, across all curing ages, microbial-OPC mortar categories exhibited higher flexural strengths than their corresponding PPC-microbial categories. OPC-LB (LB) exhibited the highest flexural strength as well as the highest percentage gain in flexural strength than the other mortar categories. The highest flexural strength and percent flexural strength gain was observed at the 56^{th} day of curing at 10.0 Mpa and 37.0 % respectively. There was observed a statistically significant difference in flexural strength and percent flexural strength gain both from one curing age to another as well as from one microbial mortar category to another for all microbial mortar categories. The increase in flexural strength is attributed to the materials precipitated by the microbes being involved in the hydration process forming a C-S-H bond responsible for strength development. The added Ca^{2+} together with calcium acetate, in presence of the microbial cell-wall nucleation site readily combine with the, precipitated siliceous bavenite compound and perhaps crystallizes out as C-S-H bond or as a C-S-H bond containing material. Bavenite also increases the microbial mortar/concrete bulk densification which could also be attributed to the increase in the strengths.

In this study, it has been found that *Bacillus megaterium*, *Sporosarcina pasteurii,* and *Lysinibacillus sphaericus* biomineralization process enhance the flexural strength hence improving durability properties of the cementitious structures. The enhanced MICP process could also be ascribed to the metabolic conversion of the organic acetate added

as a microbial feed in form of calcium acetate which was aerobically oxidized under improved alkaline conditions by these ureolytic alkaliphilic *Bacillus* species (Chahal, *et al.*, 2012; Luo and Qjan, 2016; Qian, *et al.*, 2018). Mortars prepared using *Lysinbacillus sphaericus* precipitate a more crystalline $CaCO_3$ as shown in Figure 4.1. *Bacillus megaterium* and *Sporosarcina pasteurii* prepared mortars, exhibit amorphous $CaCO_3$ precipitate as shown in Figure 4.2 and Figure 4.3 SEM images respectively. This could suggest that, the more crystalline MICP deposits, the stronger the C-S-H bonding. This results to enhanced flexural strength gain by *Lysinbacillus sphaericus* than the other two species.

4.11 Water sorptivity

The percent change in water sorptivity with exposure duration was determined according to equation 3.5. The results are summarized in Figure 4.12, Figure 4.13, and Figure 4.14 representing *Sporosarcina pasteurii, Bacillus megaterium,* and *Lysinibacillus sphaericus* respectively. The results depict a gradual water uptake with time.

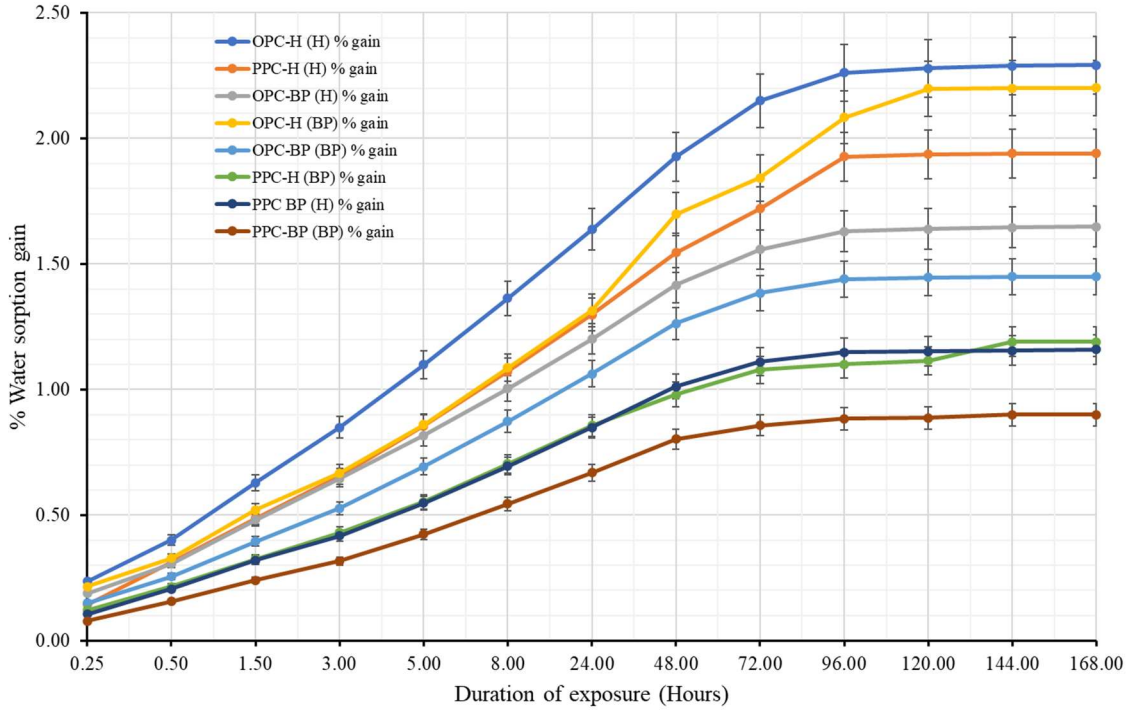

Figure 4.12: Percent water sorption gain for varied *Sporosarcina pasteurii* mortars after the 28th day of curing

From the graphical representation, the non-bacterial treated OPC mortar absorbed the highest amount of water, while the PPC mortar prepared and cured using a solution containing *Sporosarcina pasteurii* absorbed the least water content. After the 120th hour of water absorption, there was no further water uptake across both bacterial treated as well as non-bacterial treated mortars.

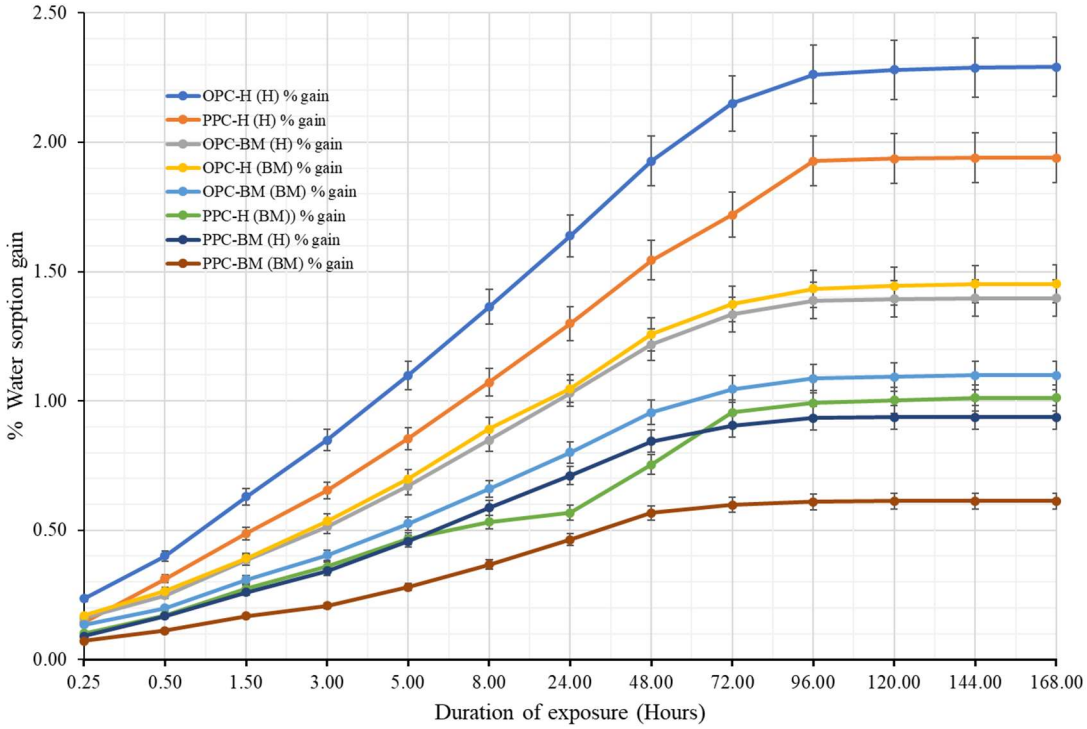

Figure 4.13: Percent water sorption for varied *Bacillus megaterium* mortars after the 28th day of curing

From the graphical representation, the non-bacterial treated OPC mortar absorbed the highest amount of water, while the PPC mortar prepared and cured using a solution containing *Bacillus megaterium* absorbed the least water content. After the 120th hour of water absorption, there was no further water uptake across both bacterial treated as well as non-bacterial treated mortars. This could imply that the mortar matrix pores were saturated disallowing further water uptake.

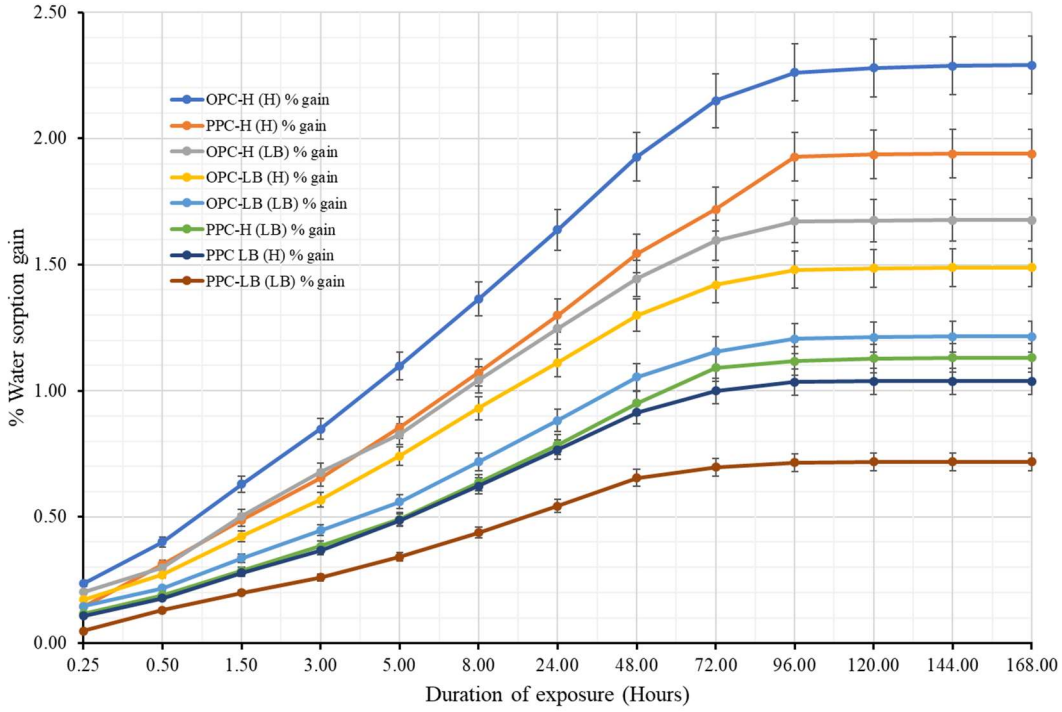

Figure 4.14: Percent water sorption for varied *Lysinibacillus sphaericus* mortars after the 28th day of curing

From the graphical representation, the non-bacterial treated OPC mortar absorbed the highest amount of water, while the PPC mortar prepared and cured using a solution containing *Lysinibacillus sphaericus* absorbed the least water content. After the 120th hour of water absorption, there was no further water uptake across both bacterial treated and non-bacterial treated mortars.

The percentage drop in water sorptivity for microbial treated mortars was determined using equation 3.7. The results are summarized in Table 4.7.

Table 4.7 is a summary of a percent drop in water sorptivity for varied microbial mortars after the 120th hour of water exposure after the 28th day of curing.

Table 4.7: Percent drop water sorptivity for varied microbial mortars after the 28th day of curing.

Bacteria	OPC		PPC	
	Microbial mortar category	Percent water drop	Microbial mortar category	Percent water drop
Bacillus megaterium	OPC-H (BM)	36.56	PPC-H (BM)	47.83
	OPC-BM (H)	38.95	PPC-BM (H)	51.73
	OPC-BM (BM)	52.00	PPC-BM (BM)	68.37
Lysinibacillus sphaericus	OPC-H (LB)	26.77	PPC-H (LB)	41.74
	OPC-LB (H)	34.95	PPC-LB (H)	46.53
	OPC-LB (LB)	46.89	PPC-LB (LB)	62.97
Sporosarcina pasteurii	OPC-H (BP)	3.86	PPC-H (BP)	38.65
	OPC-BP (H)	28.07	PPC-BP (H)	40.43
	OPC-BP (BP)	36.67	PPC-BP (BP)	53.60

This comparative summary in Figures 4.12 to 4.14 and Table 4.7 demonstrates the water sorptivity prevailing effect by the type of cement, *Bacillus species* bacteria, the preparation regime, and the curing regime.

Percent of water sorption increases gradually with exposure duration but after the 120th hour of water exposure, the water sorption almost became constant. Perhaps the mortars became water-saturated such that they could not absorb more water. OPC-H (H), exhibited the highest percent water sorption throughout the water exposure duration, with a high of 2.2914 % after the 120th hour of exposure. For all the three test bacteria, the microbial mortars prepared and cured in microbial solution, PPC-BM (BM), PPC-LB (LB), PPC-BP (BP), exhibited the lowest percentage water sorption across their respective microbial test mortars. The percent water sorption after the 120th hour of exposure was at 0.6136 %, 0.7183 %, and 0.9001 % for PPC-BM (BM), PPC-LB (LB), and PPC-BP (BP) respectively. For the OPC test mortar categories, across the three test

bacteria, the OPC microbial mortars, prepared and cured in the microbial solution again exhibited the lowest water sorption gain. Among the OPC microbial mortars, OPC-BM (BM) recorded the lowest water sorption gain of 1.0984 % after the 120^{th} hour of exposure. This could imply that preparing and curing either OPC or PPC mortars using a microbial solution allows sufficient MICP precipitation which seals the water pathways enhancing water sorption resistivity into the mortar. Dhami, *et al.*, (2012), Achal, *et al.*, (2016) and Supritha, *et al.*, (2016) made similar observations. They attributed this to the availability of nucleation sites. MICP process provides $CaCO_3$ which packs between the mortar aggregates and cement granules which physically seals the pores in the resultant mortar matrix (Al-Salloum, *et al.*, 2017; Karanja, *et al.*, 2019). The $CaCO_3$ sedimentation seals the water migration pathways thus improving on the mortar's porosity resulting in lowered water sorption. All PPC mortar categories already have narrower pores than the OPC mortars. The narrowed pores could be attributed either to the presence of pozzolana or as a result of secondary hydration products. Pozzolanic material improves mortar densification by providing fine particles that pack between the mortar aggregates and cement grains which physically decrease the resultant mortar pore space (Marchand, *et al.*, 2000; Beaudoin and Alizadeh, 2010; Jeffrey, *et al.*, 2012; Mutitu, *et al.*, 2014). Pozzolana reacts with the resultant $Ca(OH)_2$, producing additional cementitious material during the secondary hydration process (Jeffrey, *et al.*, 2012; Liu, *et al.*, 2015; Luo and Qjan, 2016).

Water sorptivity decreased from 3.86 % to 52.00 % for OPC microbial mortars for OPC-H (BP) and OPC-BM (BM) respectively. For PPC microbial mortars, water sorptivity decreased from 38.65 % to 68.37 % for PPC-H (BP) and PPC-BM (BM) respectively. Generally, the OPC microbial mortars exhibited lower water sorptivity drop than the microbial PPC mortars across the three bacterial under study. The mortars prepared and cured using microbial solution exhibited better improvements with the highest drops in water sorption for both OPC and PPC mortar categories. The enhanced water sorptivity percent drop, reflect an improved pore structure. Microbial mortars prepared using water but cured in microbial treated solutions exhibited lower water sorptivity drops than those mortars prepared using the microbial solution but cured in water or those prepared using

the microbial solution and cured in microbial solution. For OPC mortar categories, OPC-BP (H) exhibited the lowest drop at 28.07 % while OPC-BM (H) exhibited the highest drop at 38.95 %. For PPC mortar categories, PPC-BP (H) exhibited the lowest drop at 40.43 % while PPC-BM (H) exhibited the highest drop at 51.73 %.

It was noted that there was a statistically significant effect on water sorptivity by the type of cement used (OPC or PPC), the *Bacillus species*, the preparation regime as well as the curing regime. The effect was more significant from the type of *Bacillus species* used than the other factors. Arunachalan, *et al.*, (2010), Siddique and Chahal, (2011) and Chahal, *et al.*, (2012) observed similar trends. They attributed this to $CaCO_3$ precipitation content. Perhaps, this could also be attributed to the form of $CaCO_3$ precipitated.

Bacillus megaterium mortars had the highest water sorptivity drop than *Lysinibacillus sphaericus* with *Sporosarcina pasteurii* species recording the lowest drop across all mortar categories. This implies that *Bacillus megaterium* is the most suitable species among the three bacteria species under study in lowering water sorption into a mortar structure. It microbially precipitates either the highest quantity of $CaCO_3$ or the form of $CaCO_3$ precipitate is the most compatible with the hydrated cement compounds. Further, upon its precipitate mixing with the cement hydrated compounds, it forms a product with cementitious characteristics which contributes to pore-sealing. The SEM images summarized in Figures 4.1 to 4.6 corroborates this assertion, with the densest calcite precipitates observed in the *Bacillus megaterium* mortars. Pei *et al.*, (2013), Achal., *et al.*, (2016) and Siddique, *et al.*, (2016) observed similar trends. They attributed this to $CaCO_3$ precipitation.

4.11.1 Sorptivity coefficients

Figure 4.15 is a graphical presentation of comparative water sorptivity coefficients for varied microbial OPC mortars, prepared and cured using the respective microbial solution.

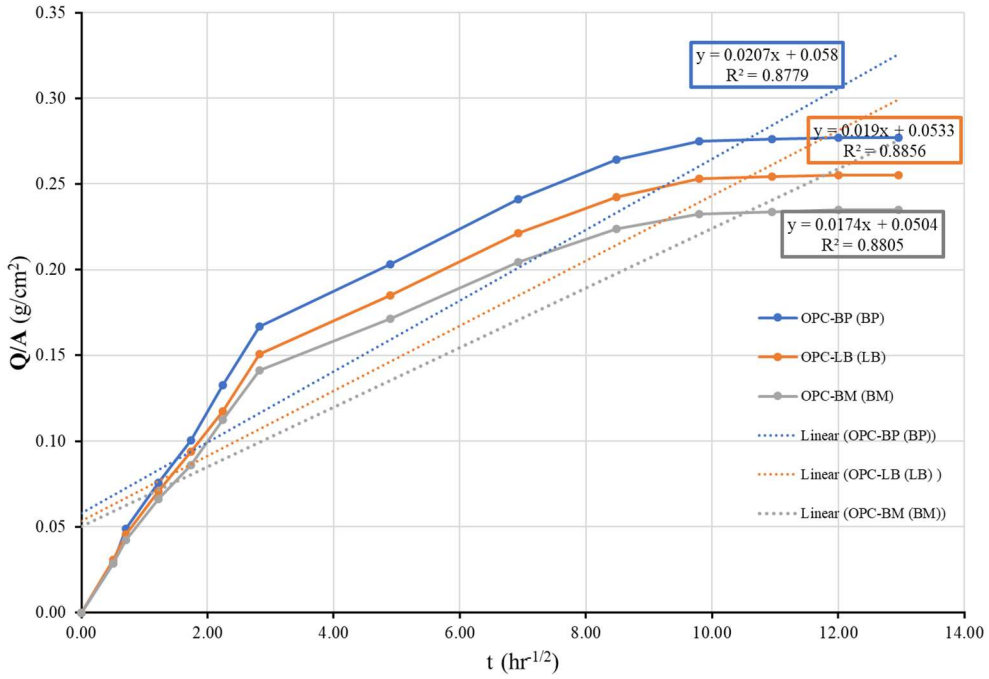

Figure 4.15: Comparative Sorptivity coefficients for OPC-BP (BP), OPC-LB (LB) and OPC BM (BM) mortars after 28th day of curing

As shown in Figure 4.15 it is evident that cement mortars have inherent water uptake pathways. Li and Herbert, (2012), Alghamri, *et al.*, (2016) and Seifan, *et al.*, (2016) made similar observations. They attributed this to the presence of non-hydrated excess cement particles in the mortar matrix, which undergoes delayed or secondary hydration upon reacting with ingress water. The concern, therefore, is not how to eliminate the cracks, but how to reduce/remediate the porosity to deter ingress of excessive water or prevent the ingress of aggressive ions into the mortar/concrete matrix.

From Figure 4.15, it is evident that different bacteria have different water sorption resistance effect. Mortars prepared and cured using *Bacillus megaterium* exhibited a lower uptake than mortars prepared and cured using either of the other two bacteria under study. A decrease in water sorption is attributed to calcite precipitation. Further, it could also be attributed to the compatibility of the deposited calcite with the cement hydration products. From Figure 4.15, it could, therefore, be deduced that *Bacillus megaterium* precipitate the highest calcite content that seals the mortar pores more significantly as the

mortar undergoes hydration than both *Lysinibacillus sphaericus* and *Sporosarcina pasteurii*.

From the experimental data, the water sorption into the test mortars increased gradually with time exhibiting a curve. After the 120th hour of water exposure, the soaked mortars could not absorb any more water and the sorption curve becomes constant. To obtain the sorptivity coefficient for a given test mortar, a linear trend line was drawn on the curve. The resultant water sorptivity coefficients for all the test mortars are summarized in Table 4.8:

Table 4.8: Water sorptivity coefficients summary for varied test mortars after the 28th day of curing.

MORTAR CATEGORY	Sorptivity Coefficient
PPC-H (H)	0.0289
OPC-H (H)	0.0355
PPC-BP (BP)	0.0129
PPC-BP (H)	0.0166
PPC-H (BP)	0.0163
OPC-BP (BP)	0.0207
OPC-BP (H)	0.0231
OPC-H (BP)	0.0314
PPC-BM (BM)	0.0093
PPC-BM (H)	0.0137
PPC-H (BM)	0.0149
OPC-BM (BM)	0.0174
OPC-BM (H)	0.0217
OPC-H (BM)	0.0223
PPC-LB (LB)	0.0112
PPC-LB (H)	0.0154
PPC-H (LB)	0.0170
OPC-LB (LB)	0.0190
OPC-LB (H)	0.0228
OPC-H (LB)	0.0254

Microbial mortar prisms had a higher water sorption resistance than the non-microbial OPC-H (H) and PPC-H (H) mortar prism. The decrease in water sorption could be attributed to the calcium carbonate precipitation which is also evident in the SEM images as shown in Figure 4.1(a) and Figure 4.4(b) for OPC and PPC respectively as compared with the other images under Figure 4.1 to Figure 4.6. Other researchers though using different bacteria such as Achal *et al.*, (2016) using *Sporosarcina pasteurii* and Pei *et al.*, (2013), as well as Dhami *et al.*, (2012) using *Bacillus megaterium* bacteria also observed water sorption reduction in the microbial mortars as compared with mortars prepared without microbial media. All these studies attributed this trend to both the calcium carbonate precipitation and additional calcium silicate hydrate crystallization. The densification that results from precipitation or crystallization decreases water permeability and porosity sealing the pore connectivity in the mortar matrix inhibiting water migration (De Muycnk, *et al.*, 2010; Al-Salloum, *et al.*, 2017).

The trend in sorptivity coefficient values as summarized in Table 4.8 could imply that the incorporation of *Bacillus species* during mortar preparation is more beneficial than exposing a prepared mortar to the microbial solution during the curing process. The improved permeation properties could be attributed to the enriched densification of the resultant mortar caused by the biomineralization from the *Bacillus species* bacteria.

4.12 Chloride Ingress

4.12.1 Chloride Profiling

Results for chloride ingress into the test non-bacterial OPC and PPC mortar prisms and their respective bacterial treated mortars are graphically presented in Figure 4.16, Figure 4.17, and Figure 4.18 for *Bacillus megaterium, Lysinibacillus sphaericus,* and *Sporosarcina pasteurii* respectively. The chloride ion concentration was determined at varied depth of cover within the mortar matrix.

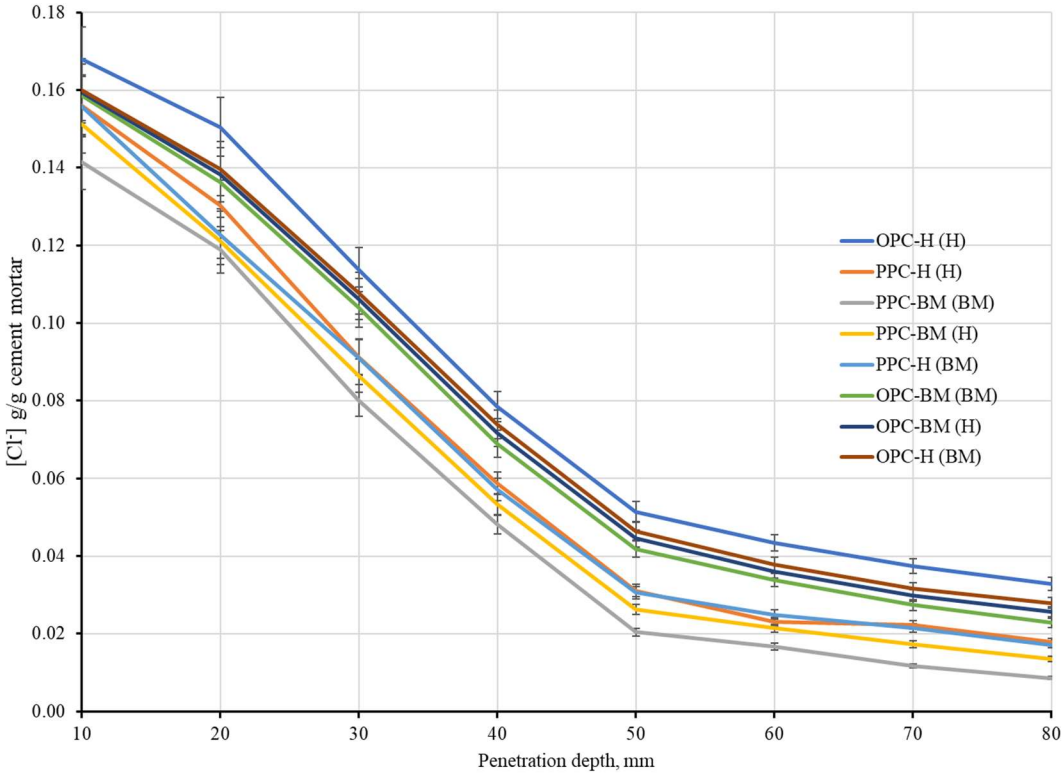

Figure 4.16: Chloride ion concentration at different depth of penetration for control and varied *Bacillus megaterium* microbial mortars.

In all cases, for both OPC and PPC mortar categories, preparation and curing regime affected the ingress of Cl^{1-}. The mortars prepared and cured in *Bacillus megaterium* exhibited the lowest ingress. This trend correlates with that observed by Chahal, *et al.*, (2012), Maes and De Belie, (2016) and Nosouhian, *et al.*, (2016). The authors attributed this to mortar densification. A similar trend was observed in the other microbial mortars as presented in Figure 4.17 and Figure 4.18.

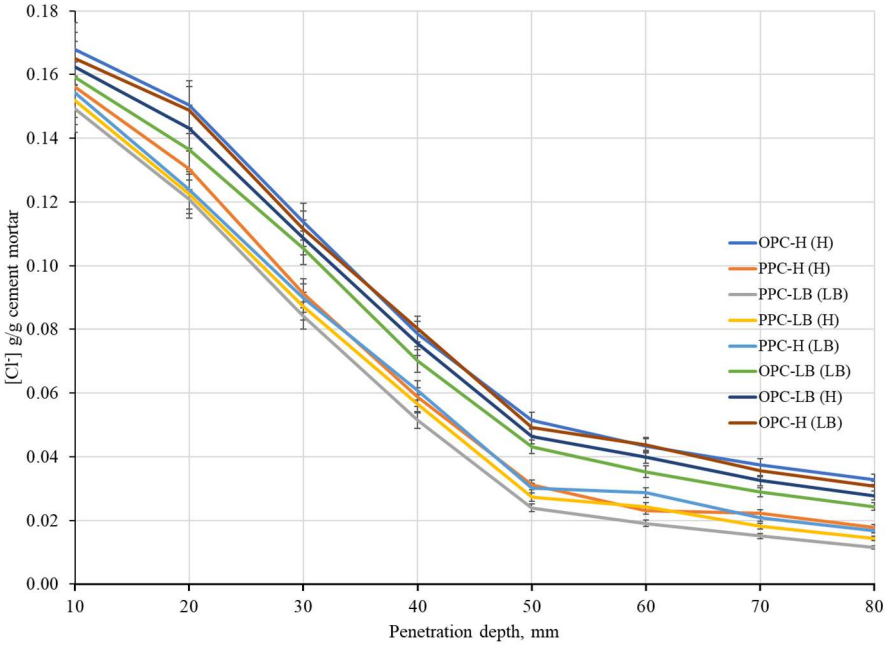

Figure 4.17: Chloride ion concentration at different depth of penetration for control and varied *Lysinibacillus sphaericus* microbial mortars.

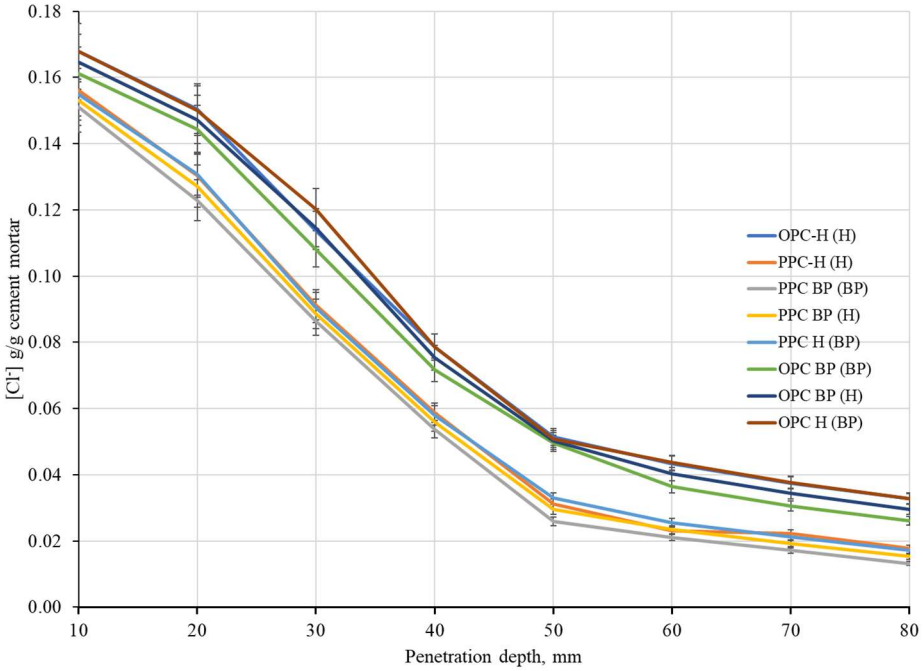

Figure 4.18: Chloride ion concentration at different depth of penetration for control and varied *Sporosarcina pasteurii* microbial mortars.

Generally, in all the mortar prisms, the chloride ion concentration gradually decreased as the depth of the mortar increased. This implies that the nearer the exposure surface is to the chloride solution, the higher is the Cl^- uptake into the mortar matrix. Across all the PPC mortars Cl^- ingress is lower than the OPC mortars. This could be attributed to the fine packing of the pozzolana particles between cement hydration products in PPC, lowering the pores within the mortar matrix. The pozzolanic reaction generates more C-S-H and C-A-H compounds which possess cementitious characteristics (Bai, *et al.*, 2007; Mehta, 2011). In all cases, the bacterial presence affected the ingress of the Cl^-. As observed, the Cl^- ingress was higher across all penetration depths in OPC-H (H) and PPC-H (H) than in all their respective microbial mortars. Perhaps this is due to the lower chloride binding capacity in OPC H (H) than in all test mortars. This could be attributed to the increased content of calcite and C-A-H gels that seal the microbial mortar pore connectivity as observed from SEM results in Figure 4.1 to 4.6. The reduction in chloride ion ingress in microbial mortars across the three test bacterial prepared and cured using microbial solution was higher than in the ones, either, prepared or cured in microbial solutions. This could also be attributed to more packing of MICP precipitates in mortar hydration compounds, further decreasing the permeability.

The presence of microbes in the mortar matrix establishes nucleation sites around which more biochemical calcite precipitation occurs. The trend correlates with that observed by Chahal *et al.*, (2012) and Nosouhian *et al.*, (2016) though involving other types of *Bacillus spp* bacteria. The authors attributed the higher chloride ingress in OPC-H (H) than PPC-H (H) and microbial mortars to continuous and interlinked voids through which the ions ingress. The higher Cl^- ingress observed in OPC mortars could be attributed to lack of a pozzolanic reaction hence the absence of pore refinement hydration products (Abo-El-Enein, *et al.*, 2013). $Ca(OH)_2$ produced during the hydration of OPC mortars is relatively soluble and can readily react with Cl^- forming non-cementitious, amorphous, and expansive products. Perhaps the products formed within the mortar upon ingress of Cl^- increases its porosity leading to more voids (Chahal, *et al.*, 2012; Mutitu, *et al.*, 2014).

Sporosarcina pasteurii OPC and PPC microbial mortars prepared using water but cured using the microbial solution, they exhibited higher Cl^- ingress than OPC-H (H) and PPC-H (H) respectively. However, for *Bacillus megaterium* and *Lysinibacillus sphaericus* mortars all their microbial mortars showed lower chloride ingress than the OPC and PPC mortars prepared and cured using water. The Cl^- ingress was more pronounced in *Bacillus megaterium* mortars than in both *Lysinibacillus sphaericus* and *Sporosarcina pasteurii* microbial mortars. This could be attributed to lowered permeability and porosity due to the calcium carbonate precipitation which seals the pores in the mortar matrix inhibiting chloride ion ingress. The more enhanced Cl^- ingress resistivity by *Bacillus megaterium* than the other two microbes under study, could be attributed to more crystallized content of $CaCO_3$ precipitation. For *Sporosarcina pasteurii*, the calcite precipitation was more amorphous as shown by SEM images represented in Figure 4.3 and of lesser quantity as summarized in Tables 4.3 and A8 for OPC and PPC microbial mortars respectively.

The MICP deposition serves as a barrier as it fills any pore/pathway reducing porosity and thus improves impermeability and ingress resistance. The difference in MICP crystallinity and the quantity between the three test bacteria explains why *Lysinibacillus sphaericus* is a better flexural strength enhancer while *Bacillus megaterium* improves impermeability thus a better chloride ingress inhibitor. Similar observations have been made by other researchers, Chahal *et al.,* (2012), Abo-El-Enein *et al*., (2013), Kim *et al.*, (2013) and Azadi *et al.*, (2017) though using other bacteria species.

4.12.2 Chloride Apparent Diffusivity coefficients

Graphical representation for the chloride error function fitting curve for OPC-BM (BM), is presented in Figure 4.19.

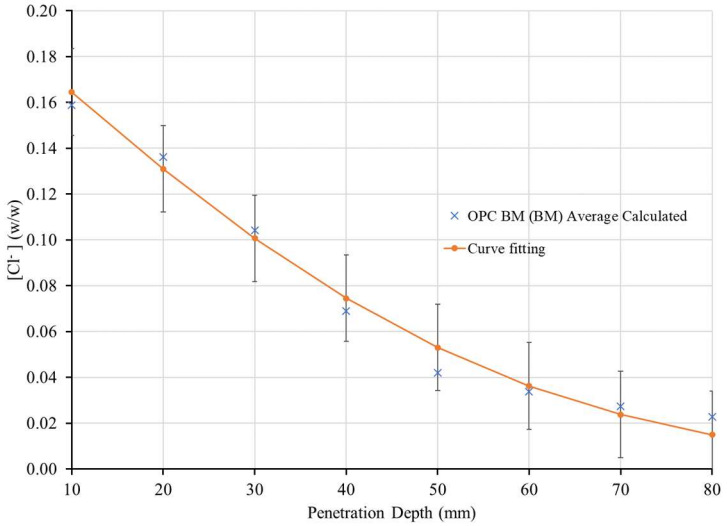

Figure 4.19: Error function fitting for OPC-BM (BM), D_{app} = 3.6407 × 10^{-10} m^2/s and C_s = 0.2016 % (r^2 = 0.9860).

OPC-BM (BM) mortar exhibited a gradual decrease in chloride ingress with depth. The D_{app} value was within the range of 10^{-9} to 10^{-10} m^2/s as reported by other authors (Marchard, *et al.*, 1998; Bertolini, *et al.*, 2004; Mutitu, *et al.*, 2014). The D_{app} value depends on the type/category of mortar/concrete. Results obtained from the chloride error function fitting curve for all the test mortars showing their corresponding D_{app} and D_{mig} with chloride surface concentration (C_s) and r^2 values from the test bacteria under study using 3.5 % by mass sodium chloride solution are summarized in Table 4.9.

Table 4.9: C_S, D_{mig}, D_{app}, and r^2 – values for different microbial mortars in NaCl

MORTAR	C_s (%)	$D_{mig.}$ x 10^{-9} (m^2/s)	$D_{app.}$ x 10^{-10} (m^2/s)	r^2
PPC-H (H)	0.1811	6.9676	3.5340	0.9798
OPC-H (H)	0.2025	9.4792	4.8079	0.9755
PPC-BP (BP)	0.1564	6.6016	3.3484	0.9800
PPC-BP (H)	0.1713	6.7149	3.4059	0.9809
PPC-H (BP)	0.1890	6.4892	3.2914	0.9856
OPC-BP (BP)	0.1997	7.7783	3.9452	0.9848
OPC-BP (H)	0.1945	7.9013	4.0076	0.9842
OPC-H (BP)	0.1941	8.7891	4.4579	0.9816
PPC-BM (BM)	0.1867	5.0174	2.5449	0.9890
PPC-BM (H)	0.1919	5.2161	2.6456	0.9901
PPC-H (BM)	0.1938	6.2674	3.1789	0.9879
OPC-BM (BM)	0.2016	7.1779	3.6407	0.9860
OPC-BM (H)	0.2073	7.9013	4.0076	0.9828
OPC-H (BM)	0.1999	9.3176	4.7260	0.9776
PPC-LB (LB)	0.1926	5.4186	2.7484	0.9881
PPC-LB (H)	0.1971	5.6250	2.8531	0.9877
PPC-H (LB)	0.1965	6.3778	3.2349	0.9848
OPC-LB (LB)	0.2092	7.6563	3.8833	0.9838
OPC-LB (H)	0.2147	7.9013	4.0076	0.9801
OPC-H (LB)	0.2046	9.45219	4.7942	0.9724

OPC-BM (BM), OPC-LB (LB), and OPC-BP (BP) mortars exhibited the lowest apparent diffusion coefficient (D_{app}) than the other OPC microbial mortars. Further, PPC-BM (BM), PPC-LB (LB), and PPC-BP (BP) had the lowest D_{app} values for PPC mortar categories. In both OPC and PPC microbial mortar categories, *Bacillus megaterium* (BM) mortars exhibited the lowest D_{app} values regardless of the preparation and curing regime. This could be attributed to the more crystalline quantity of calcite precipitated by *Bacillus megaterium* mortars than in *Lysinibacillus sphaericus* and *Sporosarcina pasteurii*

mortars. These *Bacillus* bacteria also propagate crystallization of bavenite and additional calcium silicate hydrates. These biomineralization deposits present in the microbial mortars, upon reacting with cement hydration products results in the additional cementitious material. These biominerals make the resultant mortars denser with increased resistivity to Cl^- ingress and lower chloride diffusivity. Chahal, *et al.*, (2012), Uysal, *et al.*, (2012) and Azadi, *et al.*, (2017) observed a similar trend. Similarly, the bacteria cell walls as illustrated in equation 2.9 provide a nucleation site. This is suitable for calcite precipitation among other microbial cement hydrates which add to the densification of the mortar matrix lowering aggressive ion ingress.

4.13 Sulphate Ingress

4.13.1 Sulphate Profiling

Results for sulphate ingress into the test microbial mortars determined at the varied depth of cover within the mortar are graphically presented in Figure 4.20, Figure 4.21 and Figure 4.22 for mortars prepared using water and cured in microbial solution, mortars prepared using the microbial solution and cured in water and mortars prepared and cured using microbial solution respectively.

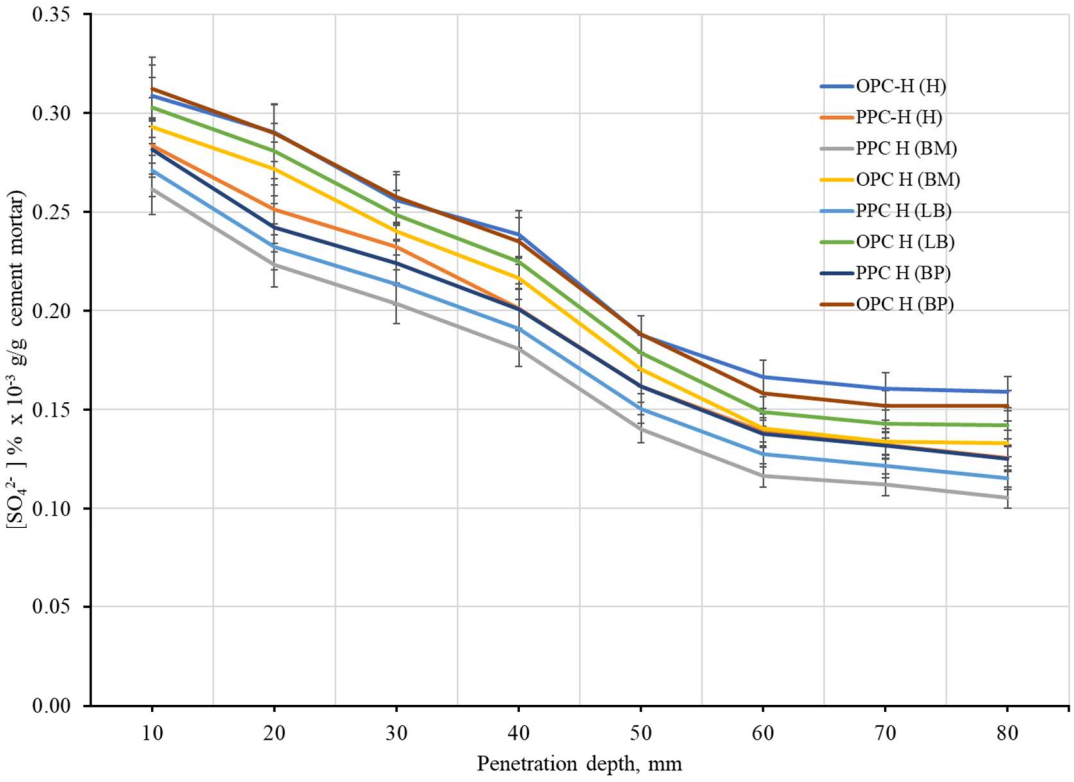

Figure 4.20: Sulphate ion concentration at different depth of penetration for control and varied *Bacillus* microbial mortars prepared using water and cured in microbial solution.

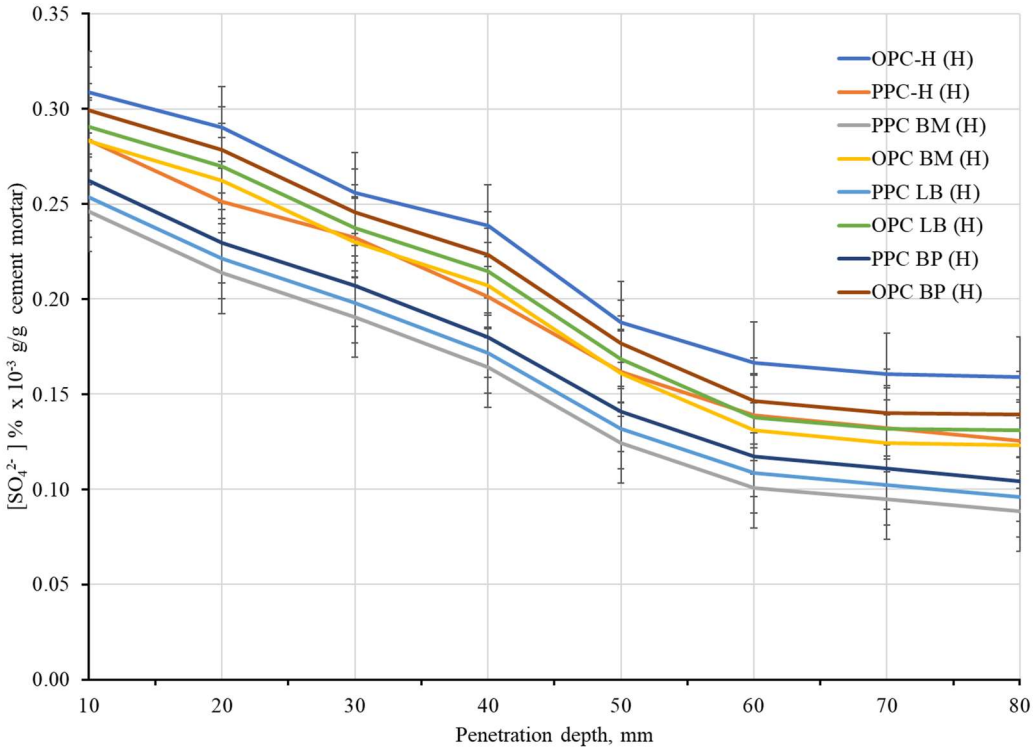

Figure 4.21: Sulphate ion concentration at different depth of penetration for control and varied *Bacillus* microbial mortars prepared using the microbial solution and cured in water.

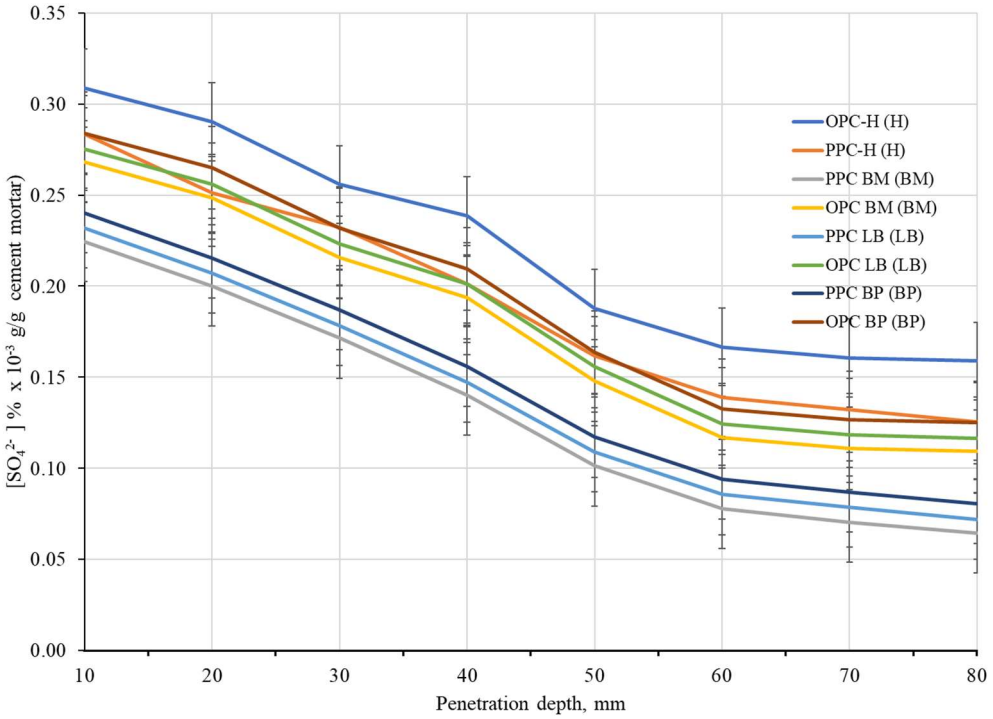

Figure 4.22: Sulphate ion concentration at different depth of penetration for control and varied *Bacillus* microbial mortars prepared and cured using the microbial solution.

Generally, the OPC mortar categories exhibited a higher ingress by the SO_4^{2-} than the PPC mortar categories. This could be attributed to the formation of expansive products within the OPC mortar matrix as shown with equations 4.2 to 4.4. The $Ca(OH)_2$ is mopped up during the pozzolanic reaction within the PPC mortar matrix, forming additional C-S-H which is beneficial. As observed in the SEM images shown in Figure 4.1 to 4.6 as well as in XRD results as summarized in Table 4.3 and Table 4.4, OPC mortar categories showed higher $Ca(OH)_2$ content than PPC mortar categories.

Mostly, the deterioration caused by SO_4^{2-} ingress is as a result of ettringite, $3CaO.Al_2O_3.3CaSO_4 .32H_2O$ or gypsum, $CaSO_4.2H_2O$ formation (De Muynck, *et al.*, 2007; Mutitu *et al.,* 2014). In presence of calcium carbonate in solution, at low

temperatures, thaumasite, $Ca_6[Si(OH)_6]_2(CO_3)_2(SO_4)_2.24H_2O$, formation is favoured (Collepardi, 1999; Barnett, 2000; Bensted, 2002; Hartshorn, *et al.*, 2002).

$Ca(OH)_2$, react with SO_4^{2-} that has ingressed into the cementitious material to form the expansive gypsum according to Equation 4.7.

$$Na_2SO_4 + Ca(OH)_2 + 2H_2O \rightarrow CaSO_4.2H_2O + 2NaOH \qquad 4.7$$

Cement phases such as $3CaO.Al_2O_3$, $4CaO.Al_2O_3.13H_2O$, and $CaSO_4.2H_2O$ can react with sulphate salts to form ettringite, $3CaO.Al_2O_3.3CaSO_4.32H_2O$. Ettringite formation depends on the sulphate salt in pore water, as shown in Equations 4.8 to 4.10

$$3CaO.Al_2O_3 + 3Na_2SO_4 + 3Ca(OH)_2 + 32H_2O \rightarrow 3NaOH + 3CaO.Al_2O_3.3CaSO_4.32H_2O \qquad 4.8$$

$$3(3CaO.Al_2O_3.CaSO_4.12H_2O) + 3Na_2SO_4 \rightarrow 3NaOH + Al_2O_3.3H_2O + 21H_2O + 2(3CaO.Al_2O_3.3CaSO_4.32H_2O) \qquad 4.9$$

$$4CaO.Al_2O_3.13H_2O + CaSO_4.H_2O + 14H_2O \rightarrow Ca(OH)_2 + 3CaO.Al_2O_3.3CaSO_4.32H_2O \qquad 4.10$$

The formation of ettringite is usually accompanied by expansion, softening, or cracking of the cement structure leading to structural degradation (Zhang, *et al.,* 2017). SO_4^{2-} and salts that convert to sulphate usually attack the $Ca(OH)_2$ and $4CaO.Al_2O_3.13H_2O$ phases of hydrated cement thereby degrading it (Muthengia, 2009; Jeffrey, *et al.*, 2012; Mutitu, *et al.*, 2014).

Gypsum and ettringite being expansive could be attributed to the micro-cracks or voids that form in mortars prepared and cured using water in this study. This may result in aggressive ion pathways. Perhaps, the MICP sedimentation that forms in microbial mortars matrix deposits within these micro-cracks and voids sealing them. The calcite deposits form an effective barrier that hinders the ingress of water and aggressive ions.

Thaumasite formation is deleterious as it reacts with hydration products (Bensted, 2002; Barnett 2000). Thaumasite could be formed in pore water in the presence of calcium

carbonate, calcium silicate hydrate, and a sulphate salt in the mortar/concrete matrix. This may occur according to Equation 4.11:

$$Ca_3Si_2O_7.3H_2O + 2CaSO_4.2H_2O + 2CaCO_3 + 24H_2O \rightarrow Ca_6[Si(OH)_6]_2.(CO_3)_2(SO_4)_2.24H_2O + Ca(OH)_2 \quad 4.11$$

In this study, perhaps, the thaumasite formation occured through nucleation over the surfaces of ettringite crystals. This could be supported by the SEM morphologies in which ettringite crystals were visualized as shown by figures 4.3 (a) and (b), Figure 4.5 (a) and (c) and Figure 4.6 (b) and (c). Direct crystallization of thaumasite has been reported to be rare, at temperatures above 15 °C (Nobst and Stark, 2002; Köhler, *et al.*, 2006).

4.13.2 Sulphate Apparent Diffusivity coefficients

Sulphate error function fitting curve for OPC-BM (BM) is presented using Figure 4.23. Results obtained from the sulphate error function fitting curve for the test mortars both for the control and microbial OPC and PPC are summarized in Table 4.10 showing the D_{app} and D_{mig} with corresponding sulphate surface concentration (Cs) and r^2 values of the test mortars from the three bacteria under study using 3.5 % by mass sodium sulphate solution.

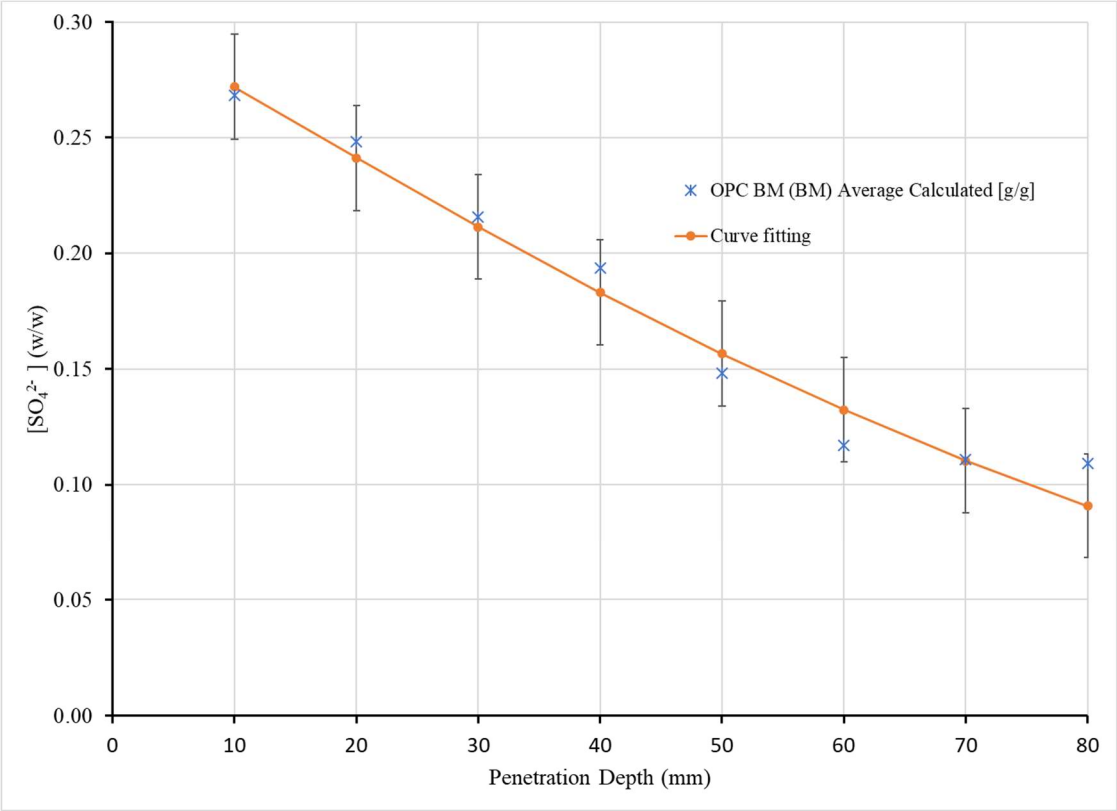

Figure 4.23: Error function fitting for OPC-BM (BM), D_{app} = 5.8124 × 10^{-11} m^2/s and C_s = 0.3033 % (r^2 = 0.9714)

An error function fitting curve was drawn against the experimental values to obtain the D_{app} value. The D_{app} value was within the range of 10^{-11} to 10^{-13} as reported by other researchers (Kawai, *et al.*, 2008; Mutitu, 2013). As reported by these researchers, the D_{app} value depends on the type/category of the mortar/concrete. Results obtained from the sulphate error function fitting curve for all the test mortars showing their corresponding D_{app} and D_{mig} with sulphate surface concentration (C_s) and r^2 values from the test bacteria under study using 3.5 % by mass sodium sulphate solution are summarized in Table 4.10.

Table 4.10: C_S, D_{mig}, D_{app}, and r^2 – values for different microbial mortars in Na_2SO_4

MORTAR TYPE	C_s (%)	$D_{mig.} \times 10^{-9}$ (m^2/s)	$D_{app.} \times 10^{-11}$ (m^2/s)	r^2
OPC-H (H)	0.3512	2.9232	7.4132	0.9618
PPC-H (H)	0.3159	2.5556	6.4810	0.9772
PPC-BM (BM)	0.2493	1.7815	4.5179	0.9824
PPC-BM (H)	0.2762	1.9717	5.0003	0.9809
PPC-H (BM)	0.2800	1.9717	5.0003	0.9909
OPC-BM (BM)	0.3033	2.2919	5.8124	0.9714
OPC-BM (H)	0.3229	2.4241	6.1476	0.9708
OPC-H (BM)	0.3229	2.4241	6.1476	0.9760
PPC-LB (LB)	0.2593	1.7815	4.5179	0.9829
PPC-LB (H)	0.2851	2.0505	5.2001	0.9812
PPC-H (LB)	0.2851	2.0505	5.2001	0.9699
OPC-LB (LB)	0.3128	2.3810	6.0384	0.9706
OPC-LB (H)	0.3321	2.4675	6.2577	0.9699
OPC-H (LB)	0.3321	2.4675	6.2577	0.9765
PPC-BP (BP)	0.2703	1.8564	4.7079	0.9821
PPC-BP (H)	0.2944	2.1715	5.5071	0.9811
PPC-H (BP)	0.2944	2.1715	5.5071	0.9778
OPC-BP (BP)	0.3248	2.4241	6.1476	0.9702
OPC-BP (H)	0.3411	2.6451	6.7082	0.9688
OPC-H (BP)	0.3411	2.64515	6.7082	0.9696

Generally, PPC mortars displayed lower apparent diffusion coefficients (D_{app}) than the OPC mortars both for the control as well across all the test microbial mortars. The lower permeability is attributed to the pozzolanic reaction and packaging of pozzolana grains (Mutitu, 2013). Pozzolana is added to cement to increase compressive strength, lower aggressive ions ingress or water absorption and generally improve the durability of

resultant mortar/concrete (Mutitu, 2013; Muthengia, 2009). Silica fume and a majority of volcanic tuff when used as pozzolana admixture, it enhances durability primarily by decreasing the permeability of the mortar/concrete (Sarsale, *et al.*, 1980; Stocks-Fischer, *et al.*, 1999; Kawai, *et al.*, 2008; Mortureux, *et al.*, 2011). With its reduced permeability pozzolana cement has been extensively used in the construction of marine structures such as bridge decks, walls of buildings, or water tunnels. The pozzolana offers the benefit in reducing the permeability of SO_4^{2-}, Cl^{1-} or any other aggressive ingress ion into the structure (Mutitu, 2013; Muthengia, 2009).

The SO_4^{2-} ingress into OPC-H (H) and OPC-BM (BM) results presented in Figure 4.23 shows that there was lesser SO_4^{2-} ingress in OPC-BM (BM) than in OPC-H (H) at any given depth. A similar trend was observed in other microbial treated mortars as compared with the non-microbial treated ones. Generally, mortars prepared and cured using a microbial solution exhibited lower D_{app} values across the three bacterial mortars. Biocementation in PPC lowers SO_4^{2-} ingress and permeability into the cement matrix (De Muynck, *et al.,* 2010). Stocks-Fischer, *et al., (*1999), observed that this is due to the refinement of the pore structure. SO_4^{2-} penetrate a pore system and form sulphate salts which may crystallize within the pores inducing internal cracks. The cracks affect the physicochemical and beneficial properties of concrete/mortar (Dousti, *et al.*, 2011; Theodore and Karen, 2012; Munyao, *et al.*, 2020).

Many theories have been advanced explaining the expansion of ettringite. Hime and Mather, (1999), for example, proposed that when SO_4^{2-} ingress into a cementitious structure, the resultant gypsum, is formed in solution, and hence it is not expansive. Tian and Cohen, (2000), Mutitu (2013), Yu *et al.*, (2018) and Munyao *et al.*, (2020) in the alternative proposed that on SO_4^{2-} ingress into mortar/concrete structure, ettringite formation leads to expansion, spalling and cracking on concrete/mortar surfaces.

Concrete/mortar microbiological precipitation produces calcium carbonate which seals the pores that appear within its matrix. Calcite also seals/repair cracks that appear on the

structure's surface (Jeffrey, *et al.,* 2012; De Belie and Wang, 2016; Rao and Meena, 2017). These microbial precipitates could also set up nucleation sites that improve the early cement hydration process leading to enhanced sorptivity resistance and lowered ingress of aggressive ions.

Specific *Bacillus species* with a calcium-based feed are mixed during the preparation of concrete/mortar (Karanja, *et al.,* 2019). The insoluble calcium carbonate is precipitated (Theodore and Karen, 2012; Ersan, *et al.,* 2015). This precipitate formed on the cracked surface seal and or cause narrowing of the ingress pathways. The densification of such cementitious material due to microbial reaction is important in reducing the permeability by aggressive ions.

CHAPTER FIVE

CONCLUSIONS AND RECOMMENDATIONS

5.1 Conclusions

The following conclusions were deduced during this research work based on the analysis and discussion of the results obtained.

1. There was significant MICP biomineralization by *Sporosarcina pasteurii, Lysinibacillus sphaericus,* and *Bacillus megaterium* as confirmed by SEM, XRD, and FTIR analysis results.
2. The incorporation of *Bacillus megaterium*, *Lysinibacillus sphaericus, or Sporosarcina pasteurii* to the fresh cement paste, lowered the normal consistency, and accelerated the setting time. CH_3COO^{1-} was a better setting time accelerator than the Cl^{1-}. The addition of either of the test *Bacillus* bacteria into the fresh cement paste in this study did not influence the soundness. Calcite and Bavenite hydration compounds formed across all test microbial treated mortars improved porosity through densification as well as the additional cementitious material. Porosity improvement was more pronounced in PPC than OPC and by *Bacillus megaterium* than the other test *Bacillus* species.
3. *Lysinibacillus sphaericus* MICP leads to enhanced flexural and compressive strength than both *Bacillus megaterium* and *Sporosarcina pasteurii*. The improvement was more pronounced in OPC than in PPC.
4. Mortars prepared and cured using microbial solution exhibited improved water sorption resistivity, lowered chloride, and sulphate apparent diffusivity coefficients than the ones either prepared or cured using a microbial solution. *Bacillus megaterium* MICP provides a better inhibitor for water sorption, chloride and sulphate ingress than both *Lysinibacillus sphaericus* and *Sporosarcina pasteurii.*

5.2 Recommendations

From the findings of this study, the following are recommendations drawn:

5.2.1 Research findings recommendations

1. That use of suitable microbes for improving the physico-chemical and mechanical properties observed from this study be applied on a mortar structure *in - situ*.
2. That further investigation is carried out on the mechanism of bavenite synthesis in bacterial treated mortars.

5.2.2 Further studies

Further to the findings of this study, the following are recommendations for future research work:

1. The mode of bacteria embedment was direct, a pozzolana encapsulation mode of embedment should be adopted with the same bacteria under similar conditions.
2. Further work is necessary on optimum pH, Ca^{2+} concentration, and bacterial feed nutrients for use in improving the physico-chemical and mechanical properties of bacterial treated concrete or mortar.
3. The determination of bacterial growth kinetics and the effect of material property.
4. Determination of the relationship between the bacterial deposited components, kinetics of $CaCO_3$ deposition and the kinetics of microbial agents.

REFERENCES

Abo-El-Enein, S. Ali, A.H., Talkhan, F. N., and Abdel-Gawwad, H. (2013). Application of microbial biocementation to improve the physical-mechanical properties of cement mortar. Housing and Building National Research Center, **9:** 36 – 40.

Achal, V., Mukherjee, A., Zhang, Q.Z. (2016). Unearthing ecological wisdom from natural habitats and its ramifications on the development of biocement and sustainable cities. Landscape Urban Plan; **155**:61 – 68.

Achal, V., Mukherjee, A., Basu, P. C., and Reddy, M. S. (2013). Strain improvement of *Sporosarcina pasteurii* for enhanced urease and calcite production. Journal of Industrial Microbiology and Biotechnology, **36**: 981-988.

Adolphe, J., Loubiére, J. F., Paradas, J., Soleilhavoup, F. (1990). Method of biological treatment of an artificial surface. European patent 90400G97.

Alghamri, R., Kanellopoulos, A., Al-Tabba, A. (2016). Impregnation and encapsulation of lightweight aggregates for self-healing concrete. Constr. Build. Mater. J., **13:** 915–921.

Al-Salloum, Y., Abbas, H., Sheikh, Q. I. (2017). Effect of some biotic factors on microbially-induced calcite precipitation in cement mortar. Saudi J. Biol. Sci. **24**:286 – 294.

Al-Moudi, O. S. B., Masleuddin, M. and Abdul, Y. A. B. (2011). Role of chloride ions on expansion and strength reduction in plain and blended cements in sulphate environment. Construction and building material Journal; **13:** 38 – 43.

Alexander, Q., and Karen, L. S. (2012). Hydration of C_3S-gypsum systems, Laboratory construction materials station 12, CH-1015, Laussane, pg. 52 – 56.

Amiri, A., Azima, M., and Bundur, Z. B. (2018). Crack remediation in mortar via biomineralization: effects of chemical admixtures on biogenic calcium carbonate. *Construction and Building Materials*, **190**: 317 – 325.

Artioli, G., Valentini, L., Voltolini, M., Dalconi, M.C., Ferrari, G., Russo, V. (2015). Direct imaging of nucleation mechanisms by synchrotron diffraction micro-tomography: superplasticizer-induced change of C−S−H nucleation in cement. Cryst Growth Des. **15**:20 – 23.

Arunachalan, K. D., Sathyanarayanan, K. S., Darshan, B.S. (2010). Studies on the characterization of Biosealant properties of *Bacillus sphaericus*. Int. J. Eng. Sci. Technol., **2:**112–119

ASTM C 293 (1990). Standards of flexural strength of concrete, Part 3, effects of variations in testing procedures. American Society for Testing and Materials, Elsevier, London, pg. 34 – 39.

ASTM C 1556 (2004). A standard method for determining the apparent chloride diffusion coefficient of cementitious mixtures by bulk diffusion. American Society for Testing and Materials, Elsevier, London, pg. 596 - 616.

ASTM D 7348 (2013). Standard Test Methods for Loss on Ignition (LOI) of solid combustion residues, ASTM International, West Conshohocken, PA.

Atkins, C. P., Scantleberry, J. D., Nedwell, P. J., and Blatch, S. P. (1996). Monitoring Chloride concentrations in Hardened cement pastes using Ion Selective Electrodes, Cement and Concrete Research, **26:** 319 – 324.

Azadi, M., Ghayoomi, M., Shamskia, N. (2017). Physical and mechanical properties of reconstructed bio-cemented sand, Soils Found. **57:** 698–706.

Bai, J., Wild, S., and Sabir, B. B. (2007). Sorptivity and strength of air-cured and water-cured PC-PFA-MK, concrete, and the influence of binder composition on carbonation depth. Ellis Horwood, London, pg. 1813 – 1821.

Bamforth, P. (2003). Concrete classification for RC structures exposed to marine and other salt-laden environment. Proc. 5th International Symposia on Structural faults and repair. June, 1993, Edinburgh, pg. 31 – 40.

Bang, S., Galinat, J. and Ramakrishnan, V. (2010). Calcite precipitation induced by polyurethane-immobilzed *Bacillus pasteurii*. Enzyme Microb. Technol., **28:** 404 – 409.

Barnett, S. J., Adam, C. D., Jackson, A.R.W. (2000). Solid solutions between ettringite and thaumasite. Journal of Materials Science, **35:** 4109-4114.

Beaudoin, J. J. and Alizadeh, R. (2010). Detection of nanostructural anomalies in hydrated cement systems. Journal of Cement and Concrete Composites, **29:** 68 – 71.

Bensted, J. (2002). Thaumasite – direct, woodfordite and other possible formation routes. Proceedings of the First International Conference on Thaumasite in Cementitious Materials. Building Research Establishment.

Bertolini, L., Elsner, B., Pedeferri, P. and Polder, R. (2004). Corrosion of steel in Concrete: Prevention, Diagnosis and Repair. Wiley – VCH Verlag GMbH & Co. KGaA, Weinheim, pg. 179 – 181.

Blanks, R.F., and Kennedy, H.L. (1955). The Technology of cement and concrete. John Wiley and Sons Incorporation, New York, pg. 121 – 124, 130 - 135.

Bojes, H. K., Pope, P. G. (2007). Characterization of EPA's 16 priority pollutant polycyclic aromatic hydrocarbons (PAHs) in tank bottom solids and associated contaminated soils at oil exploration and production sites in Texas. Regulatory Toxicology and Pharmacology.

Boquet, E., Boronat, A., and Ramos-Cormenzana, A. (1973). Production of calcite (calcium carbonate) crystals by soil bacteria is a general phenomenon. *Nature* **246**: 527–529.

Bossa, N., Chaurand, P., Vicente, J. (2015). Micro- and nano-X-ray computed-tomography: a step forward in the characterization of the pore network of a leached cement paste. Cem Concr Res., **67**:138 – 147.

Botusharova, S. P. (2017) Self-healing geotechnical structures via microbial action – a thesis. Cardiff School of Engineering.

BS EN 12322 (1999). In vitro diagnostic devices – Culture media for microbiology – Performance criteria for culture media. British Standards Institute, London, pg. 21 – 23.

Carmona, J. P. S. F., Oliveira, P. J. V., Lemos, L. J. L. (2016). Biostabilization of a sandy soil using enzymatic calcium carbonate precipitation. Procedia Engineer. **143:** 1301–1308.

Castanier, S., Le Metayer-Levrel, G., and Perthuisot J. P. (1999). Ca-carbonates precipitation and limestone genesis: The microbiogeologist point of view. Journal of Sedimentary Geology, **5**: 12 – 23.

Chahal, N., Siddique, R., and Rajor, A. (2012). Influence of bacteria on the compressive strength, water absorption, and rapid chloride permeability of fly ash concrete. Journal of Construction and Building Materials, **4**: 103 – 119.

Cheng, A.; Huang, R., Wu, J. and Chen, C. (2005). Influence of GGBS on durability and corrosion behavior of reinforced concrete. Journal of Materials Chemistry and Physics, **93**: 40 **–** 45.

Cheng L. and Cord-Ruwisch, R. (2013). Selective enrichment and production of highly urease active bacteria by non-sterile chemostat culture. J Ind Microbiol. Biotechnol. **40**:1095 – 1104.

Cheng, L., Cord-Ruwisch, R., and Shahin, M. A. (2013). Cementation of sand soil by Microbially induced calcite precipitation at various degrees of saturation. Canadian Geotechnical Journal, **50:** 81 - 90.

Chindara, R., Nagulagama, R., and Yadav, S. (2014). Achievement of early compressive strength in concrete using *Sporosarcina pasteurii* bacteria as an admixture. Journal of Advanced Civil Engineering, **1**: 76 – 102.

Chollet, M., and Horgnies, M. (2011). Analyses of the surfaces of concrete by Raman and FT-IR spectroscopies: Comparative study of hardened samples after demoulding and after organic post-treatment, *Surface and Interface Analysis,* **43:**714 – 725.

Collepardi, M. (1999). Thaumasite formation and deterioration in historic buildings. Cement and Concrete Composites, **21:** 147-154

Collepardi, M; Marcialis, M. and Turriziani, R. (1972). Penetration of Chloride ions into Cement pastes and Concrete, *American Ceramic Society*, **55**: 534 – 540.

Cook, D. J. (2006). Calcined Clay, Shale, and Other Soils. Surrey University Press, Glasgow, pg. 12 – 17.

Crank, J. (1975). The Mathematics of Diffusion (2nd Edn.). Oxford University Press, New York, p. 160 – 163.

Dhami, N. K., Reddy, S.M., Mukherjee, A. (2012). Improvement in strength properties of ash bricks by bacterial calcite. Ecol. Eng. p. 39 – 43.

De Belie, N., and Wang J. (2016). Bacteria based repair and self-healing of concrete. Journal of Sustainable Cement-Based Materials, **7**: 35 – 39.

De Jong, J. T. (2013). Biogeochemical processes and geotechnical applications: Progress, opportunities, and challenges. Geotechnique Press, New Delhi, pg. 23 – 41.

Del Bosque, I.F.S., Martinez-Ramirez, S. and Blanco-Varela, M.T. (2014). FTIR study of the effect of temperature and nano-silica on the nanostructure of C–S–H gel formed by hydrating tricalcium silicate. Construction and Building Materials **52**: 314 – 323.

De Muynck, W., De Belie N. and Verstraete W. (2007). Improvement of concrete durability with the aid of bacteria. Proceedings of the First International Conference on Self Healing Materials 18 – 20 April 2007. Journal of Concrete and Materials, **3**: 124 – 139.

De Muynck, W., De Belie, N., and Verstraete, W. (2010). Microbial carbonate precipitation in construction materials. Journal of Ecological Engineering, **5**: 124 – 127.

De Weerdt, K., Orsakova, D., Muller, A.C.A, Larsen, C.K, Pedersen, B.; Geiker, M.R. (2016). Towards the understanding of chloride profiles in marine exposed concrete, the impact of leaching and moisture content, Construction and Building Materials. **Vol. 120**.

Dhami, N. K., Reddy, S. M., and Mukherjee, A. (2012). Improvement in strength properties of ash bricks by bacterial calcite. Journal of Ecological Engineering, **39**: 101 – 110.

Damidot, D., and Glasser, F. P. (1997). Thermodynamic investigation of the CaO-Al_2O_3-$CaSO_4$-$CaCl_2$.H_2O system and the influence of Na_2O, 10^{th} Congress on the Chemistry of Cement. Princeton Incorporation Press, Gothenburg, pg. 105 - 120.

Dhir, R.K., El-Mohr, M. A. K., and Dyer, T. D. (1996). Chloride binding in GGBS concrete. Journal of Cement and Concrete Research, **26**: 1767-1783.

Dong, Z. H., Shi, W., and Guo, X. P. (2011). Initiation and repassivation of pitting corrosion of carbon steel in carbonated concrete pore solution," Corrosion Science, **53:** 1322 – 1330.

Douglas, S., and Beveridge, T. J. (1998). Mineral formation by bacteria in natural microbial communities. Journal of Microbiology and Ecology, **26**: 89 – 97.

Dousti, A., Shekarchi, M., Alizadeh, R., and Taheri-Motlagh, A. (2011). Binding of externally supplied chlorides in micro silica concrete under field exposure conditions. Journal of Cement and Concrete Composites, **33**: 1071 – 1079.

Edvardsen, C. (1999) Water permeability and autogenous healing of cracks in concrete. Journal of Materials and Research **4**: 448 – 454.

Elvira, R. (2012). Advanced Statistical Methods of Analysis of large data-sets, Saunders, College Publishers, FortWorth; p. 1 – 13.

EN 196 21 (2016). Methods of testing cement – Part 21: Determination of the chloride, carbon (IV) oxide, and alkali content of cement. European Union Standards, Beckum, Germany, pg. 34 – 35.

EN 196-1 (2011) Cement part 1: Composition, specifications, and conformity criteria for common cement. European Union Standards, Beckum, Germany.

Ersan, Y.C., Hernandez-Sanabria, N., De Belie, N. (2015). Enhanced crack closure performance of microbial mortar through nitrate reduction. Cement Concrete Res. **70**:159 – 170.

Florea M. V. A. and Brouwers H. J. H. (2012). Chloride binding related to hydration products: Part I: Ordinary Portland Cement. Cement and Concrete Research, **42:** 282 – 290.

Ghosh P., Mandal S., Chattopadhyay B. D., and Pal S. (2009). Use of microorganisms to improve the strength of cement mortar. Journal of Cement and Concrete Research **35**: 1980 – 1983.

Golterman, H. L. (1978). Methods for physical and chemical analysis of freshwater. Blackwell Scientific Publication, Oxford pg. 213 – 214.

Hammad, I. A., Talkhan, F. N. T., Zoheir, A.E. (2013). Urease activity and induction of calcium carbonate precipitation by *Sporosarcina pasteurii* NCIMB 8841. Journal of Applied Science Research, **9:**1525–2013.

Hamdy, E., Ahmed, A., Mohamed, H., Mohamed S. (1999). Effect of Calcium acetate as accelerator and water reducer on the properties of silica fume blended cement. Ceramics – Silikaty, Zagazig, **43:** 29 – 33.

Hartshorn, S. A., Sharp, J. H., Swamy, R. N. (2002). The thaumasite form of sulfate attack in Portland limestone cement mortars stored in a magnesium sulfate solution. Cement and Concrete Composites, **24:** 351-359

Hime, W. G., and Mather, B. (1999). Sulfate attack, or is it? In Cement and Concrete Research, Volume 29, pg. 789-791

Holden, W. R., Page, C. L., and Short, N. R. (1983). The influence of chlorides and sulphates on durability, Symposium on Corrosion of Reinforcement in Concrete Construction. Ellis Horwood Limited, London, pg. 143 – 146.

Horgnies, M., Chen, J. J., Bouillon, C. (2013). Overview about the use of Fourier Transform Infrared spectroscopy to study cementitious materials. WIT Transactions on Engineering Sciences, St. Quentin-Fallavier, France, **77**: 251 – 260.

IS 4031-4 (1988). Methods of Physical Tests for hydraulic cement, Part 4: Determination of consistency of standard cement paste. Bureau of Indian Standards, New Delhi, India.

Jeffrey, J.W., Mondal, P., and Mideley C. M. (2012). Mechanisms of cement hydration. Journal of Cement and Concrete Research, **41:** 1208 – 1223.

Johanneson, B., and Geiker, M. (2012). Self-Healing in cementitious materials and engineered cementitious composite as a self-healing material. Journal of Construction and Building Materials, **28**: 571-578.

Jonkers, H. M., Thijssen, A., Muyzer, G., Copuroglu, O. and Schlangen, E. (2011). Application of bacteria as a self-healing agent for the development of sustainable concrete. Journal of Ecological Engineering, **14**: 325 – 412.

Jupe, A.C., Wilkinson, A.P., Funkhouser, G.P. (2012). Simultaneous study of mechanical property development and early hydration chemistry in Portland cement slurries using X-ray diffraction and ultrasound reflection. Cem Concr Res., **42**:1166 – 1173.

Karanja, D. M., Mulwa, O. M., Wachira J. M., Mwirichia, R., Thiong'o, J. K. and Marangu, J. M. (2019). Effects of biocementation on some properties of cement-based materials incorporating *Bacillus species* bacteria – a review. Journal of Sustainable cement-based Materials, Taylor and Francis, **8**: 309 – 325.

Karol, R. H. (2003). Chemical grouting and soil stabilization, Revised and Expanded. CRC Press, pg. 457 – 489.

Kawai, M. Y., Williams, W., and Nishino, S. (2008). Deterioration of cement hydrates containing mineral admixtures due to sulphuric acid attack. International Publishers Incorporation, Istanbul, pg. 1203 – 1205.

Khaliq, W., Ehsan, M. B. (2016). Crack healing in concrete using various bio influenced self-healing techniques. Construction Build. Mater., **102:** 349 **–** 357.

Khan, A. R., Al-Gadhib, A. H., and Baluch, M. H. (2010). Experimental and Computational modeling of low cycle fatigue damage of CFRP strengthened reinforced concrete beams. International Journal of Damage Mechanics, **2**: 113 – 157.

Kim, H., Park, S., Han, J., and Lee, H. (2013). Microbially mediated calcium carbonate precipitation on normal and lightweight concrete. Construction and Building materials, **38:** 1073 – 1082.

Köhler, S., Heinz, D., Urbonas, L. (2006). Effect of ettringite on thaumasite formation. Cement and Concrete Research, **36:** 697-706.

Kropp, J. and Hilsdorf, H. K. (2010). Performance criteria for concrete durability; State of the art report prepared by RILEM Technical Committee TC116-PCD, performance of cement as a criterion of its durability, E & FN Spon, London, pg. 123 – 376.

KS EAS 18 - 1 (2017). Kenya Standard Test Method for Oxides Specification of Hydraulic cement. Kenya Bureau of Standards, Nairobi, pg. 59 – 61.

KS EAS 148-3 (2017). Cement-Test methods Part 3: Determination of setting times and soundness. Kenya Bureau of Standards, Nairobi. p10 – 15.

Kumar-Jagdeesha, B. G., Prabhakara, R., and Pushpa, H. (2013). Effect of bacterial precipitate on compressive strength of mortar cubes. International Journal of Engineering and Advanced Technology, **7**: 112 **–** 128.

Larbi, J. A. (1993). Microstructures of the interfacial zone around aggregate particles in concrete: Effect of the pore system on chloride ion transport. Journal of Concrete and Materials Research, **38**: 77 - 89.

Lassen, C., Hansen, S. F., Magnusson, K., Hartmann, N. B., Rehne Jensen, P., Nielsen, T. G., & Brinch, A. (2015). Microplastics: occurrence, effects, and sources of releases to the environment in Denmark. Danish Environmental Protection Agency.

Lee, S.G. and Calhoun, D.H. (1997). Urease from a potentially pathogenic coccoid isolate: purification, characterization, and comparison to other microbial ureases, Infect. Immun., American Society of Microbiology, New York, **65**: 3991-3996.

Li, V. C., and Herbert, E. (2012). Robust self- healing concrete for sustainable infrastructure. ACT., **10:** 207–218.

Liu, C., Xu, X., Lv, Z., and Xing, L. (2020). Self-healing of concrete cracks by immobilizing microorganisms in recycled aggregate. *Journal of Advanced Concrete Technology*, JCI, **18**: 168 – 178.

Liu, X., Aranda, M.A.G., Chen, B., Wang, P., Harder, R., Robinson, I. (2015). In situ Bragg coherent diffraction imaging study of a cement phase microcrystal during hydration. Cryst Growth Des., **15**:3087 – 3091.

Luo, M., and Qjan, C. (2016). Influences of bacteria-based self-healing agents on cementitious materials hydration kinetics and compressive strength. Journal of Construction and Building materials, **3**: 81 **–** 115.

Luping, T. and Gullikers, J. (2007). On the Mathematics of Time-dependent Apparent Chloride Diffusion Coefficient in Concrete, Cement and Concrete Research; **33:** 589 **–** 593.

Machard, J., Gerald, B., and Delagrave, A. (1998). Ion transport mechanisms in cement based materials. Journal of Materials Science of Concrete, **5**: 307 – 310.

Maes, M. and De Belie, N. (2016). Service life estimation of cracked and healed concrete in a marine environment. The procedure of concrete solutions. 6th International Conference. Journal on Concrete Repair, **10**: 34 – 39.

Maheshwaran, S., Dasuru, S. S., Murthy, A. R. C., Bhuvaneshwari, B., Kumar, V. R., Palani, G. S., Iyer, N. R., Sarayu, K., and Sandhya, S. (2014). Strength improvement studies using new type wild strain *Bacillus cereus* on cement mortar. Journal of Current Science, **106**: 50 **–** 53.

Majunathan, M., Santosh, A. K., and Ashwinkumar, A. K. (2014). An experimental investigation on the strength and durability aspects of bacterial concrete with fly ash. Journal of Civil and Environmental Research, **6**: 6 – 9.

Mehta, P. K. (2011). The durability of concrete in a marine environment – A review. Performance of concrete in marine environment, Journal of Materials and Concrete Research, **68**: 1 – 15.

Miller, J .C., and Miller, J. N. (1988). Statistics for analytical chemistry. Halsted Press: A Division of John Wiley and Sons, New York, pg. 1 – 36.

Mingyu, H., Funei, L., and Mungshu, T. (2006). The Thaumasite form of Sulphate attack in Concrete of Yongan Dam, Cement and Concrete Research; **36:** 2006 – 2008.

Mobley, H. L., Hausinger, R. P. (1989). Microbial ureases: significance, regulation and molecular characterization. Microbiol. Rev. **59:** 451–480

Mortureux, B., Hornain H., Gautier E., and Regourd M. (2011). Comparison of the reactivity of different pozzolans. Proceedings of the 7th International Congress on the Chemistry of Cement IV, John Wiley, and Sons, New York, pg. 110 – 112.

Mostavi, E., Asadi, S., Hassan, M. M. (2015). Evaluation of self-healing mechanisms in concrete with double-walled sodium silicate microcapsules. J. Mater. Civil Eng., **1:** 1340–1352

Muhammad, I. I., Afifudin, H., and Mohd, S. H. (2014). *Bacillus subtilis* and *Thermus thermophilus* derived bio concrete in enhancing concrete properties. International Sustainable Civil Engineering Journal, **9**: 23 – 45.

Munyao, O. M., Thiong′o, J. K., Wachira, J. M., Mutitu, D. K., Mwirichia, R. and Murithi, G. L. (2019). Use of *Bacillus* Species Bacteria in Protecting the Concrete Structures from Sulphate Attack-A Review. Journal of Chemical Reviews, **1:** 287 – 299.

Munyao, O. M., Thiong'o, J. K., Muthengia, J. W., Mutitu, D. K., Mwirichia, R. and Murithi, G. L., Marangu, J. M. (2020). Study on the effect of *Thiobacillus intermedius* bacteria on the physico-mechanical properties of mortars of ordinary portland cement. Heliyon Journal, Elservier Ltd., pg. 1 – 8.

Muthengia, W. J. (2009). Effects of selected aggressive ions on Pozzolana based Cement made from industrial and agricultural wastes. Kenyatta University Press, Nairobi, pg. 95 – 106.

Mutitu, D. K. (2013). Diffusivity of chloride and sulphate ions into mortar cubes made using Ordinary Portland and Portland Pozzolana cement. Kenyatta University Press, Nairobi, pg. 69 – 83.

Mutitu, D. K., Wachira, J. M., Thiong'o, J. K. (2014). Diffusivity of chloride ion in mortar cubes made using PPC & OPC. IOSR Journal of Applied Chemistry (JAC), e-ISSN 2278-5736, pg. 12 – 25.

Mutitu D. K., Wachira, J. M., Mwirichia, R., Thiong'o, J. K., Munyao, O. M. and Muriithi, G. (2019). Influence of *Lysinibacillus sphaericus* on compressive strength and water sorptivity in microbial cement mortar. Journal of Chemistry, Elsevier Ltd. **5:** 1 – 8.

Mutitu D. K., Wachira, J. M., Mwirichia, R., Thiong'o, J. K., Munyao, O. M. and Muriithi, G. (2020). Biocementation Influence on flexural strength and chloride ingress by *Lysinibacillus sphaericus* and *Bacillus megaterium* in mortar structures, Journal of Chemistry, Hindawi, **2020:** 1 – 13.

NCA, (2017). The Construction industry; Analysis of the state of Built structures, p. 5.

NEMA, (2018). Provision of Sewerage in major towns in Kenya. An performance audit report. **2:** 1 – 42.

Nobst, P., and Stark, J. (2002). Investigations on the influence of cement type on the thaumasite formation. Proceedings of the First International Conference on Thaumasite in Cementitious Materials. Building Research Establishment.

Nosouhian, F., Mostofinejad, D., and Hasheminejad, H. (2016). Concrete durability improvement in a sulphate environment using bacteria. John Wiley and Sons, New York, pg. 89 – 102.

Okoya, B. O. (2013). An investigation into the Cementitious Properties of a Mixture of Rice Husks Ash with Building Lime. University of Nairobi Press, Nairobi, pg. 30 – 83.

Otsuki N., Miyazato S. and Yodsudjai W. (2003). Influence of recycled aggregate on interfacial transition zone, strength, chloride penetration, and carbonation of

concrete. Journal of Materials and Civil Engineering, **15:** 448 – 451.

Rao, V. N., Meena, T. (2017). A review on carbonation study in concrete. IOP Conference, Material Science and Engineering, **263:**1−10.

Pacheco-Torgal, F., Labrincha, J. A. (2013). Biotech cementitious materials: Some aspects of an innovative approach for concrete with enhanced durability. Constr. Build. Mater., **40:** 1136–1141.

Park, S. J., Park, Y. M., Chun, W.Y. (2010) Calcite forming bacteria for compressive strength improvement in mortar. Journal of Microbial Biotechnol. **9**:782 – 788.

Patrick, J., Aditya, K., Emmanuel, G., Robert, J. F., and Karen L. S. (2012). Effect of mixing on the early hydration of alite and OPC systems. Sika Technology Press, Zurich, pg. 2 – 8.

Pei, R., Wang, S., and Yang, M. (2013). Use of bacterial cell walls to improve the Mechanical properties of concrete. Journal of Cement and Concrete Composites, **7:** 39 – 42.

Powers, T. C. (1958). The physical structure and engineering properties of concrete. Portland Cement Association, Bulletin 90, Chicago, pg. 67 − 78.

Qian, C.X., Yu, X.N., Wang, X. (2018). A study on the cementation interface of bio-cement. Mater. Charact.; **59**:1186 – 1193.

Ramakrishnan, V., Panchalan, R. K., and Bang S. S (2007). Improvement of concrete durability by bacterial mineral precipitation. Journal of International Conference on Fracture, **3**: 102 – 159.

Rasanen, V. and Pentalla, V. (2004). The pH measurement of concrete and smoothing mortar using a concrete powder suspension. Cement and Concrete Research; **34:** 813 – 820.

Rasheeduzzafar, T.; Hussain, E. S. and Al-Saadoun, S. S. (2004). Pore solution composition of hydrated cement pastes with reference to corrosion resistance performance of reinforcing steel in concrete, Vetch Middle East NACE Corrosion Conference, Bahrain, 28-30 Oct., p. 386 – 389.

Reddy, S. M., Achal, V., and Mukerjee, A. (2013). Biogenic treatment improves the durability and remediates the cracks of concrete structures. Journal of Construction and Building Materials, **48**: 324 – 350.

Resheidat, M.R., and Ghanma, M.S. (1997). Accelerated strength and testing of concrete using blended cement. Journal of Advanced Cement-Based Materials, **5:** 49 – 51.

Rodriguez-Navarro, C., Rodriguez G., BenChekroun, K. and Gonzalez-Munoz, M.T. (2007). Conservation of ornamental stone by *Myxococcus xanthus* induced carbonate biomineralization. Journal of Application Environmental Microbiology, **69**: 2182 – 2193.

Rong H, Qian C X. (2015). Binding functions of microbe cement. Advanced Engineering Materials, **17**: 334 – 340.

Sahoo, K. K, Arakha, M., Sarkar, P. (2016). Enhancement of properties of recycled coarse aggregate concrete using bacteria. Int J. Smart Nano Mater. **9**: 903 – 910.

Salifu, E., MacLachlan, E., Iyer, K. R., (2016). Application of microbially induced calcite precipitation in erosion mitigation and stabilisation of sandy soil foreshore slopes: a preliminary investigation. Eng. Geol., **201:**96–105.

Sarsale, R. (1980). Structure and characterization of Pozzolanas and Fly ash. Proceedings of The 7th International Congress on the Chemistry of Cements. Journal of Advanced Cement-Based Materials, **5:** 4 – 7.

Schwantes-Cezaro, N., Porto, M. F., Sandoval, G. F. B. (2019). Effects of *Bacillus subtilis* biocementation on the mechanical properties of mortars. Bracon Struct Mater J. **12:**1–18

Seifan, M., Samani, A.K., Berenjian, A. (2016). Bio concrete: next generation of self healing concrete. Appl. Microbiol. Biotechnol.; **100**:2591 – 2511.

Siddique, R., Singh, K., Kunal, V., Singh, C., and Rajor, A. (2016). Properties of bacterial rice husk ash concrete. Journal of Construction and Building Materials, **121**: 34 – 43.

Siddique, R. and Chahal, N. K. (2011). Effect of ureolytic bacteria on concrete properties. Construction and Building materials, **25:** 3791 – 3801.

Sierra-Betran, M. G., Jonker, H. M., and Schlagen, E. (2014). Characterization of sustainable bio-based mortar for concrete repair. Journal of Construction and Building materials, **67**: 35 – 46.

Sookie. S., Bang, W., Galinat, J. K. (2014). Calcite precipitation induced by polyurethane-immobilized *Bacillus pasteurii*. **8:** 99–107

Stocks-Fischer, S., Galinat, J.K., Takemoto, K., and Uchikawa, H. (1999). Hydration of Pozzolanic Cement. Proceedings of the 7th International Congress on the Chemistry of Cements. John Wileys, Paris, pg. 26 – 28.

Stutzman, P. E., and Clifton, J. R. (2015). Specimen preparation for Scanning Electron Microscopy. Proceedings from the 21st International Conference on Cement Microscopy. Gaithersburg, Nevada, pg. 10 – 22.

Stutzman, P. E., Feng, P., Bullard, J. W. (2016). Phase Analysis Of Portland Cement By Combined Quantitative X-Ray Powder Diffraction And Scanning Electron Microscopy. J. Res. Natl. Inst. Stand. Technol. **121:** 47–107.

Supritha, R. M., Shashishankar, A., Shivakumaraswamy, B. (2016). IoT based home Security through image processing algorithms. Int. J. Civil Eng. Res., **7:**67–77.

Suryavanshi, A. K., Scantlebury, J. D. and Lyon, S. B. (1996). Mechanism of Friedel′s salt formation in cements rich in tri-calcium aluminate, Cement and Concrete Research, **26:** 717 – 719.

Theissing, E. M., Mebius-Van De Laar, T., and De Wind, G. (1986). The combining of sodium chloride and calcium chloride by the hardened Portland cement compounds. Proc. 8th International Symposium of Chemistry of cement, Rio de Janeiro, pg. 823 – 827.

Theodore, C., and Karen, S. (2012). Alkali fixation of CSH in blended cement pastes and its relation to alkali-silica reaction. Journal of Construction Materials, **42**: 1049 – 1054.

Thiyagarajan, H., Maheswaran, S., Mapa, M. (2016). Investigation of Bacterial activity on Compressive Strength of cement mortar in different curing Media. ACT. **14**:125 – 133.

Thompson, J. B., Schultze-Lam, S., Beveridge, T. J., and Des Marais, D. J. (1997). Whiting events: biogenic origin due to the photosynthetic activity of cyanobacterial picoplankton. Limnol. Oceanogr. 42, 133–141.

Tian, B., and Cohen, M. D. (2000). Does gypsum formation during sulphate attack on concrete lead to expansion? Cement Concr. Res. **30:** 117–123.

Tziviloglou, E., Wiktor, V., Jonkers, H. M., and Schlangen, E. (2016). Bacteria-based self-healing concrete to increase the liquid tightness of cracks. Journal of Construction and Building Materials, **122**:14 – 19.

Uysal, M., Yilmaz, K., and Ipek, M. (2012). The effect of mineral admixtures on mechanical properties, chloride ion permeability, and impermeability of self-compacting concrete. Construction and Building Materials **27:** 263–270.

Van Tittelboom, K., De Belie, N. (2013). Use of bacteria to repair cracks. Cement Conrete Res. **40:**157–166.

Vekariya, M. S., and Pitroda, J. (2013). Bacterial Concrete. A new era for the construction industry. Intern. J. of Eng. Trends and Tech. (IJETT) **4**: 9 – 16.

Venkateswara V.R., Ramana, N.V., Gnaneswar, K., and Sashidhar, C. (2011). Influence of strong alkaline substances in mixing water on strength and setting properties of concrete. Journal of Indian Engineering and Material Science, **5:** 125 – 133.

Verma, R.K., Chaurasia, L., Bisht, V. (2015). Bio-mineralization and Bacterial carbonate precipitation in Mortar and Concrete. Biosci. Bioeng.**1:** 5–11.

Vijay, K., Murmu, M., Deo, S. V. (2017). Bacteria based self-healing concrete – A review. Constr Build Mater., **152:** 1008–1014.

Vijay, K., and Murmu, M. (2018). Effect of Calcium Lactate on compressive strength and self-healing of cracks in microbial concrete. Front Struct. Civ. Eng.; **5**:1 – 11.

Wachira, J. M. (2012). Chloride Ingress in Pozzolana Based Cement, 7th Kenya Chemical Society International Conference, Abstract Book, Held in Maseno University between 15th – 19th October, 2012.

Walker, S., and Bloem, D. L. (1994). Studies of flexural strength of concrete, Part 3, Effects of variations in testing procedures. Prentice-Hall, New Jersey, pg. 21 – 24.

Wang, J., Basheer, P. M., Nanukuttan, S. V.and Bai, Y. (2014). "Influence of compressive loading on chloride ingress through concrete," in Proceedings of the Civil Engineering Research Association of Ireland (CERAI).

Wang, J. Y. (2013). Self-healing concrete by use of microencapsulated carbonate precipitating bacterial [Ph.D. thesis]. Ghent University Belgium; 131 – 137.

Wang, J. Y., Dewanckele, J., Cnudde, V., Vlierberghe, S.V., Verstraete, W. and De Belie, N., (2014). X-ray computed tomography proof of bacterial-based self-healing in concrete. Cement and Concrete Composites, **53**: 289 – 304.

Williams, S. L., Kirisits, M. J., Ferron, R. D. (2016). Influence of concrete-related environmental stressors on biomineralizing bacteria used in self-healing concrete. Constr Build Mater., **10:** 121–138.

Xu, J., Wang, X. Z., Zuo, J. Q. and Liu, X. Y. (2018). Self-healing of concrete cracks by a ceramsite-loaded microorganism. Advances in Materials science and Engineering.

Yang, C. C., and Cho, S.W. (2003). An electrochemical method for accelerated chloride migration test of the diffusion coefficient in cement-based materials. Journal of Materials Chemistry and Physics, **81:** 116 – 119.

Young, J. F., Mindess, S., Gray, R.J., and Bentur, A. (1998). The science and technology of civil engineering materials. Journal on Science and Technology of Civil Engineering Materials, **4**: 91 – 94.

Yu, X. N., Qian, C. X., Sun, L. Z. (2018). The influence of the number of injections of bio-composite cement on the properties of bio-sandstone cemented by bio-composite cement. Constr Build Mater., **164:** 682–687.

Zhang, J. G., Liu, Y. Z., Feng, T., Zhou, M. J., Zhao, L., Zhou, A. J., and Li, Z., (2017). Immobilizing bacteria in expanded perlite for the crack self-healing in concrete. Construction and Building Materials, **148**: 610 – 617.

Zhang, Y., Guo, H. X., Cheng, X. H., (2014). Influences of calcium sources on microbially induced carbonate precipitation in porous media. Mater. Res. Innov., **18**: 79 – 84.

Zhu, T., and Dittrich, M. (2016). Carbonate Precipitation through Microbial Activities in Natural Environment, and Their Potential in Biotechnology: A Review. Front. Bioeng. Biotechnol.

APPENDICES

APPENDIX A: Raw data for chemical analysis for OPC and PPC

Table A1 OPC and PPC Chemical Analysis Results

Cement Sample	**Cement metal oxides composition % w/w ±S.D**									
	Al_2O_3	**SiO_2**	**SO_3**	**Na_2O**	**K_2O**	**CaO**	**MgO**	**Fe_2O_3**	**MnO**	**LOI**
O1	3.643	22.120	2.697	0.410	0.978	64.678	2.090	3.411	0.170	1.521
O2	3.646	22.000	2.723	0.411	0.975	64.746	2.140	3.397	0.170	1.515
O3	3.641	22.426	2.664	0.410	0.973	64.456	2.021	3.400	0.180	1.520
OPC Average	**3.643 ±0.010**	**22.182 ±0.010**	**2.695 ±0.021**	**0.410 ±0.001**	**0.975 ±0.006**	**64.627 ±0.042**	**2.084 ±0.025**	**3.403 ±0.012**	**0.173 ±0.006**	**1.519 ±0.001**
P1	5.322	33.423	1.454	0.979	1.810	47.413	1.879	4.680	0.234	2.679
P2	5.327	33.412	1.433	0.961	1.867	47.434	1.870	4.562	0.236	2.653
P3	5.202	33.430	1.461	0.986	1.862	47.432	1.890	4.612	0.231	2.671
PPC Average	**5.284 ±0.010**	**33.422±0 .036**	**1.449 ±0.010**	**0.975 ±0.006**	**1.846 ±0.006**	**47.426 ±0.306**	**1.880 ±0.015**	**4.618 ±0.034**	**0.234 ±0.006**	**2.668 ±0.003**

Table A2 Raw data for phase composition of OPC and PPC test cement from Bogue's calculations

Cement category	Sample	Percent phase composition from Bogue's calculations			
		Phase % (w/w) ± S.D.			
		C_3S	**C_2S**	**C_3A**	**C_4AF**
OPC	Sample 1	65.786	13.802	3.884	10.380
	Sample 2	66.975	12.561	3.916	10.338
	Sample 3	62.585	17.094	3.897	10.347
	Average	**65.115 ± 0.854**	**14.485 ± 0.913**	**3.899 ± 0.013**	**10.355 ± 0.018**
PPC	Sample 1	28.381	58.024	6.187	14.242
	Sample 2	29.412	58.125	6.400	13.883
	Sample 3	26.985	59.564	5.984	14.035
	Average	**28.259 ± 0.146**	**58.571 ± 0.893**	**6.190 ± 0.170**	**14.053 ± 0.147**

Table A3 Fresh paste tests Raw data

Test Cement	Setting Time (Minutes)		Normal Consistency (%)	Soundness (mm)
	IST (min)	FST (min)		
Sample 1	98	178	27.9	0.9
Sample 2	90	180	28.1	1.0
Sample 3	98	178	28.0	1.0
OPC- H	98 ± 10	178 ± 10	28.0 ± 0.05	1.0 ± 0.05
Sample 1	80	170	27.4	1.0
Sample 2	90	170	27.5	0.9
Sample 3	80	170	27.4	1.0
OPC-BM	80 ± 10	170 ± 10	27.4 ± 0.05	1.0 ± 0.05
Sample 1	78	167	26.3	0.9
Sample 2	70	160	26.4	1.0
Sample 3	78	167	26.4	1.0
OPC-LB	78 ± 10	167 ± 10	26.4 ± 0.05	1.0 ± 0.05
Sample 1	89	175	22.2	1.0
Sample 2	95	180	22.3	1.0
Sample 3	89	175	22.3	1.0
OPC-BP	89 ± 10	175 ± 10	22.3 ± 0.05	1.0 ± 0.05
Sample 1	150	210	31.2	0.8
Sample 2	140	220	31.2	0.8
Sample 3	160	220	31.2	0.9
PPC-H	150 ± 10	220 ± 10	31.2 ± 0.05	0.8 ± 0.05
Sample 1	135	190	30.2	0.9
Sample 2	140	200	30.3	1.0
Sample 3	135	200	30.2	1.0
PPC-BM	135 ± 10	200 ± 10	30.2 ± 0.05	1.0 ± 0.05
Sample 1	130	190	29.1	1.0
Sample 2	130	180	29.2	1.0

Sample 3	120	190	29.1	1.0
PPC-LB	130 ± 10	190 ± 10	29.1 ± 5	1.0 ± 0.05
Sample 1	140	209	29.3	0.9
Sample 2	130	209	29.4	0.9
Sample 3	140	200	29.4	1.0
PPC-BP	140 ± 10	209 ± 10	29.4 ± 0.05	1.0 ± 0.05

Table A4 EDX Chemical Analysis for varied OPC and PPC paste categories Results

Metal Oxide	Mortar Category							
	OPC-H	**OPC-BM**	**OPC-BP**	**OPC-LB**	**PPC-H**	**PPC-BM**	**PPC-BP**	**PPC-LB**
SiO_2	22.182 ± 0.002	23.984 ± 0.022	23.912 ± 0.002	23.915 ± 0.101	35.422 ± 0.002	36.235 ± 0.004	36.231 ± 0.400	36.294 ± 0.020
CaO	64.226 ± 0.031	64.418 ± 0.005	64.406 ± 0.015	64.479 ± 0.024	47.426 ± 0.001	47.421 ± 0.021	47.615 ± 0.421	47.517 ± 0.014
MgO	2.084 ± 0.061	2.115 ± 0.018	2.203 ± 0.001	2.218 ± 0.070	1.880 ± 0.019	1.921 ± 0.018	1.967 ± 0.038	1.984 ± 0.025
Fe_2O_3	3.313 ± 0.004	1.863 ± 0.028	2.047 ± 0.002	1.773 ± 0.067	4.615 ± 0.013	3.224 ± 0.065	3.391 ± 0.078	2.741 ± 0.017
Al_2O_3	3.643 ± 0.003	3.324 ± 0.017	3.268 ± 0.005	3.279 ± 0.036	5.404 ± 0.012	5.675 ± 0.053	5.456 ± 0.044	5.556 ± 0.013
Na_2O	0.410 ± 0.054	0.345 ± 0.065	0.397 ± 0.044	0.324 ± 0.061	1.175 ± 0.018	0.905 ± 0.049	0.899 ± 0.302	0.886 ± 0.018
K_2O	0.975 ± 0.014	0.633 ± 0.056	0.601 ± 0.051	0.614 ± 0.022	1.846 ± 0.019	1.712 ± 0.091	1.745 ± 0.009	1.729 ± 0.002
WO_3	0.018 ± 0.002	0.083 ± 0.006	0.043 ± 0.041	0.077 ± 0.029	0.011 ± 0.071	0.097 ± 0.033	0.049 ± 0.010	0.086 ± 0.032
SO_3	2.695 ± 0.007	2.202 ± 0.078	2.195 ± 0.019	2.205 ± 0.042	1.449 ± 0.065	1.224 ± 0.054	1.217 ± 0.008	1.353 ± 0.006
BeO	0.081 ± 0.004	0.252 ± 0.069	0.256 ± 0.056	0.263 ± 0.019	0.097 ± 0.088	0.423 ± 0.021	0.414 ± 0.051	0.435 ± 0.002
SrO	0.012 ± 0.007	0.098 ± 0.033	0.067 ± 0.002	0.101 ± 0.022	0.043 ± 0.091	0.113 ± 0.044	0.105 ± 0.061	0.184 ± 0.046
MnO	0.173 ± 0.005	0.188 ± 0.076	0.183 ± 0.006	0.197 ± 0.013	0.234 ± 0.086	0.194 ± 0.079	0.236 ± 0.045	0.254 ± 0.017
TiO_2	0.034 ± 0.041	0.096 ± 0.098	0.071 ± 0.079	0.104 ± 0.066	0.071 ± 0.018	0.171 ± 0.019	0.112 ± 0.056	0.175 ± 0.031

Sc_2O_3	0.011	0.068	0.055	0.076	0.039	0.101	0.097	0.118
	± 0.032	± 0.026	± 0.005	± 0.002	± 0.023	± 0.017	± 0.045	± 0.033
Y_2O_3	0.045	0.104	0.094	0.121	0.095	0.154	0.143	0.197
	± 0.036	± 0.096	± 0.098	± 0.003	± 0.018	± 0.026	± 0.069	± 0.047
RbO_2	0.009	0.019	0.011	0.022	0.014	0.071	0.066	0.092
	± 0.002	± 0.083	± 0.061	± 0.001	± 0.042	± 0.007	± 0.003	± 0.091
NbO	0.048	0.112	0.102	0.119	0.091	0.186	0.135	0.209
	± 0.054	± 0.079	± 0.002	± 0.002	± 0.034	± 0.062	± 0.031	± 0.073
ZrO_2	0.041	0.096	0.089	0.113	0.088	0.173	0.122	0.191
	± 0.087	± 0.004	± 0.051	± 0.045	± 0.031	± 0.012	± 0.002	± 0.058
Total	100.000	100.000	100.000	100.000	100.000	100.000	100.000	100.000

Table A5: Raw data for compressive strength of test mortars at the 14th, 28th and 56th day of curing

Test Cement/Mortar	Compressive Strength (Mpa)		
	14th day	**28th day**	**56th day**
Sample 1	43.2	48.3	49.1
Sample 2	43.4	48.1	48.9
Sample 3	43.6	48.6	48.8
OPC -H (H)	**43.4 ± 0.2**	**48.3 ± 0.2**	**48.9 ± 0.1**
Sample 1	44.7	53.5	55.0
Sample 2	44.5	53.2	54.7
Sample 3	44.4	53.3	54.6
OPC-H (BM)	**44.5 ± 0.1**	**53.3 ± 0.1**	**54.8 ± 0.2**
Sample 1	45.8	55.8	57.2
Sample 2	45.5	56.3	57.3
Sample 3	45.6	56.1	57.5
OPC-BM (BM)	**45.6 ± 0.1**	**56.1 ± 0.2**	**57.3 ± 0.1**
Sample 1	45.3	54.8	56.2
Sample 2	45.1	54.5	56.4
Sample 3	45.0	54.3	56.7
OPC-BM (H)	**45.1 ± 0.1**	**54.5 ± 0.2**	**56.4 ± 0.2**
Sample 1	44.5	52.9	54.6
Sample 2	44.0	52.7	54.4
Sample 3	44.2	52.6	54.2
OPC-H (LB)	**44.2 ± 0.2**	**52.7 ± 0.1**	**54.3 ± 0.2**
Sample 1	46.0	55.1	57.9
Sample 2	45.6	55.4	57.8
Sample 3	46.2	55.6	57.5
OPC-LB (H)	**45.9 ± 0.2**	**55.4 ± 0.2**	**57.7 ± 0.2**
Sample 1	46.3	56.7	58.8
Sample 2	46.5	56.5	58.9

Sample 3	46.6	56.3	58.1
OPC-LB (LB)	**46.4 ± 0.1**	**56.5 ± 0.2**	**58.6 ± 0.4**
Sample 1	43.8	52.4	54.0
Sample 2	43.7	52.6	53.6
Sample 3	44.1	52.3	53.7
OPC-H (BP)	**43.9 ± 0.2**	**52.4 ± 0.1**	**53.8 ± 0.2**
Sample 1	44.2	53.0	55.5
Sample 2	44.4	53.6	55.3
Sample 3	44.6	53.6	55.1
OPC-BP (H)	**44.4 ± 0.2**	**53.4 ± 0.3**	**55.3 ± 0.2**
Sample 1	44.3	54.9	56.0
Sample 2	44.8	54.7	56.5
Sample 3	44.9	54.5	56.4
OPC-BP (BP)	**44.7 ± 0.3**	**54.7 ± 0.2**	**56.3 ± 0.2**
Sample 1	32.3	36.4	37.2
Sample 2	32.4	36.5	37.1
Sample 3	32.6	36.0	37.0
PPC-H (H)	**32.5 ± 0.1**	**36.3 ± 0.2**	**37.1 ± 0.1**
Sample 1	33.5	41.2	42.9
Sample 2	33.1	40.9	42.5
Sample 3	33.3	41.0	42.7
PPC-BM (BM)	**33.3 ± 0.2**	**41.0 ± 0.1**	**42.7 ± 0.2**
Sample 1	32.9	39.9	42.4
Sample 2	32.5	40.2	42.1
Sample 3	33.3	40.0	42.1
PPC-BM (H)	**32.9 ± 0.3**	**40.0 ± 0.1**	**42.2 ± 0.1**
Sample 1	32.6	40.1	41.3
Sample 2	32.9	39.7	41.1
Sample 3	33.1	39.9	40.8
PPC-H (BM)	**32.9 ± 0.2**	**39.9 ± 0.2**	**41.1 ± 0.2**

Sample 1	34.6	41.8	43.6
Sample 2	34.0	41.4	43.9
Sample 3	34.3	41.3	44.0
PPC-LB (LB)	**34.3 ± 0.2**	**41.5 ± 0.2**	**43.8 ± 0.2**
Sample 1	34.0	40.4	42.9
Sample 2	33.8	40.7	43.0
Sample 3	33.9	41.1	43.3
PPC-LB (H)	**33.9 ± 0.1**	**40.7 ± 0.3**	**43.1 ± 0.2**
Sample 1	33.3	39.9	40.4
Sample 2	33.1	39.5	40.9
Sample 3	32.8	39.4	40.7
PPC-H (LB)	**33.1 ± 0.2**	**39.6 ± 0.2**	**40.7 ± 0.2**
Sample 1	33.3	40.1	41.7
Sample 2	33.1	39.9	42.0
Sample 3	33.2	40.5	41.7
PPC-BP (BP)	**33.2 ± 0.1**	**40.2 ± 0.2**	**41.8 ± 0.1**
Sample 1	32.6	39.5	41.1
Sample 2	32.9	39.5	40.9
Sample 3	33.2	38.8	40.7
PPC-BP (H)	**32.9 ± 0.2**	**39.3 ± 0.3**	**40.9 ± 0.2**
Sample 1	33.1	39.1	40.6
Sample 2	32.6	38.7	40.2
Sample 3	32.7	38.9	40.4
PPC-H (BP)	**32.8 ± 0.2**	**38.9 ± 0.2**	**40.4 ± 0.2**

Table A6: Raw data for flexural strength of test mortars at the 14th, 28th and 56th day of curing

Test Cement/Mortar	Compressive Strength (Mpa)		
	14th day	**28th day**	**56th day**
Sample 1	6.5	7.3	7.3
Sample 2	6.5	7.1	7.2
Sample 3	6.6	7.1	7.4
OPC -H (H)	**6.5± 0.05**	**7.2 ± 0.09**	**7.3 ± 0.08**
Sample 1	7.6	9.1	9.5
Sample 2	7.5	9.2	9.3
Sample 3	7.6	9.3	9.4
OPC-BM (BM)	**7.6 ± 0.05**	**9.2 ± 0.08**	**9.4 ± 0.08**
Sample 1	7.3	8.9	9.2
Sample 2	7.5	9.0	9.3
Sample 3	7.5	8.9	9.1
OPC-BM (H)	**7.4 ± 0.09**	**8.9 ± 0.05**	**9.2 ± 0.08**
Sample 1	7.2	8.7	9.1
Sample 2	7.3	8.8	9.0
Sample 3	7.3	8.6	9.0
OPC-H (BM)	**7.3 ± 0.05**	**8.7 ± 0.08**	**9.0 ± 0.05**
Sample 1	7.9	9.3	9.7
Sample 2	7.8	9.4	9.8
Sample 3	7.9	9.4	9.8
OPC-LB (H)	**7.9 ± 0.05**	**9.4 ± 0.05**	**9.8 ± 0.05**
Sample 1	7.6	9.2	9.6
Sample 2	7.8	9.1	9.5
Sample 3	7.7	9.1	9.7
OPC-H (LB)	**7.7 ± 0.05**	**9.1 ± 0.05**	**9.6 ± 0.08**
Sample 1	8.0	9.7	10.1
Sample 2	8.1	9.5	9.8

Sample 3	8.1	9.6	10.0
OPC-LB (LB)	**8.1 ± 0.05**	**9.6 ± 0.08**	**10.0 ± 0.12**
Sample 1	6.7	8.3	8.5
Sample 2	6.8	8.2	8.6
Sample 3	6.6	8.5	8.7
OPC-H (BP)	**6.7 ± 0.05**	**8.3 ± 0.06**	**8.6 ± 0.05**
Sample 1	6.8	8.6	8.8
Sample 2	6.9	8.4	8.8
Sample 3	6.9	8.5	8.7
OPC-BP (H)	**6.9 ± 0.05**	**8.5 ± 0.08**	**8.8 ± 0.05**
Sample 1	7.1	8.8	9.1
Sample 2	7.3	8.7	9.2
Sample 3	7.2	8.7	8.9
OPC-BP (BP)	**7.2 ± 0.08**	**8.7 ± 0.05**	**9.1 ± 0.12**
Sample 1	4.9	5.6	5.7
Sample 2	4.9	5.4	5.8
Sample 3	4.8	5.2	5.5
PPC-H (H)	**4.9 ± 0.05**	**5.4 ± 0.16**	**5.7 ± 0.12**
Sample 1	5.7	6.9	7.1
Sample 2	5.4	6.7	6.9
Sample 3	5.6	6.4	6.9
PPC-BM (BM)	**5.6 ± 0.12**	**6.7 ± 0.21**	**7.0 ± 0.09**
Sample 1	5.3	6.6	6.6
Sample 2	5.4	6.4	6.6
Sample 3	5.4	6.4	6.8
PPC-BM (H)	**5.4 ± 0.05**	**6.5 ± 0.09**	**6.7 ± 0.09**
Sample 1	5.0	6.2	6.6
Sample 2	4.8	5.8	6.4
Sample 3	5.0	6.0	6.5
PPC-H (BM)	**5.0 ± 0.05**	**6.0 ± 0.16**	**6.5 ± 0.08**

Sample 1	5.9	7.0	7.3
Sample 2	5.9	7.2	7.4
Sample 3	5.8	7.2	7.6
PPC-LB (LB)	**5.9 ± 0.05**	**7.1 ± 0.09**	**7.4 ± 0.12**
Sample 1	5.8	6.9	7.3
Sample 2	5.6	6.7	7.1
Sample 3	5.9	7.1	7.4
PPC LB (H)	**5.8 ± 0.12**	**6.9 ± 0.16**	**7.2 ± 0.17**
Sample 1	5.2	6.0	6.3
Sample 2	5.3	6.3	6.5
Sample 3	5.1	6.1	6.5
PPC-H (LB)	**5.2 ± 0.08**	**6.1 ± 0.12**	**6.4 ± 0.09**
Sample 1	5.3	6.2	6.7
Sample 2	5.4	6.4	6.4
Sample 3	5.2	6.2	6.5
PPC-BP (BP)	**5.3 ± 0.08**	**6.3 ± 0.09**	**6.5 ± 0.12**
Sample 1	5.2	6.2	6.6
Sample 2	5.2	5.9	6.3
Sample 3	5.1	6.0	6.2
PPC BP (H)	**5.2 ± 0.05**	**6.0 ± 0.12**	**6.4 ± 0.17**
Sample 1	5.1	5.9	6.2
Sample 2	5.1	5.7	6.3
Sample 3	5.0	5.8	5.9
PPC-H (BP)	**5.1 ± 0.08**	**5.8 ± 0.08**	**6.1 ± 0.17**

Table A7: XRD (% w/w ± S. D. values) summary for hydrated OPC microbial mortars prepared and cured in respective the microbial solution against control OPC mortar after the 28th day of curing

		MORTAR CATEGORY (% w/w ± S. D.)			
HYDRATION COMPOUND		**OPC-H**	**OPC-LB**	**OPC-BM**	**OPC-BP**
Bavenite, $Al_2Be_2Ca_4H_2O_{28}Si_9$	Sample 1	-	2.55	1.36	1.99
	Sample 2	-	2.52	1.33	2.14
	Sample 3	-	2.51	1.29	2.12
% Average ± S. D.		-	**2.53 ± 0.02**	**1.33 ± 0.03**	**2.08 ± 0.07**
Dellaite, $Ca_6H_2O_{13}Si_3$	Sample 1	83.89	83.49	84.21	83.90
	Sample 2	83.95	83.47	84.18	83.87
	Sample 3	83.94	83.45	84.16	83.88
% Average ± S.D.		**83.93 ± 0.03**	**83.47 ± 0.02**	**84.18 ± 0.02**	**83.69 ± 0.03**
Calcite, $CaCO_3$	Sample 1	0.67	10.26	10.24	10.21
	Sample 2	0.63	10.22	10.29	10.23
	Sample 3	0.61	10.21	10.27	10.19
% Average ± S.D.		**0.64 ± 0.02**	**10.23 ± 0.02**	**10.27 ± 0.02**	**10.21 ± 0.02**
Portlandite, $Ca(OH)_2$	Sample 1	15.43	3.79	4.21	3.83
	Sample 2	15.48	3.75	4.17	3.82
	Sample 3	15.49	3.78	4.19	3.79
% Average ± S.D.		**15.47 ± 0.03**	**3.77 ± 0.02**	**4.19 ± 0.02**	**3.81 ± 0.02**

Table A8: XRD (% w/w ± S. D. values) summary for hydrated PPC microbial mortars prepared and cured in the respective microbial solution against non-microbial PPC mortar after 28th day of curing

HYDRATION COMPOUND		MORTAR CATEGORY (% w/w ± S. D.)			
		PPC-H	PPC-LB	PPC-BM	PPC-BP
Bavenite, $Al_2Be_2Ca_4H_2O_{28}Si_9$	Sample 1	-	12.33	14.92	13.88
	Sample 2	-	12.30	14.89	13.85
	Sample 3	-	12.28	14.90	13.87
% Average ± S.D.		**-**	**12.30 ± 0.02**	**14.90 ± 0.01**	**13.87 ± 0.01**
Dellaite, $Ca_6H_2O_{13}Si_3$	Sample 1	93.78	80.43	75.29	77.25
	Sample 2	93.82	80.38	75.32	77.22
	Sample 3	93.79	80.40	75.28	77.21
% Average ± S.D.		**93.80 ± 0.02**	**80.40 ± 0.02**	**75.30 ± 0.02**	**77.23 ± 0.02**
Calcite, $CaCO_3$	Sample 1	0.88	6.14	7.52	7.21
	Sample 2	0.91	6.09	7.49	7.21
	Sample 3	0.92	6.11	7.48	7.18
% Average ± S.D.		**0.90 ± 0.02**	**6.11 ±0.02**	**7.50 ± 0.02**	**7.20 ± 0.01**
Portlandite, $Ca(OH)_2$	Sample 1	5.33	1.23	2.33	1.72
	Sample 2	5.28	1.19	2.28	1.69
	Sample 3	5.29	1.18	2.29	1.69
% Average ± S.D.		**5.30 ± 0.02**	**1.20 ± 0.02**	**2.30 ± 0.02**	**1.70 ± 0.01**

APPENDIX B: XRD Diffractograms and Sorptivity coefficient analysis for OPC and PPC mortars

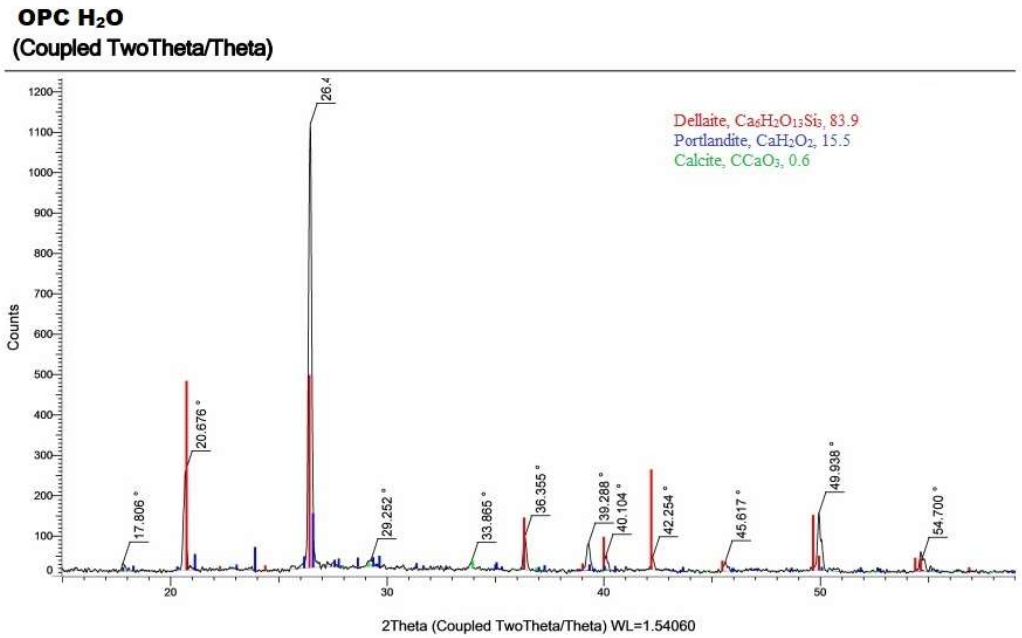

Figure B1: XRD Diffractograms for OPC-H (H)

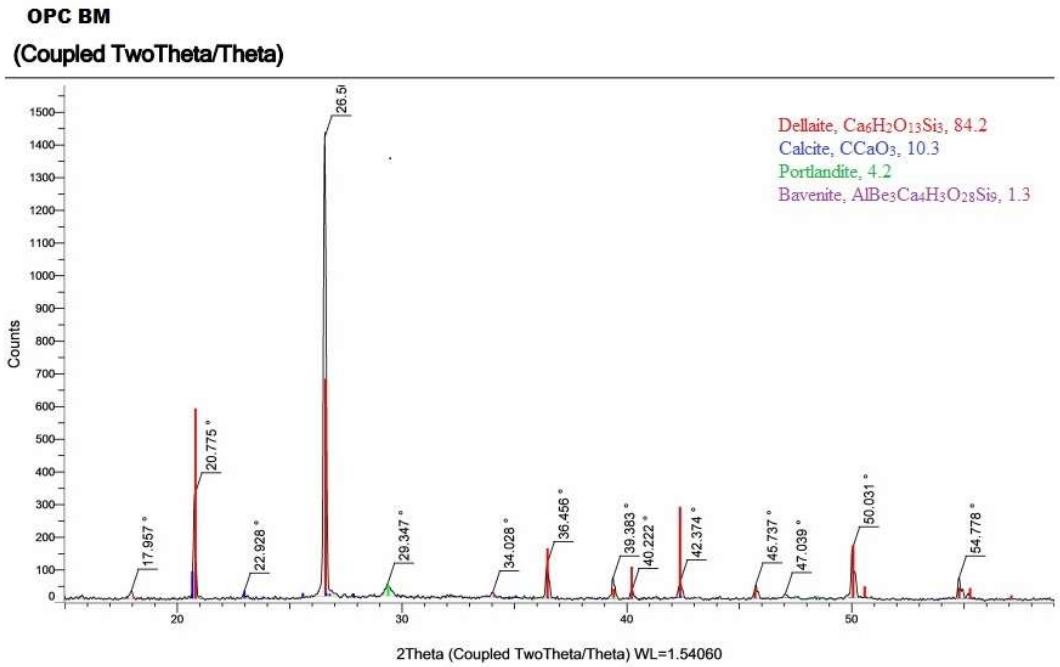

Figure B2: XRD Diffractograms for OPC-BM (BM).

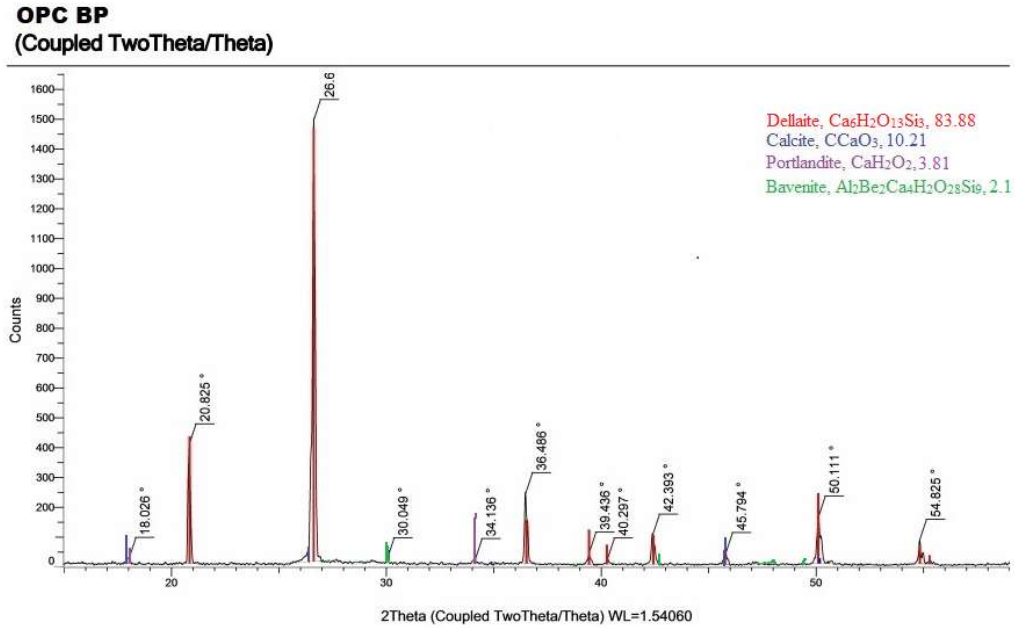

Figure B3: XRD Diffractograms for OPC-BP (BP).

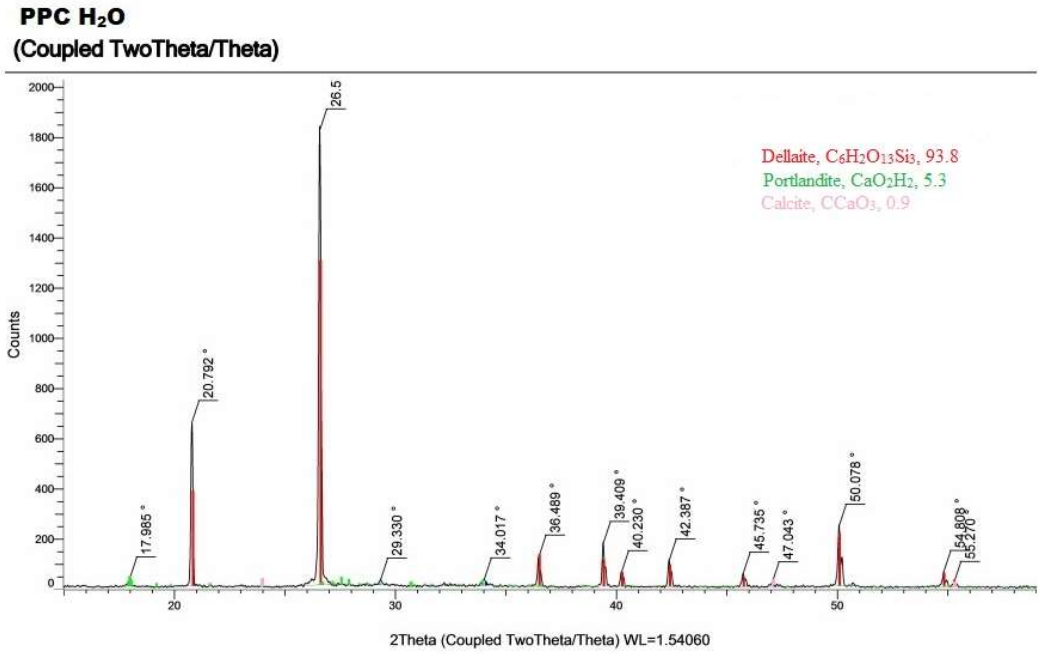

Figure B4: XRD diffractograms for PPC-H (H).

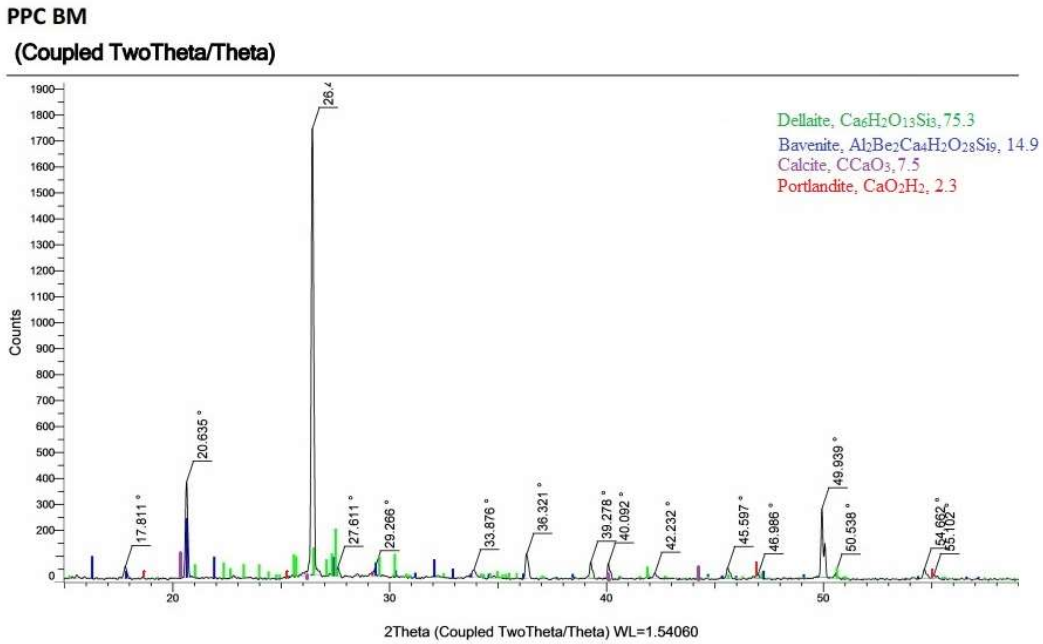

Figure B5: XRD diffractograms for PPC-BM (BM).

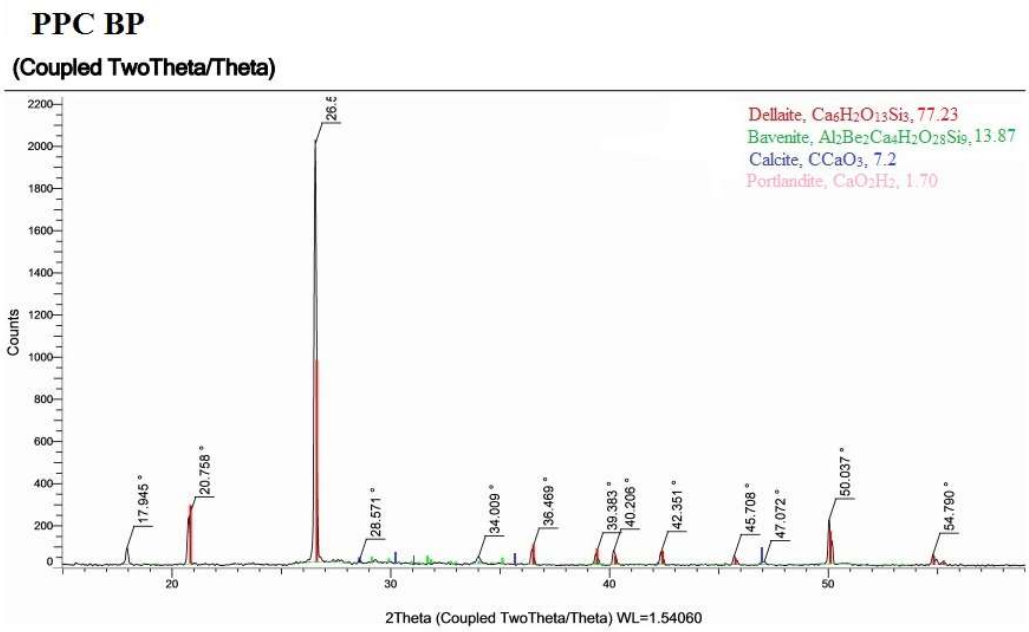

Figure B6: XRD diffractograms for PPC-BP (BP).

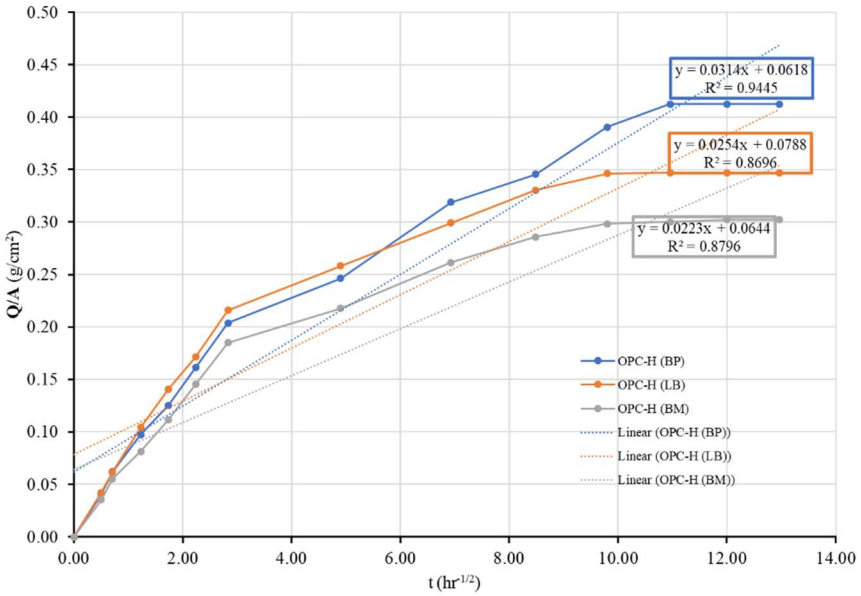

Figure B7: Comparative Sorptivity coefficients for OPC-H (BP), OPC-H (LB) and OPC-H (BM) mortars after 28th day of curing

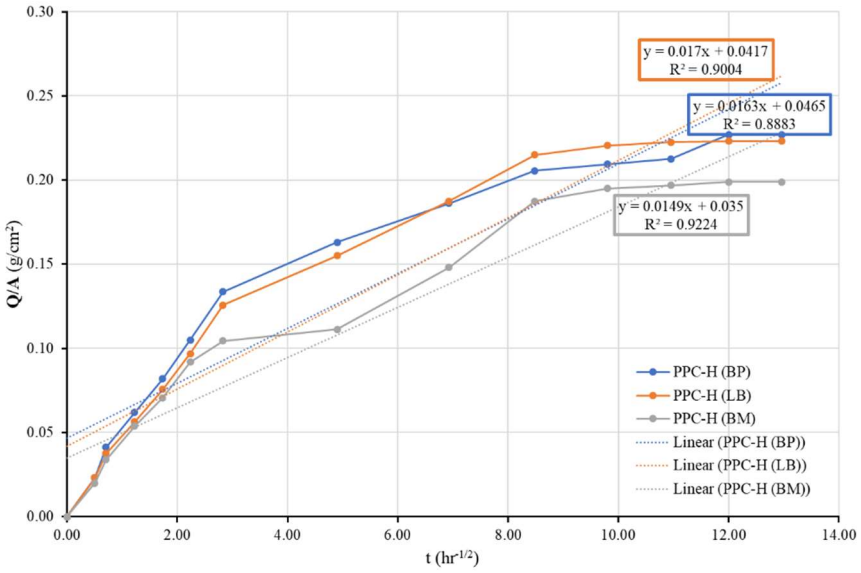

Figure B8: Comparative Sorptivity coefficients for PPC mortar after 28th day of curing in microbial solution

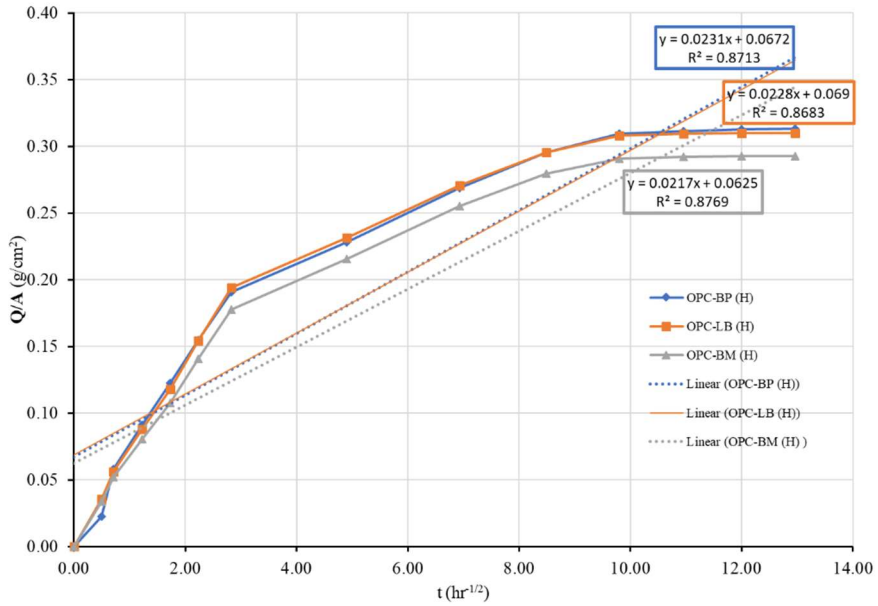

Figure B9: Comparative Sorptivity coefficients for OPC-BP (H), OPC-LB (H) and OPC BM (H) mortars after 28th day of curing

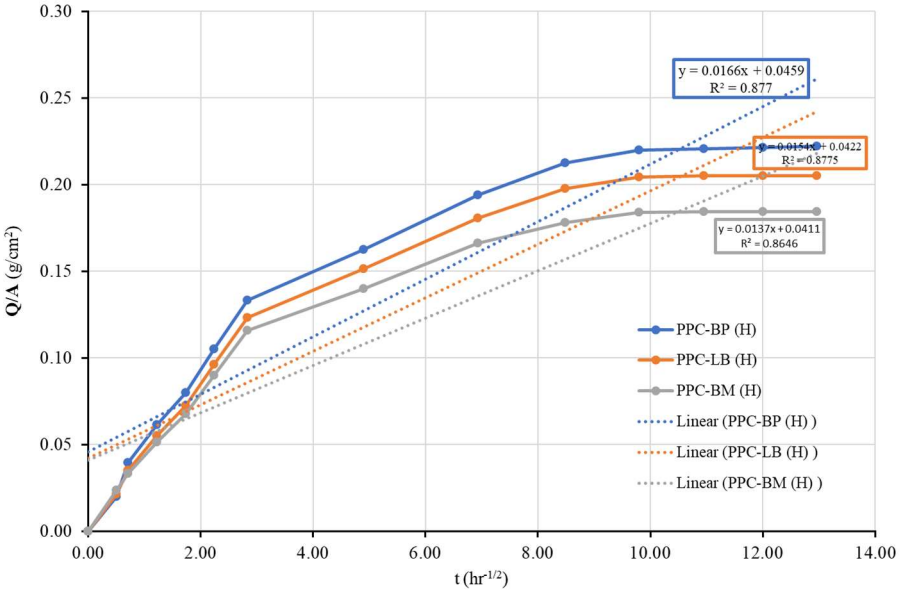

Figure B10: Comparative Sorptivity coefficients for varied microbial mortars after 28th day of curing in water

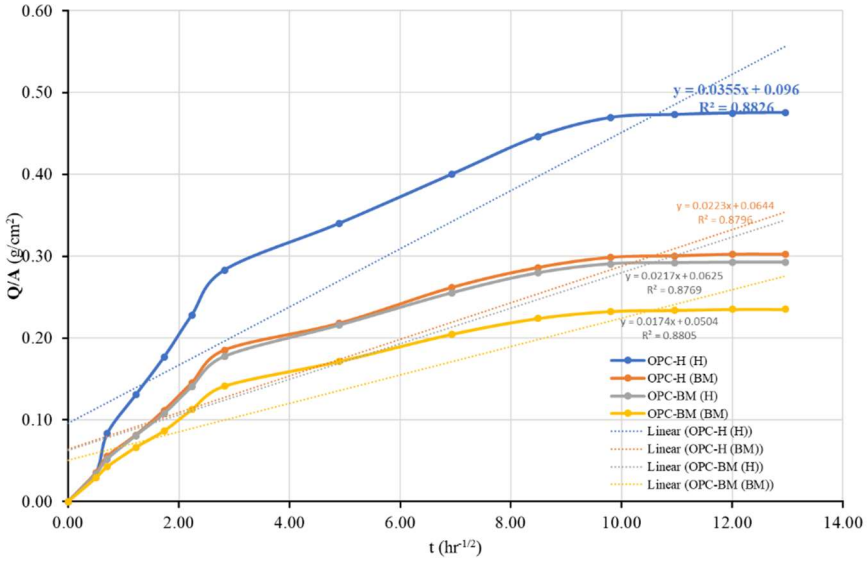

Figure B11: Sorptivity coefficients for varied *Bacillus megaterium*-OPC mortars after 28th day of curing

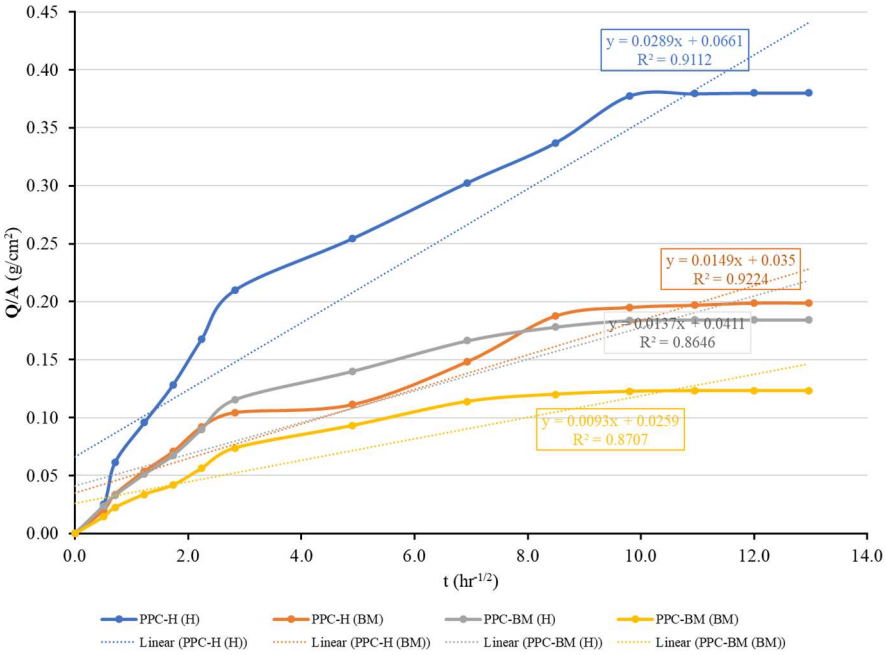

Figure B12: Sorptivity coefficients for varied *Bacillus megaterium*-PPC mortars after 28th day of curing

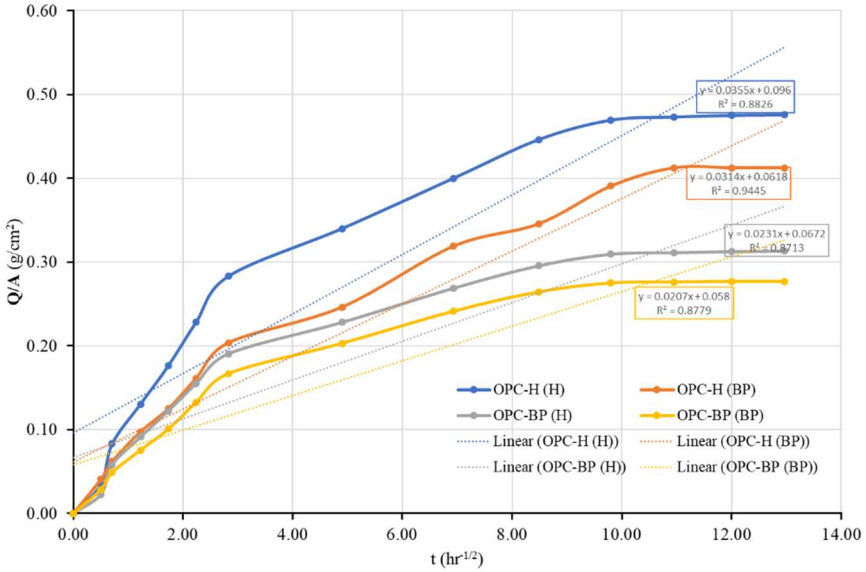

Figure B13: Sorptivity coefficients for varied *Sporosarcina pasteurii*-OPC mortars after 28th day of curing

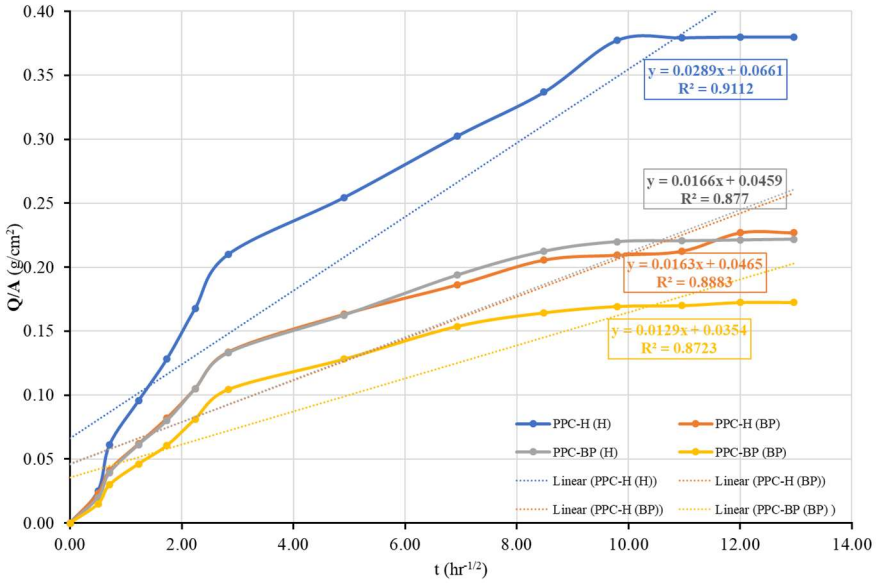

Figure B14: Sorptivity coefficients for varied *Sporosarcina pasteurii*-PPC mortars after 28th day of curing

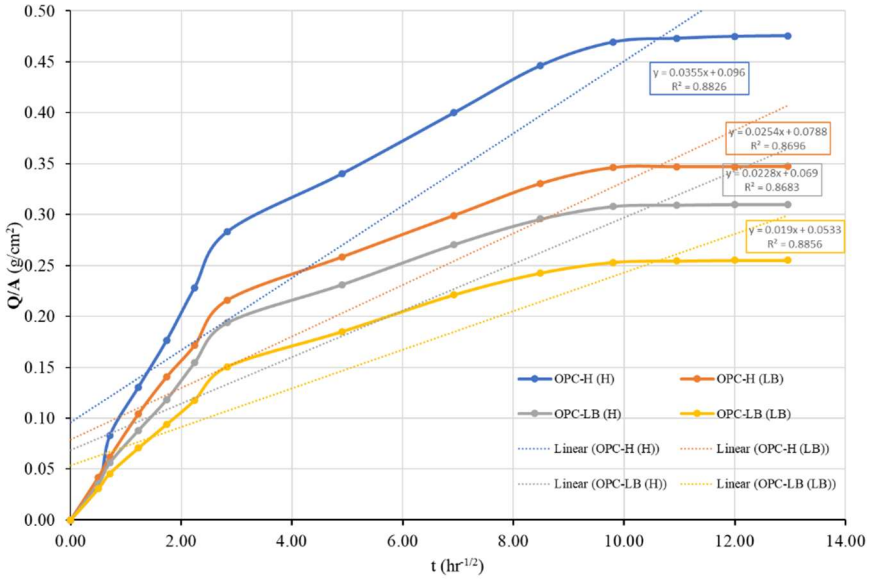

Figure B15: Sorptivity coefficients for varied *Lysinibacillus sphaericus*-OPC mortars after 28th day of curing

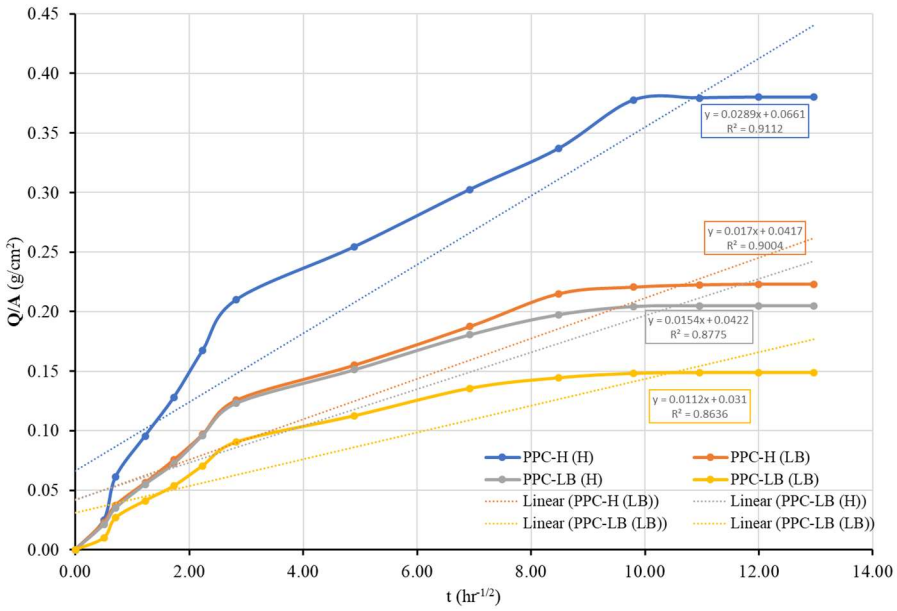

Figure B16: Sorptivity coefficients for varied *Lysinibacillus sphaericus*-PPC mortars after 28th day of curing

APPENDIX C: Raw data for Chloride and Sulphate analysis

Raw data for Chloride analysis

Table C1 Raw data for chloride analysis for OPC-H (H)

Depth (mm)	Chloride ions concentration in g/g cement					
	Sample 1	Sample 2	Sample 3	Average Calculated	Standard Deviation	Curve fitting
10	0.1677	0.1681	0.1679	0.1679	± 0.0002	0.1701
20	0.1504	0.1506	0.1505	0.1505	± 0.0001	0.1390
30	0.1138	0.1139	0.1137	0.1138	± 0.0001	0.1104
40	0.0787	0.0785	0.0784	0.0785	± 0.0001	0.0850
50	0.0513	0.0515	0.0514	0.0514	± 0.0001	0.0634
60	0.0433	0.0435	0.0435	0.0434	± 0.0001	0.0458
70	0.0376	0.0376	0.0374	0.0375	± 0.0001	0.0320
80	0.0329	0.0327	0.0328	0.0328	± 0.0001	0.0216

Table C2 Raw data for chloride analysis for PPC-H (H)

Depth (mm)	Chloride ions concentration in g/g cement					
	Sample 1	Sample 2	Sample 3	Average Calculated	Standard Deviation	Curve fitting
10	0.1561	0.1559	0.1562	0.1561	± 0.0001	0.1474
20	0.1303	0.1305	0.1302	0.1303	± 0.0001	0.1155
30	0.0911	0.0914	0.0913	0.0913	± 0.0001	0.0870
40	0.0588	0.0589	0.0585	0.0587	± 0.0002	0.0628
50	0.0313	0.0312	0.0309	0.0311	± 0.0002	0.0434
60	0.0230	0.0233	0.0231	0.0231	± 0.0001	0.0286
70	0.0221	0.0222	0.0222	0.0222	± 0.0000	0.0180
80	0.0179	0.0180	0.0176	0.0178	± 0.0002	0.0108

Table C3 Raw data for chloride analysis for OPC-H (BM)

Depth (mm)	Chloride ions concentration in g/g cement					
	Sample 1	Sample 2	Sample 3	Average Calculated	Standard Deviation	Curve fitting
10	0.1603	0.1600	0.1601	0.1601	± 0.0001	0.1619
20	0.1395	0.1399	0.1397	0.1397	± 0.0002	0.1311
30	0.1076	0.1077	0.1080	0.1078	± 0.0002	0.1028
40	0.0742	0.0740	0.0739	0.0740	± 0.0001	0.0780
50	0.0463	0.0465	0.0467	0.0465	± 0.0002	0.0572
60	0.0376	0.0381	0.0377	0.0378	± 0.0002	0.0405
70	0.0314	0.0317	0.0318	0.0316	± 0.0002	0.0277
80	0.0276	0.0282	0.0279	0.0279	± 0.0002	0.0182

Table C4 Raw data for chloride analysis for OPC-H (LB)

Depth (mm)	Chloride ions concentration in g/g cement					
	Sample 1	Sample 2	Sample 3	Average Calculated	Standard Deviation	Curve fitting
10	0.1648	0.1652	0.1650	0.1650	± 0.0002	0.1677
20	0.1490	0.1487	0.1486	0.1488	± 0.0002	0.1367
30	0.1120	0.1113	0.1115	0.1116	± 0.0003	0.1083
40	0.0802	0.0804	0.0798	0.0801	± 0.0002	0.0831
50	0.0491	0.0489	0.0495	0.0492	± 0.0002	0.0618
60	0.0437	0.0436	0.0441	0.0438	± 0.0002	0.0444
70	0.0357	0.0356	0.0354	0.0356	± 0.0001	0.0309
80	0.0305	0.0308	0.0311	0.0308	± 0.0002	0.0207

Table C5 Raw data for chloride analysis for OPC-H (BP)

Depth (mm)	Chloride ions concentration in g/g cement					
	Sample 1	Sample 2	Sample 3	Average Calculated	Standard Deviation	Curve fitting
10	0.1551	0.1547	0.1549	0.1549	± 0.0002	0.1583
20	0.1309	0.1307	0.1312	0.1309	± 0.0002	0.1224
30	0.0903	0.0907	0.0906	0.0905	± 0.0002	0.0905
40	0.0582	0.0577	0.0578	0.0579	± 0.0002	0.0639
50	0.0326	0.0331	0.0329	0.0329	± 0.0002	0.0430
60	0.0252	0.0254	0.0258	0.0255	± 0.0002	0.0275
70	0.0211	0.0216	0.0213	0.0213	± 0.0002	0.0167
80	0.0170	0.0174	0.0173	0.0172	± 0.0002	0.0097

Table C6 Raw data for chloride analysis for OPC-BM (H)

Depth (mm)	Chloride ions concentration in g/g cement					
	Sample 1	Sample 2	Sample 3	Average Calculated	Standard Deviation	Curve fitting
10	0.1593	0.1597	0.1595	0.1595	± 0.0002	0.1605
20	0.1383	0.1385	0.1379	0.1382	± 0.0002	0.1281
30	0.1062	0.1058	0.1065	0.1062	± 0.0003	0.0987
40	0.0719	0.0717	0.0718	0.0718	± 0.0001	0.0733
50	0.0442	0.0448	0.0445	0.0445	± 0.0002	0.0524
60	0.0363	0.0365	0.0356	0.0361	± 0.0004	0.0360
70	0.0297	0.0296	0.0301	0.0298	± 0.0002	0.0237
80	0.0256	0.0254	0.0260	0.0257	± 0.0002	0.0150

Table C7 Raw data for chloride analysis for OPC-LB (H)

Depth (mm)	Chloride ions concentration in g/g cement					
	Sample 1	Sample 2	Sample 3	Average Calculated	Standard Deviation	Curve fitting
10	0.1620	0.1626	0.1622	0.1623	± 0.0002	0.1710
20	0.1428	0.1435	0.1430	0.1431	± 0.0003	0.1365
30	0.1086	0.1091	0.1087	0.1088	± 0.0002	0.1052
40	0.0753	0.0758	0.0755	0.0755	± 0.0002	0.0781
50	0.0461	0.0468	0.0464	0.0464	± 0.0003	0.0558
60	0.0397	0.0403	0.0396	0.0399	± 0.0003	0.0383
70	0.0327	0.0319	0.0328	0.0325	± 0.0004	0.0253
80	0.0275	0.0279	0.0280	0.0278	± 0.0002	0.0160

Table C8 Raw data for chloride analysis for OPC-BP (H)

Depth (mm)	Chloride ions concentration in g/g cement					
	Sample 1	Sample 2	Sample 3	Average Calculated	Standard Deviation	Curve fitting
10	0.1644	0.1650	0.1647	0.1647	± 0.0002	0.1772
20	0.1469	0.1478	0.1472	0.1473	± 0.0004	0.1414
30	0.1142	0.1149	0.1147	0.1146	± 0.0003	0.1089
40	0.0751	0.0756	0.0752	0.0753	± 0.0002	0.0809
50	0.0499	0.0505	0.0503	0.0502	± 0.0002	0.0578
60	0.0401	0.0406	0.0399	0.0402	± 0.0003	0.0397
70	0.0339	0.0344	0.0345	0.0343	± 0.0003	0.0262
80	0.0300	0.0295	0.0293	0.0296	± 0.0003	0.0166

Table C9 Raw data for chloride analysis for OPC-BM (BM)

Depth (mm)	Chloride ions concentration in g/g cement					
	Sample 1	Sample 2	Sample 3	Average Calculated	Standard Deviation	Curve fitting
10	0.1588	0.1585	0.1589	0.1587	± 0.0002	0.1645
20	0.1366	0.1359	0.1362	0.1362	± 0.0003	0.1310
30	0.1042	0.1045	0.1037	0.1041	± 0.0003	0.1007
40	0.0687	0.0689	0.0691	0.0689	± 0.0002	0.0745
50	0.0423	0.0418	0.0417	0.0419	± 0.0003	0.0530
60	0.0339	0.0340	0.0335	0.0338	± 0.0002	0.0362
70	0.0273	0.0272	0.0276	0.0274	± 0.0002	0.0238
80	0.0227	0.0230	0.0227	0.0228	± 0.0001	0.0149

Table C10 Raw data for chloride analysis for OPC-LB (LB)

Depth (mm)	Chloride ions concentration in g/g cement					
	Sample 1	Sample 2	Sample 3	Average Calculated	Standard Deviation	Curve fitting
10	0.1589	0.1593	0.1591	0.1591	± 0.0002	0.1646
20	0.1365	0.1366	0.1362	0.1364	± 0.0002	0.1296
30	0.1053	0.1057	0.1055	0.1055	± 0.0002	0.0981
40	0.0699	0.0703	0.0702	0.0701	± 0.0002	0.0713
50	0.0429	0.0433	0.0432	0.0431	± 0.0002	0.0497
60	0.0354	0.0356	0.035	0.0353	± 0.0002	0.0331
70	0.0287	0.0291	0.0289	0.0289	± 0.0002	0.0211
80	0.0241	0.0246	0.0242	0.0243	± 0.0002	0.0128

Table C11 Raw data for chloride analysis for OPC-BP (BP)

Depth (mm)	Chloride ions concentration in g/g cement					
	Sample 1	Sample 2	Sample 3	Average Calculated	Standard Deviation	Curve fitting
10	0.1615	0.1609	0.1611	0.1612	± 0.0002	0.1720
20	0.1446	0.1442	0.1442	0.1443	± 0.0002	0.1367
30	0.1085	0.1080	0.1081	0.1082	± 0.0002	0.1047
40	0.0716	0.0714	0.0721	0.0717	± 0.0003	0.0772
50	0.0492	0.0499	0.0495	0.0495	± 0.0003	0.0547
60	0.0362	0.0366	0.0364	0.0364	± 0.0002	0.0372
70	0.0307	0.0308	0.0303	0.0306	± 0.0002	0.0243
80	0.0259	0.0263	0.0261	0.0261	± 0.0002	0.0152

Table C12 Raw data for chloride analysis for PPC-H (BM)

Depth (mm)	Chloride ions concentration in g/g cement					
	Sample 1	Sample 2	Sample 3	Average Calculated	Standard Deviation	Curve fitting
10	0.1560	0.1557	0.1558	0.1558	± 0.0001	0.1526
20	0.1231	0.1226	0.1229	0.1228	± 0.0002	0.1183
30	0.0913	0.0910	0.0912	0.0911	± 0.0001	0.0878
40	0.0573	0.0572	0.0571	0.0572	± 0.0001	0.0623
50	0.0309	0.0305	0.0307	0.0306	± 0.0002	0.0421
60	0.0251	0.0248	0.0249	0.0249	± 0.0001	0.0271
70	0.0216	0.0217	0.0214	0.0215	± 0.0001	0.0166
80	0.0174	0.0171	0.0172	0.0172	± 0.0001	0.0097

Table C13 Raw data for chloride analysis for PPC-H (LB)

Depth (mm)	Chloride ions concentration in g/g cement					
	Sample 1	Sample 2	Sample 3	Average Calculated	Standard Deviation	Curve fitting
10	0.1539	0.1543	0.1544	0.1542	± 0.0002	0.1558
20	0.1241	0.1237	0.1239	0.1239	± 0.0002	0.1201
30	0.0896	0.0902	0.0898	0.0899	± 0.0002	0.0885
40	0.0610	0.0606	0.0609	0.0608	± 0.0002	0.0622
50	0.0300	0.0302	0.0305	0.0302	± 0.0002	0.0416
60	0.0289	0.0286	0.0285	0.0287	± 0.0002	0.0265
70	0.0206	0.0210	0.0207	0.0208	± 0.0002	0.0160
80	0.0168	0.0166	0.0172	0.0169	± 0.0002	0.0091

Table C14 Raw data for chloride analysis for PPC-H (BP)

Depth (mm)	Chloride ions concentration in g/g cement					
	Sample 1	Sample 2	Sample 3	Average Calculated	Standard Deviation	Curve fitting
10	0.1551	0.1547	0.1549	0.1549	± 0.0002	0.1583
20	0.1309	0.1307	0.1312	0.1309	± 0.0002	0.1224
30	0.0903	0.0907	0.0906	0.0905	± 0.0002	0.0905
40	0.0582	0.0577	0.0578	0.0579	± 0.0002	0.0639
50	0.0326	0.0331	0.0329	0.0329	± 0.0002	0.0430
60	0.0252	0.0254	0.0258	0.0255	± 0.0002	0.0275
70	0.0211	0.0216	0.0213	0.0213	± 0.0002	0.0167
80	0.0170	0.0174	0.0173	0.0172	± 0.0002	0.0097

Table C15 Raw data for chloride analysis for PPC-BM (H)

Depth (mm)	Chloride ions concentration in g/g cement					
	Sample 1	Sample 2	Sample 3	Average Calculated	Standard Deviation	Curve fitting
10	0.1514	0.1513	0.1511	0.1513	± 0.0001	0.1388
20	0.1212	0.1210	0.1211	0.1211	± 0.0001	0.1082
30	0.0866	0.0865	0.0862	0.0864	± 0.0002	0.0809
40	0.0535	0.0534	0.0531	0.0533	± 0.0002	0.0578
50	0.0261	0.0264	0.0260	0.0262	± 0.0002	0.0395
60	0.0213	0.0212	0.0216	0.0214	± 0.0002	0.0258
70	0.0175	0.0174	0.0171	0.0173	± 0.0002	0.0160
80	0.0135	0.0134	0.0136	0.0135	± 0.0001	0.0094

Table C16 Raw data for chloride analysis for PPC-LB (H)

Depth (mm)	Chloride ions concentration in g/g cement					
	Sample 1	Sample 2	Sample 3	Average Calculated	Standard Deviation	Curve fitting
10	0.1520	0.1517	0.1521	0.1519	± 0.0002	0.1508
20	0.1223	0.1227	0.1225	0.1225	± 0.0002	0.1125
30	0.0875	0.0872	0.0871	0.0873	± 0.0002	0.0796
40	0.0565	0.0568	0.0563	0.0565	± 0.0002	0.0531
50	0.0271	0.0276	0.0272	0.0273	± 0.0002	0.0334
60	0.0241	0.0243	0.0244	0.0243	± 0.0001	0.0197
70	0.0184	0.0179	0.0183	0.0182	± 0.0002	0.0109
80	0.0146	0.0143	0.0143	0.0144	± 0.0001	0.0057

Table C17 Raw data for chloride analysis for PPC-BP (H)

Depth (mm)	Chloride ions concentration in g/g cement					
	Sample 1	Sample 2	Sample 3	Average Calculated	Standard Deviation	Curve fitting
10	0.1535	0.1528	0.1531	0.1531	± 0.0003	0.1564
20	0.1269	0.1273	0.1271	0.1271	± 0.0002	0.1183
30	0.0887	0.0890	0.0882	0.0886	± 0.0003	0.0852
40	0.0555	0.0563	0.0558	0.0559	± 0.0003	0.0581
50	0.0294	0.0298	0.0296	0.0296	± 0.0002	0.0375
60	0.0233	0.0231	0.0239	0.0234	± 0.0003	0.0229
70	0.0193	0.0189	0.0197	0.0193	± 0.0003	0.0132
80	0.0150	0.0156	0.0153	0.0153	± 0.0002	0.0071

Table C18 Raw data for chloride analysis for PPC-BM (BM)

Depth (mm)	Chloride ions concentration in g/g cement					
	Sample 1	Sample 2	Sample 3	Average Calculated	Standard Deviation	Curve fitting
10	0.1413	0.1416	0.1414	0.1414	± 0.0001	0.1265
20	0.1187	0.1189	0.1190	0.1189	± 0.0001	0.0983
30	0.0802	0.0803	0.0799	0.0801	± 0.0002	0.0732
40	0.0483	0.0481	0.0480	0.0481	± 0.0001	0.0522
50	0.0204	0.0206	0.0202	0.0204	± 0.0002	0.0355
60	0.0169	0.0165	0.0167	0.0167	± 0.0002	0.0230
70	0.0119	0.0115	0.0118	0.0117	± 0.0002	0.0142
80	0.0085	0.0089	0.0084	0.0086	± 0.0002	0.0083

Table C19 Raw data for chloride analysis for PPC-LB (LB)

Depth (mm)	Chloride ions concentration in g/g cement					
	Sample 1	Sample 2	Sample 3	Average Calculated	Standard Deviation	Curve fitting
10	0.1489	0.1493	0.1494	0.1492	± 0.0002	0.1459
20	0.1211	0.1209	0.1208	0.1209	± 0.0001	0.1081
30	0.0843	0.0845	0.0841	0.0843	± 0.0002	0.0757
40	0.0513	0.0515	0.0517	0.0515	± 0.0002	0.0499
50	0.0237	0.0239	0.0242	0.0239	± 0.0002	0.0309
60	0.0192	0.0194	0.0188	0.0191	± 0.0002	0.0180
70	0.0149	0.0152	0.0151	0.0151	± 0.0001	0.0098
80	0.0114	0.0116	0.0115	0.0115	± 0.0001	0.0050

Table C20 Raw data for chloride analysis for PPC-BP (BP)

Depth (mm)	Chloride ions concentration in g/g cement					
	Sample 1	Sample 2	Sample 3	Average Calculated	Standard Deviation	Curve fitting
10	0.1508	0.1513	0.1512	0.1511	± 0.0002	0.1521
20	0.1231	0.1226	0.1229	0.1229	± 0.0002	0.1143
30	0.0866	0.0868	0.0862	0.0865	± 0.0002	0.0816
40	0.0538	0.0535	0.0537	0.0537	± 0.0001	0.0550
50	0.0256	0.0262	0.0258	0.0259	± 0.0002	0.0351
60	0.0213	0.0214	0.0207	0.0211	± 0.0003	0.0211
70	0.0168	0.0173	0.0172	0.0171	± 0.0002	0.0119
80	0.0133	0.0135	0.0129	0.0132	± 0.0002	0.0063

Raw data for Sulphate analysis

Table C21 Raw data for sulphate analysis for OPC-H (H)

Depth (mm)	Sulphate ions concentration in g/g cement					
	Sample 1	Sample 2	Sample 3	Average Calculated	Standard Deviation	Curve fitting
10	0.3087	0.3083	0.3091	0.3087	± 0.0003	0.3191
20	0.2898	0.2903	0.2902	0.2901	± 0.0002	0.2874
30	0.2555	0.2561	0.2558	0.2558	± 0.0002	0.2565
40	0.2382	0.2387	0.2386	0.2385	± 0.0002	0.2268
50	0.1877	0.1881	0.1879	0.1879	± 0.0002	0.1987
60	0.1669	0.1663	0.1668	0.1667	± 0.0003	0.1723
70	0.1603	0.1608	0.1607	0.1606	± 0.0002	0.1480
80	0.1589	0.1585	0.1592	0.1589	± 0.0003	0.1258

Table C22 Raw data for sulphate analysis for PPC-H (H)

Depth (mm)	Sulphate ions concentration in g/g cement					
	Sample 1	Sample 2	Sample 3	Average Calculated	Standard Deviation	Curve fitting
10	0.2831	0.2837	0.2834	0.2834	± 0.0002	0.2850
20	0.2509	0.2514	0.2511	0.2511	± 0.0002	0.2546
30	0.2320	0.2327	0.2325	0.2324	± 0.0003	0.2251
40	0.2011	0.2014	0.2008	0.2011	± 0.0002	0.1968
50	0.1616	0.1620	0.1621	0.1619	± 0.0002	0.1703
60	0.1390	0.1386	0.1388	0.1388	± 0.0002	0.1456
70	0.1325	0.1318	0.1320	0.1321	± 0.0003	0.1231
80	0.1259	0.1255	0.1257	0.1257	± 0.0002	0.1029

Table C23 Raw data for sulphate analysis for OPC-H (BM)

Depth (mm)	Sulphate ions concentration in g/g cement					
	Sample 1	Sample 2	Sample 3	Average Calculated	Standard Deviation	Curve fitting
10	0.2873	0.2879	0.2875	0.2876	± 0.0002	0.2905
20	0.2597	0.2599	0.2595	0.2597	± 0.0002	0.2586
30	0.2409	0.2412	0.2412	0.2411	± 0.0001	0.2277
40	0.2122	0.2127	0.2124	0.2124	± 0.0002	0.1982
50	0.1688	0.1682	0.1684	0.1685	± 0.0002	0.1706
60	0.1341	0.1338	0.1346	0.1342	± 0.0003	0.1450
70	0.1291	0.1287	0.1288	0.1289	± 0.0002	0.1218
80	0.1206	0.1212	0.1210	0.1209	± 0.0002	0.1010

Table C24 Raw data for sulphate analysis for OPC-H (LB)

Depth (mm)	Sulphate ions concentration in g/g cement					
	Sample 1	Sample 2	Sample 3	Average Calculated	Standard Deviation	Curve fitting
10	0.2989	0.2985	0.2986	0.2987	± 0.0002	0.2991
20	0.2722	0.2724	0.2726	0.2724	± 0.0002	0.2665
30	0.2409	0.2413	0.2412	0.2411	± 0.0002	0.2350
40	0.2189	0.2183	0.2187	0.2186	± 0.0002	0.2049
50	0.1731	0.1735	0.1732	0.1733	± 0.0002	0.1766
60	0.1429	0.1425	0.1426	0.1427	± 0.0002	0.1505
70	0.1371	0.1373	0.1376	0.1373	± 0.0002	0.1267
80	0.1318	0.1319	0.1315	0.1317	± 0.0002	0.1053

Table C25 Raw data for sulphate analysis for OPC-H (BP)

Depth (mm)	Sulphate ions concentration in g/g cement					
	Sample 1	Sample 2	Sample 3	Average Calculated	Standard Deviation	Curve fitting
10	0.2994	0.3001	0.2996	0.2997	± 0.0003	0.3083
20	0.2809	0.2813	0.2812	0.2811	± 0.0002	0.2760
30	0.2472	0.2474	0.2470	0.2472	± 0.0002	0.2446
40	0.2779	0.2775	0.2776	0.2277	± 0.0002	0.2146
50	0.1810	0.1811	0.1815	0.1812	± 0.0002	0.1862
60	0.1495	0.1490	0.1491	0.1492	± 0.0002	0.1599
70	0.1432	0.1434	0.1437	0.1434	± 0.0002	0.1357
80	0.1410	0.1414	0.1409	0.1411	± 0.0002	0.1139

Table C26 Raw data for sulphate analysis for OPC-BM (H)

Depth (mm)	Sulphate ions concentration in g/g cement					
	Sample 1	Sample 2	Sample 3	Average Calculated	Standard Deviation	Curve fitting
10	0.2833	0.2826	0.2828	0.2829	± 0.0003	0.2905
20	0.2619	0.2618	0.2626	0.2621	± 0.0004	0.2586
30	0.2304	0.2299	0.2300	0.2301	± 0.0002	0.2277
40	0.2075	0.2068	0.2070	0.2071	± 0.0003	0.1982
50	0.1609	0.1611	0.1616	0.1612	± 0.0003	0.1706
60	0.1308	0.1314	0.1305	0.1309	± 0.0004	0.1450
70	0.1245	0.1237	0.1247	0.1243	± 0.0004	0.1218
80	0.1229	0.1236	0.1231	0.1232	± 0.0003	0.1010

Table C27 Raw data for sulphate analysis for OPC-LB (H)

Depth (mm)	Sulphate ions concentration in g/g cement					
	Sample 1	Sample 2	Sample 3	Average Calculated	Standard Deviation	Curve fitting
10	0.2901	0.2906	0.2911	0.2906	± 0.0004	0.2991
20	0.2701	0.2698	0.2695	0.2698	± 0.0002	0.2665
30	0.2374	0.2377	0.2369	0.2373	± 0.0003	0.2350
40	0.2148	0.2139	0.2145	0.2144	± 0.0004	0.2049
50	0.1687	0.1683	0.1685	0.1685	± 0.0002	0.1766
60	0.1375	0.1384	0.1378	0.1379	± 0.0004	0.1505
70	0.1316	0.1323	0.1318	0.1319	± 0.0003	0.1267
80	0.1307	0.1312	0.1308	0.1309	± 0.0002	0.1053

Table C28 Raw data for sulphate analysis for OPC-BP (H)

Depth (mm)	Sulphate ions concentration in g/g cement					
	Sample 1	Sample 2	Sample 3	Average Calculated	Standard Deviation	Curve fitting
10	0.2993	0.2985	0.2995	0.2991	± 0.0004	0.3083
20	0.2783	0.2780	0.2786	0.2783	± 0.0002	0.2760
30	0.2450	0.2458	0.2457	0.2455	± 0.0004	0.2446
40	0.2228	0.2233	0.2235	0.2232	± 0.0003	0.2146
50	0.1770	0.1768	0.1763	0.1767	± 0.0003	0.1862
60	0.1467	0.1464	0.1461	0.1464	± 0.0002	0.1599
70	0.1405	0.1398	0.1406	0.1403	± 0.0004	0.1357
80	0.1392	0.1399	0.1391	0.1394	± 0.0004	0.1139

Table C29 Raw data for sulphate analysis for OPC-BM (BM)

Depth (mm)	Sulphate ions concentration in g/g cement					
	Sample 1	Sample 2	Sample 3	Average Calculated	Standard Deviation	Curve fitting
10	0.2685	0.2680	0.2684	0.2683	± 0.0002	0.2720
20	0.2487	0.2479	0.2486	0.2484	± 0.0004	0.2412
30	0.2155	0.2160	0.2159	0.2158	± 0.0002	0.2114
40	0.1933	0.1938	0.1937	0.1936	± 0.0002	0.1831
50	0.1483	0.1485	0.1478	0.1482	± 0.0003	0.1567
60	0.1167	0.1171	0.1169	0.1169	± 0.0002	0.1323
70	0.1108	0.1113	0.1106	0.1109	± 0.0003	0.1103
80	0.1089	0.1096	0.1094	0.1093	± 0.0003	0.0908

Table C30 Raw data for sulphate analysis for OPC-LB (LB)

Depth (mm)	Sulphate ions concentration in g/g cement					
	Sample 1	Sample 2	Sample 3	Average Calculated	Standard Deviation	Curve fitting
10	0.2755	0.2753	0.2751	0.2753	± 0.0002	0.2811
20	0.2565	0.2559	0.2562	0.2561	± 0.0002	0.2499
30	0.2230	0.2233	0.2236	0.2233	± 0.0002	0.2198
40	0.2009	0.2011	0.2016	0.2012	± 0.0003	0.1910
50	0.1560	0.1553	0.1558	0.1557	± 0.0003	0.1641
60	0.1245	0.1243	0.1238	0.1242	± 0.0003	0.1392
70	0.1180	0.1187	0.1185	0.1184	± 0.0003	0.1166
80	0.1163	0.1168	0.1170	0.1167	± 0.0003	0.0965

Table C31 Raw data for sulphate analysis for OPC-BP (BP)

Depth (mm)	Sulphate ions concentration in g/g cement					
	Sample 1	Sample 2	Sample 3	Average Calculated	Standard Deviation	Curve fitting
10	0.2835	0.2842	0.2837	0.2838	± 0.0003	0.2922
20	0.2649	0.2648	0.2656	0.2651	± 0.0004	0.2601
30	0.2318	0.2315	0.2321	0.2318	± 0.0002	0.2290
40	0.2090	0.2098	0.2094	0.2094	± 0.0003	0.1994
50	0.1633	0.1638	0.1640	0.1637	± 0.0003	0.1716
60	0.1330	0.1327	0.1324	0.1327	± 0.0002	0.1459
70	0.1268	0.1270	0.1263	0.1267	± 0.0003	0.1225
80	0.1251	0.1255	0.1247	0.1251	± 0.0003	0.1016

Table C32 Raw data for sulphate analysis for PPC-H (BM)

Depth (mm)	Sulphate ions concentration in g/g cement					
	Sample 1	Sample 2	Sample 3	Average Calculated	Standard Deviation	Curve fitting
10	0.2577	0.2582	0.2578	0.2579	± 0.0002	0.2455
20	0.2239	0.2241	0.2242	0.2241	± 0.0001	0.2153
30	0.1929	0.1926	0.1926	0.1927	± 0.0001	0.1864
40	0.1709	0.1711	0.1712	0.1711	± 0.0001	0.1590
50	0.1333	0.1331	0.1332	0.1332	± 0.0001	0.1338
60	0.1123	0.1126	0.1123	0.1124	± 0.0001	0.1108
70	0.0989	0.0986	0.0985	0.0987	± 0.0002	0.0905
80	0.0898	0.0905	0.0899	0.0901	± 0.0003	0.0727

Table C33 Raw data for sulphate analysis for PPC-H (LB)

Depth (mm)	Sulphate ions concentration in g/g cement					
	Sample 1	Sample 2	Sample 3	Average Calculated	Standard Deviation	Curve fitting
10	0.2627	0.2624	0.2619	0.2623	± 0.0003	0.2540
20	0.2306	0.2309	0.2312	0.2309	± 0.0002	0.2235
30	0.2002	0.1997	0.1995	0.1998	± 0.0003	0.1941
40	0.1782	0.1786	0.1785	0.1784	± 0.0002	0.1663
50	0.1344	0.1340	0.1343	0.1342	± 0.0002	0.1405
60	0.1111	0.1115	0.1112	0.1113	± 0.0002	0.1170
70	0.1178	0.1175	0.1173	0.1175	± 0.0002	0.0961
80	0.1011	0.1006	0.1009	0.1009	± 0.0002	0.0777

Table C34 Raw data for sulphate analysis for PPC-H (BP)

Depth (mm)	Sulphate ions concentration in g/g cement					
	Sample 1	Sample 2	Sample 3	Average Calculated	Standard Deviation	Curve fitting
10	0.2719	0.2714	0.2715	0.2716	± 0.0002	0.2632
20	0.2308	0.2313	0.2312	0.2311	± 0.0002	0.2325
30	0.2131	0.2126	0.2127	0.2128	± 0.0002	0.2029
40	0.1819	0.1815	0.1816	0.1817	± 0.0002	0.1749
50	0.1486	0.1488	0.1484	0.1486	± 0.0002	0.1487
60	0.1218	0.1213	0.1214	0.1215	± 0.0002	0.1248
70	0.1155	0.1153	0.1159	0.1156	± 0.0002	0.1033
80	0.1116	0.1111	0.1112	0.1113	± 0.0002	0.0843

Table C35 Raw data for sulphate analysis for PPC-BM (H)

Depth (mm)	Sulphate ions concentration in g/g cement					
	Sample 1	Sample 2	Sample 3	Average Calculated	Standard Deviation	Curve fitting
10	0.2459	0.2464	0.2463	0.2462	± 0.0002	0.2455
20	0.2138	0.2137	0.2133	0.2136	± 0.0002	0.2153
30	0.1904	0.1902	0.1906	0.1904	± 0.0002	0.1864
40	0.1645	0.1638	0.1640	0.1641	± 0.0003	0.1590
50	0.1240	0.1244	0.1245	0.1243	± 0.0002	0.1338
60	0.1010	0.1009	0.1005	0.1008	± 0.0002	0.1108
70	0.0952	0.0946	0.0949	0.0949	± 0.0002	0.0905
80	0.0884	0.0887	0.0890	0.0887	± 0.0002	0.0727

Table C36 Raw data for sulphate analysis for PPC-LB (H)

Depth (mm)	Sulphate ions concentration in g/g cement					
	Sample 1	Sample 2	Sample 3	Average Calculated	Standard Deviation	Curve fitting
10	0.2541	0.2536	0.2531	0.2536	± 0.0004	0.2540
20	0.2207	0.2212	0.2214	0.2211	± 0.0003	0.2235
30	0.1975	0.1984	0.1978	0.1979	± 0.0004	0.1941
40	0.1714	0.1711	0.1720	0.1715	± 0.0004	0.1663
50	0.1323	0.1320	0.1317	0.1320	± 0.0002	0.1405
60	0.1084	0.1088	0.1092	0.1088	± 0.0003	0.1170
70	0.1028	0.1021	0.1023	0.1024	± 0.0003	0.0961
80	0.0958	0.0965	0.0960	0.0961	± 0.0003	0.0777

Table C37 Raw data for sulphate analysis for PPC-BP (H)

Depth (mm)	Sulphate ions concentration in g/g cement					
	Sample 1	Sample 2	Sample 3	Average Calculated	Standard Deviation	Curve fitting
10	0.2623	0.2628	0.2621	0.2624	± 0.0003	0.2632
20	0.2296	0.2299	0.2293	0.2296	± 0.0002	0.2325
30	0.2068	0.2066	0.2073	0.2069	± 0.0003	0.2029
40	0.1802	0.1795	0.1797	0.1798	± 0.0003	0.1749
50	0.1404	0.1412	0.1411	0.1409	± 0.0004	0.1487
60	0.1179	0.1170	0.1173	0.1174	± 0.0004	0.1248
70	0.1104	0.1113	0.1107	0.1108	± 0.0004	0.1033
80	0.1038	0.1047	0.1044	0.1043	± 0.0004	0.0843

Table C38 Raw data for sulphate analysis for PPC-BM (BM)

Depth (mm)	Sulphate ions concentration in g/g cement					
	Sample 1	Sample 2	Sample 3	Average Calculated	Standard Deviation	Curve fitting
10	0.2244	0.2240	0.2245	0.2243	± 0.0002	0.2201
20	0.2005	0.2000	0.1998	0.2001	± 0.0003	0.1916
30	0.1712	0.1718	0.1715	0.1715	± 0.0002	0.1643
40	0.1403	0.1400	0.1406	0.1403	± 0.0002	0.1386
50	0.1016	0.1011	0.1015	0.1014	± 0.0002	0.1151
60	0.0779	0.0783	0.0781	0.0781	± 0.0002	0.0941
70	0.0703	0.0707	0.0705	0.0705	± 0.0002	0.0755
80	0.0645	0.0649	0.0644	0.0646	± 0.0002	0.0596

Table C39 Raw data for sulphate analysis for PPC-LB (LB)

Depth (mm)	Sulphate ions concentration in g/g cement					
	Sample 1	Sample 2	Sample 3	Average Calculated	Standard Deviation	Curve fitting
10	0.2315	0.2322	0.2317	0.2318	± 0.0003	0.2290
20	0.2066	0.2074	0.2073	0.2071	± 0.0004	0.1993
30	0.1785	0.1782	0.1788	0.1785	± 0.0002	0.1708
40	0.1478	0.1469	0.1472	0.1473	± 0.0004	0.1442
50	0.1087	0.1092	0.1088	0.1089	± 0.0002	0.1198
60	0.0853	0.0856	0.0859	0.0856	± 0.0002	0.0978
70	0.0789	0.0787	0.0782	0.0786	± 0.0003	0.0786
80	0.0716	0.0718	0.0723	0.0719	± 0.0003	0.0620

Table C40 Raw data for sulphate analysis for PPC-BP (BP)

Depth (mm)	Sulphate ions concentration in g/g cement					
	Sample 1	Sample 2	Sample 3	Average Calculated	Standard Deviation	Curve fitting
10	0.2397	0.2407	0.2405	0.2403	± 0.0004	0.2393
20	0.2158	0.2151	0.2153	0.2154	± 0.0003	0.2090
30	0.1879	0.1865	0.1869	0.1871	± 0.0006	0.1799
40	0.1562	0.1555	0.1557	0.1558	± 0.0003	0.1525
50	0.1167	0.1175	0.1171	0.1171	± 0.0003	0.1273
60	0.0938	0.0940	0.0945	0.0941	± 0.0003	0.1046
70	0.0864	0.0872	0.0868	0.0868	± 0.0003	0.0846
80	0.0806	0.0801	0.0808	0.0805	± 0.0003	0.0672

APPENDIX D: T-test summary for test mortars at varied preparation and curing regimes

Table D1 T-test summary for varied OPC and PPC mortar paste

Mortar category	Setting Time (Minutes)		Normal Consistency (%)	Soundness (mm)
	IST (min)	FST (min)		
OPC-H_2O vs OPC-BM	0.0578	0.0029	0.0013	0.0237
OPC-H_2O vs OPC-BP	0.0298	0.3060	0.0001	0.2113
OPC-H_2O vs OPC-LB	0.0066	0.0320	0.0001	0.0500
OPC-BM vs OPC-LB	0.0506	0.2113	0.0001	0.0237
OPC-BP vs OPC-LB	0.0016	0.0506	0.0001	0.2113
OPC-BM vs OPC-BP	0.0066	0.0918	0.0001	0.0189
OPC-H_2O vs PPC-H_2O	0.0021	0.0030	0.0002	0.0382
PPC-H_2O vs PPC-BM	0.0412	0.0066	0.0006	0.0382
PPC-H_2O vs PPC-BP	0.0668	0.0506	0.0002	0.0566
PPC-H_2O vs PPC-LB	0.0178	0.0016	0.0001	0.0364
PPC-BM vs PPC-LB	0.1151	0.0506	0.0001	0.2113
PPC-BP vs PPC-LB	0.0506	0.0066	0.0039	0.0918
PPC-BM vs PPC-BP	0.2593	0.0506	0.0001	0.2593
OPC-BM vs PPC-BM	0.0003	0.0076	0.0001	0.0237
OPC-BP vs PPC-BP	0.0016	0.0016	0.0001	0.0918
OPC-LB vs PPC-LB	0.0002	0.0066	0.0001	0.2113

Table D2 Compressive strength t-test summary for OPC versus PPC at 28th day of curing

	OPC-H (H)	PPC-H (H)
OPC-H (H)	5.0000×10^{-1}	2.9051×10^{-7}

Table D3 Flexural strength t-test summary for OPC versus PPC at 28th day of curing

	OPC-H (H)	PPC-H (H)
OPC-H (H)	5.0000×10^{-1}	3.3259×10^{-4}

Table D4 $T_{Calc.}$ Values summary for microbial treated mortars against the non-microbial mortar and among varied microbial treated mortar categories compressive strength on the 28th day of curing. ($T_{Crit.}$ = 0.5, p = 0.05)

MORTAR CATEGORY	Tcalc. values × 10^{-6}										
	OPC-H (H)	PPC-H (H)	OPC-BP (H)	OPC-H (BP)	OPC-H (LB)	OPC-LB (H)	OPC-BM (H)	OPC-H (BM)	OPC-BP (BP)	OPC-LB (LB)	OPC-BM (BM)
OPC-H (H)	5000000	0.2905	33.290	39.980	2.1732	31.706	1.4883	3.5930	3.4785	1.3512	20.831
PPC-H (H)	0.2905	5000000	0.3183	0.7029	0.0464	0.6627	0.0401	0.0554	0.0928	0.0655	0.0591
OPC-BP (H)	33.290	0.3183	5000000	12851	981.56	31033	335.40	6275.5	4651.5	319.23	390990
OPC-H (BP)	39.980	0.7029	12851	5000000	119.75	36963	59.429	355.52	76.523	8.7336	977.84
OPC-H (LB)	2.1732	0.0464	981.56	119.75	5000000	170.31	13555	7702.6	12462	2136.6	394.68
OPC-LB (H)	31.706	0.6627	31033	36963	170.31	5000000	78.819	585.05	129.16	11.619	4290.5
OPC-BM (H)	1.4883	0.0401	335.40	59.429	13555	78.819	5000000	861.73	1097.6	41583	150.81
OPC-H	3.5930	0.0554	6275.5	2153.4	7702.6	585.05	861.73	5000000	211170	290.07	2125.4

(BM)											
OPC-BP (BP)	3.4785	0.0928	4651.5	76.523	12462	129.16	1097.6	211170	5000000	192.53	487.75
OPC-LB (LB)	1.3512	0.0655	319.23	8.7336	2136.6	11.619	41583	290.07	192.53	5000000	22.158
OPC-BM (BM)	20.831	0.5908	390990	977.84	394.68	4290.5	150.81	2125.4	487.75	22.158	5000000
PPC-H (BP)	0.7811	131.34	2.3416	0.0979	0.0939	0.09018	0.0801	0.1144	0.0342	0.0222	0.0769
PPC-BP (H)	12.576	466.37	0.8599	29.367	1.8442	27.722	1.5994	2.2031	6.7304	4.8756	24.797
PPC-BP (BP)	2.6085	44.645	0.5871	5.5343	0.2382	5.1548	0.2002	0.2960	0.7726	0.5167	4.4944
PPC-H (LB)	1.0418	53.552	0.7094	1.4615	0.0989	1.3573	0.0832	0.1228	0.1936	0.1273	1.1766
PPC-LB (H)	8.3850	52.6550	0.7657	170.82	0.7831	15.942	0.6611	0.9684	2.9624	2.0168	13.955
PPC-LB (LB)	2.7661	8.8337	1.2339	2.4397	0.1651	2.2374	0.1356	0.2113	0.3193	0.1984	1.8944
PPC-H (BM)	1.1959	39.679	2.9427	0.1304	0.1192	0.1194	0.1007	0.1471	0.0444	0.0281	0.1006
PPC-BM (H)	3.9291	75.354	10.825	0.0307	0.5198	0.0279	0.4487	0.6250	0.0725	0.0470	0.0232
PPC-BM (BM)	5.9968	35.382	13.403	0.0429	0.6493	0.0387	0.5548	0.7901	0.0944	0.0594	0.0317

Table D5 $T_{Calc.}$ Values summary for microbial treated mortars against the non-microbial mortar and among varied microbial treated mortar categories flexural strength on the 28th day of curing. ($T_{Crit.}$ = 0.5, p = 0.05)

MORTAR CATEGORY	Tcalc. values × 10^{-5}										
	OPC-H (H)	PPC-H (H)	OPC-BP (H)	OPC-H (BP)	OPC-H (LB)	OPC-LB (H)	OPC-BM (H)	OPC-H (BM)	OPC-BP (BP)	OPC-LB (LB)	OPC-BM (BM)
OPC-H (H)	50000	33.259	6.3676	32.9104	6.8664	4.9426	9.4017	3.7064	13.364	0.61408	1.2371
PPC-H (H)	33.259	50000	9.0504	2.9445	20.928	18.175	23.788	7.5355	27.241	3.7149	4.9828
OPC-BP (H)	6.3676	9.0504	50000	10009	94.375	35.318	302.53	3524.2	1782.6	8.7818	50.833
OPC-H (BP)	32.910	2.9445	10009	50000	305.70	160.98	621.82	1609.9	1633.6	30.910	110.25
OPC-H (LB)	6.8664	20.928	94.375	305.70	50000	388.13	661.78	302.53	52.878	241.69	19340
OPC-LB (H)	4.9426	18.175	35.318	160.98	388.13	50000	38.895	80.436	8.8776	1782.6	4122.1
OPC-BM (H)	9.4017	23.788	302.53	621.82	661.78	38.895	50000	1782.6	661.78	80.436	1240.9
OPC-H (BM)	3.7064	7.5355	3524.2	1609.9	302.53	80.436	1782.6	50000	32473	19.253	180.11
OPC-BP (BP)	13.364	27.241	1782.6	1633.6	52.878	8.8776	6.61.78	32473	50000	35.318	241.69

OPC-LB (LB)	0.61408	3.7149	8.7818	30.910	241.69	1782.6	80.436	19.253	35.318	50000	402.49
OPC-BM (BM)	1.2371	4.9828	50.833	110.25	19340	4122.1	1240.9	180.11	241.69	402.49	50000
PPC-H (BP)	5.7878	2739.3	0.24937	2.9031	0.48498	0.39065	0.59105	0.18752	0.72974	0.063748	0.0993
PPC-BP (H)	36.552	699.09	3.1813	2.5440	9.8508	8.1833	11.681	2.4344	14.020	0.89609	1.3490
PPC-BP (BP)	33.630	302.53	0.85814	4.0522	2.2728	1.8061	2.8104	0.61408	3.5331	0.17953	0.29594
PPC-H (LB)	51.009	4.3172	3.6665	3.0336	10.712	8.8458	12.776	2.7757	5831.6	0.98817	1.5063
PPC-LB (H)	6679.2	39.006	62.291	41.049	69.057	54.838	85.832	44.258	109.08	13.562	21.669
PPC-LB (LB)	37076	35.318	5.7878	29.714	6.5363	4.7293	8.9008	3.4098	12.566	0.58232	1.1611
PPC-H (BM)	121.82	1065.6	16.984	6.8750	31.457	26.618	3.6.669	13.562	43.207	5.8390	8.2466
PPC-BM (H)	87.831	160.63	1.2371	5.8976	2.8104	2.1969	3.5331	0.85814	4.5281	0.22868	0.38999
PPC-BM (BM)	2852.7	144.11	123.68	74.930	116.22	95.284	139.93	9.4.669	171.34	36.590	53.558

Table D6: Sorptivity Test Raw Data

MORTAR CATEGORY / Duration, t (hr)	0	0.25	0.5	1.5	3	5	8	24	48	72	96	120	144	168
$t^{1/2}$ (hr^{-1})	**0.0000**	**0.5000**	**0.7071**	**1.2247**	**1.7321**	**2.2361**	**2.8284**	**4.8990**	**6.9282**	**8.4853**	**9.7980**	**10.955**	**12.000**	**12.962**
OPC-H [H] (g)	332.110	332.660	333.440	334.200	334.930	335.760	336.640	337.550	338.510	339.250	339.620	339.680	339.710	339.720
OPC-H [H] % gain	0.0000	0.1656	0.4005	0.6293	0.8491	1.0990	1.3640	1.6380	1.9271	2.1499	2.2613	2.2794	2.2884	2.2914
OPC-H [H] H absorbed (g)		0.5500	1.3300	2.0900	2.8200	3.6500	4.5300	5.4400	6.4000	7.1400	7.5100	7.5700	7.6000	7.6100
OPC-H [H] Q/A	0.0000	0.0344	0.0831	0.1306	0.1763	0.2281	0.2831	0.3400	0.4000	0.4462	0.4694	0.4731	0.4750	0.4756
PPC-H [H] (g)	313.410	313.860	314.390	314.940	315.460	316.090	316.770	317.480	318.250	318.800	319.450	319.480	319.490	319.490
PPC-H [H]		0.1436	0.3127	0.4882	0.6541	0.8551	1.0721	1.2986	1.5443	1.7198	1.9272	1.9368	1.9400	1.9400

% gain														
PPC-H [H] H absorbed (g)	0.0000	0.4500	0.9800	1.5300	2.0500	2.6800	3.3600	4.0700	4.8400	5.3900	6.0400	6.0700	6.0800	6.0800
PPC-H [H] Q/A	0.0000	0.0281	0.0612	0.0956	0.1281	0.1675	0.2100	0.2544	0.3025	0.3369	0.3775	0.3794	0.3800	0.3800
OPC-BP [H] (g)	303.750	304.110	304.680	305.210	305.710	306.230	306.800	307.400	308.050	308.480	308.700	308.730	308.750	308.760
OPC-BP [H] % gain		0.1185	0.3062	0.4807	0.6453	0.8165	1.0041	1.2016	1.4156	1.5572	1.6296	1.6395	1.6461	1.6494
OPC-BP [H] H absorbed (g)	0.0000	0.3600	0.9300	1.4600	1.9600	2.4800	3.0500	3.6500	4.3000	4.7300	4.9500	4.9800	5.0000	5.0100
OPC-BP [H] Q/A	0.0000	0.0225	0.0581	0.0912	0.1225	0.1550	0.1906	0.2281	0.2688	0.2956	0.3094	0.3113	0.3125	0.3131
OPC-H [BP] (g)	300.120	300.770	301.110	301.680	302.120	302.700	303.380	304.060	305.220	305.650	306.370	306.720	306.720	306.720
OPC-H [BP] % gain		0.2166	0.3299	0.5198	0.6664	0.8597	1.0862	1.3128	1.6993	1.8426	2.0825	2.1991	2.1991	2.1991
OPC-H [BP] H absorbed (g)		0.6500	0.9900	1.5600	2.0000	2.5800	3.2600	3.9400	5.1000	5.5300	6.2500	6.6000	6.6000	6.6000
OPC-H [BP] Q/A		0.0406	0.0619	0.0975	0.1250	0.1612	0.2037	0.2463	0.3188	0.3456	0.3906	0.4125	0.4125	0.4125
OPC-LB [H] (g)	333.190	333.760	334.090	334.600	335.080	335.660	336.290	336.890	337.520	337.920	338.120	338.140	338.150	338.150

OPC-LB [H] % gain		0.1711	0.2701	0.4232	0.5672	0.7413	0.9304	1.1105	1.2996	1.4196	1.4796	1.4856	1.4886	1.4886
OPC-LB [H] H absorbed (g)		0.5700	0.9000	1.4100	1.8900	2.4700	3.1000	3.7000	4.3300	4.7300	4.9300	4.9500	4.9600	4.9600
OPC-LB [H] Q/A		0.0356	0.0562	0.0881	0.1181	0.1544	0.1938	0.2312	0.2706	0.2956	0.3081	0.3094	0.3100	0.3100
OPC-H [LB] (g)	331.340	332.011	332.326	333.008	333.586	334.080	334.794	335.472	336.126	336.627	336.879	336.891	336.892	336.894
OPC-H [LB] % gain		0.2027	0.2978	0.5034	0.6779	0.8271	1.0426	1.2472	1.4447	1.5958	1.6719	1.6754	1.6759	1.6765
OPC-H [LB] H absorbed (g)		0.6716	0.9867	1.6680	2.2462	2.7405	3.4546	4.1325	4.7869	5.2875	5.5397	5.5513	5.5529	5.5549
OPC-H [LB] Q/A		0.0420	0.0617	0.1042	0.1404	0.1713	0.2159	0.2583	0.2992	0.3305	0.3462	0.3470	0.3471	0.3472
OPC-BM [H] (g)	335.000	335.540	335.830	336.290	336.720	337.250	337.840	338.450	339.080	339.470	339.650	339.670	339.680	339.680
OPC-BM [H] % gain		0.1612	0.2478	0.3851	0.5134	0.6716	0.8478	1.0299	1.2179	1.3343	1.3881	1.3940	1.3970	1.3970
OPC-BM [H] H absorbed (g)		0.5400	0.8300	1.2900	1.7200	2.2500	2.8400	3.4500	4.0800	4.4700	4.6500	4.6700	4.6800	4.6800

OPC-BM [H] Q/A		0.0338	0.0519	0.0806	0.1075	0.1406	0.1775	0.2156	0.2550	0.2794	0.2906	0.2919	0.2925	0.2925
OPC-H [BM] (g)	332.677	333.240	333.560	333.980	334.460	335.000	335.640	336.160	336.860	337.250	337.450	337.480	337.510	337.510
OPC-H [BM] % gain		0.1692	0.2654	0.3917	0.5360	0.6983	0.8907	1.0470	1.2574	1.3746	1.4347	1.4437	1.4528	1.4528
OPC-H [BM] H absorbed (g)		0.5630	0.8830	1.3030	1.7830	2.3230	2.9630	3.4830	4.1830	4.5730	4.7730	4.8030	4.8330	4.8330
OPC-H [BM] Q/A		0.0352	0.0552	0.0814	0.1114	0.1452	0.1852	0.2177	0.2614	0.2858	0.2983	0.3002	0.3021	0.3021
OPC-BP [BP] (g)	305.690	306.150	306.470	306.900	307.300	307.810	308.360	308.940	309.550	309.920	310.090	310.110	310.120	310.120
OPC-BP [BP] % gain		0.1505	0.2552	0.3958	0.5267	0.6935	0.8734	1.0632	1.2627	1.3838	1.4394	1.4459	1.4492	1.4492
OPC-BP [BP] absorbed		0.4600	0.7800	1.2100	1.6100	2.1200	2.6700	3.2500	3.8600	4.2300	4.4000	4.4200	4.4300	4.4300
OPC-BP [BP] Q/A		0.0287	0.0488	0.0756	0.1006	0.1325	0.1669	0.2031	0.2413	0.2644	0.2750	0.2763	0.2769	0.2769
OPC-LB[LB] (g)	335.730	336.220	336.460	336.860	337.230	337.610	338.140	338.690	339.270	339.610	339.780	339.800	339.810	339.810

OPC-LB [LB]		0.1460	0.2174	0.3366	0.4468	0.5600	0.7178	0.8817	1.0544	1.1557	1.2063	1.2123	1.2153	1.2153
% gain														
OPC-LB [LB] H		0.4900	0.7300	1.1300	1.5000	1.8800	2.4100	2.9600	3.5400	3.8800	4.0500	4.0700	4.0800	4.0800
absorbed (g)														
OPC-LB [LB]		0.0306	0.0456	0.0706	0.0938	0.1175	0.1506	0.1850	0.2212	0.2425	0.2531	0.2544	0.2550	0.2550
Q/A														
OPC-BM [BM]	342.330	342.790	343.010	343.390	343.710	344.130	344.590	345.070	345.600	345.910	346.050	346.070	346.090	346.090
(g)														
OPC-BM [BM]		0.1344	0.1986	0.3096	0.4031	0.5258	0.6602	0.8004	0.9552	1.0458	1.0867	1.0925	1.0984	1.0984
% gain														
OPC-BM [BM]		0.4600	0.6800	1.0600	1.3800	1.8000	2.2600	2.7400	3.2700	3.5800	3.7200	3.7400	3.7600	3.7600
H absorbed (g)														
OPC-BM [BM]		0.0288	0.0425	0.0663	0.0862	0.1125	0.1412	0.1713	0.2044	0.2238	0.2325	0.2338	0.2350	0.2350
Q/A														
PPC BP [H] (g)	306.330	306.650	306.960	307.310	307.610	308.010	308.460	308.930	309.430	309.730	309.850	309.860	309.870	309.880
PPC-BP [H]		0.1045	0.2057	0.3199	0.4179	0.5484	0.6953	0.8488	1.0120	1.1099	1.1491	1.1524	1.1556	1.1589
% gain														
PPC-BP [H] H		0.3200	0.6300	0.9800	1.2800	1.6800	2.1300	2.6000	3.1000	3.4000	3.5200	3.5300	3.5400	3.5500

absorbed (g)													
PPC-BP [H] Q/A		0.0200	0.0394	0.0613	0.0800	0.1050	0.1331	0.1625	0.1938	0.2125	0.2200	0.2206	0.2213	0.2219
PPC-H [BP] (g)	304.720	305.090	305.380	305.710	306.030	306.400	306.860	307.330	307.700	308.010	308.070	308.120	308.350	308.350
PPC-H [BP] % gain		0.1214	0.2166	0.3249	0.4299	0.5513	0.7023	0.8565	0.9779	1.0797	1.0994	1.1158	1.1913	1.1913
PPC-H [BP] H absorbed (g)		0.3700	0.6600	0.9900	1.3100	1.6800	2.1400	2.6100	2.9800	3.2900	3.3500	3.4000	3.6300	3.6300
PPC-H [BP] Q/A		0.0231	0.0412	0.0619	0.0819	0.1050	0.1337	0.1631	0.1862	0.2056	0.2094	0.2125	0.2269	0.2269
PPC LB [H] (g)	316.230	316.570	316.790	317.110	317.390	317.770	318.200	318.650	319.120	319.390	319.500	319.510	319.510	319.510
PPC LB [H] % gain		0.1075	0.1771	0.2783	0.3668	0.4870	0.6230	0.7653	0.9139	0.9993	1.0341	1.0372	1.0372	1.0372
PPC-LB [H] H. absorbed (g)		0.3400	0.5600	0.8800	1.1600	1.5400	1.9700	2.4200	2.8900	3.1600	3.2700	3.2800	3.2800	3.2800
PPC-LB [H] Q/A		0.0212	0.0350	0.0550	0.0725	0.0962	0.1231	0.1512	0.1806	0.1975	0.2044	0.2050	0.2050	0.2050
PPC-H [LB] (g)	315.840	316.210	316.440	316.740	317.050	317.390	317.850	318.320	318.840	319.280	319.370	319.400	319.410	319.410
PPC-H (LB) % gain		0.1171	0.1900	0.2850	0.3831	0.4908	0.6364	0.7852	0.9498	1.0892	1.1177	1.1272	1.1303	1.1303

PPC-H [LB] H absorbed (g)		0.3700	0.6000	0.9000	1.2100	1.5500	2.0100	2.4800	3.0000	3.4400	3.5300	3.5600	3.5700	3.5700
PPC-H [LB] Q/A		0.0231	0.0375	0.0563	0.0756	0.0969	0.1256	0.1550	0.1875	0.2150	0.2206	0.2225	0.2231	0.2231
PPC-BM [H] (g)	315.010	315.390	315.540	315.830	316.090	316.450	316.860	317.250	317.670	317.860	317.950	317.960	317.960	317.960
PPC-BM [H] % gain		0.1206	0.1682	0.2603	0.3428	0.4571	0.5873	0.7111	0.8444	0.9047	0.9333	0.9365	0.9365	0.9365
PPC-BM [H] H absorbed (g)		0.3800	0.5300	0.8200	1.0800	1.4400	1.8500	2.2400	2.6600	2.8500	2.9400	2.9500	2.9500	2.9500
PPC-BM [H] Q/A		0.0237	0.0331	0.0512	0.0675	0.0900	0.1156	0.1400	0.1663	0.1781	0.1838	0.1844	0.1844	0.1844
PPC-H [BM] (g)	314.550	314.870	315.090	315.410	315.680	316.020	316.220	316.330	316.920	317.550	317.670	317.700	317.730	317.730
PPC-H [BM] % gain		0.1017	0.1717	0.2734	0.3592	0.4673	0.5309	0.5659	0.7535	0.9537	0.9919	1.0014	1.0110	1.0110
PPC-H [BM] H absorbed (g)		0.3200	0.5400	0.8600	1.1300	1.4700	1.6700	1.7800	2.3700	3.0000	3.1200	3.1500	3.1800	3.1800
PPC-H [BM] Q/A		0.0200	0.0337	0.0538	0.0706	0.0919	0.1044	0.1112	0.1481	0.1875	0.1950	0.1969	0.1988	0.1988
PPC-BP [BP] (g)	306.640	306.880	307.120	307.380	307.610	307.940	308.310	308.690	309.100	309.270	309.350	309.360	309.400	309.400

PPC-BP [BP] % gain		0.0783	0.1565	0.2413	0.3163	0.4239	0.5446	0.6685	0.8022	0.8577	0.8838	0.8870	0.9001	0.9001
PPC-BP [BP] H absorbed (g)		0.2400	0.4800	0.7400	0.9700	1.3000	1.6700	2.0500	2.4600	2.6300	2.7100	2.7200	2.7600	2.7600
PPC-BP [BP] Q/A		0.0150	0.0300	0.0463	0.0606	0.0813	0.1044	0.1281	0.1538	0.1644	0.1694	0.1700	0.1725	0.1725
PPC-LB [LB] (g)	331.35	331.510	331.780	332.010	332.210	332.480	332.800	333.150	333.520	333.660	333.720	333.730	333.730	333.730
PPC-LB [LB] % gain		0.0483	0.1298	0.1992	0.2595	0.3410	0.4376	0.5432	0.6549	0.6971	0.7153	0.7183	0.7183	0.7183
PPC-LB [LB] H absorbed (g)		0.1600	0.4300	0.6600	0.8600	1.1300	1.4500	1.8000	2.1700	2.3100	2.3700	2.3800	2.3800	2.3800
PPC-LB [LB] Q/A		0.0100	0.0269	0.0412	0.0537	0.0706	0.0906	0.1125	0.1356	0.1444	0.1481	0.1488	0.1488	0.1488
PPC-BM [BM] (g)	321.06	321.290	321.420	321.600	321.730	321.960	322.240	322.550	322.880	322.980	323.020	323.030	323.030	323.030
PPC-BM [BM] % gain		0.0716	0.1121	0.1682	0.2087	0.2803	0.3675	0.4641	0.5669	0.5980	0.6105	0.6136	0.6136	0.6136
PPC-BM [BM]		0.2300	0.3600	0.5400	0.6700	0.9000	1.1800	1.4900	1.8200	1.9200	1.9600	1.9700	1.9700	1.9700

H absorbed (g)													
PPC-BM [BM] Q/A	0.0144	0.0225	0.0338	0.0419	0.0562	0.0738	0.0931	0.1138	0.1200	0.1225	0.1231	0.1231	0.1231